IOWA STATE UNIVERSITY
Digital Repository

2010

Effect of heat generation from cement hydration on mass concrete placement

Soo Geun Kim
Iowa State University

Follow this and additional works at: http://lib.dr.iastate.edu/etd

 Part of the Civil and Environmental Engineering Commons

Recommended Citation

Effect of heat generation from cement hydration on mass concrete placement

by

Soo Geun Kim

A thesis submitted to the graduate faculty

in partial fulfillment of the requirements for the degree of

MASTER OF SCIENCE

Major: Civil Engineering (Geotechnical Engineering)

Program of Study Committee:
Kejin Wang, Major Professor
Chris Williams
Charles Jahren
Roy Gu

Iowa State University

Ames, Iowa

2010

TABLE OF CONTENTS

LIST OF FIGURES

LIST OF TABLES

ACKNOWEDGEMENT

I would like to express my sincere thanks to my advisor Dr. Kejin Wang for her motivation, inspiration, encouragement, and unstinted guidance. I also extend my thanks to Dr. Chris Williams, Dr. Charles Jahren, and Dr. Roy Gu for serving as my thesis committee and providing critical review on my thesis.

I extend my deep appreciation to Dr. Sung-Hwan Kim, Dr. Gilson Lomboy, and Mr. Chethan Hazaree. Their constant advices and encouragement helped me in every step of this research. I would also like to acknowledge the PCC Research Lab Manger Bob Steffes for his help in my experiments.

I am grateful to the K-water for the financial support of my Master of Science studying special thanks to the president Kuen-Ho Kim, my co-workers Dr. Bong-Suk Jang, Tae-Geun Kim, Sung-Won Jung, Min-Sup Kang, Bung-Su Chae, Jae-An Jung, and Jong-Hyun Lee. Without their help, much of this work would not have been possible.

I earnestly thank my family, especially to my wife Mi-Suk Cho, my beautiful daughter Chae-Won, and my lovely son Geon-Woo for their love, support and patience during the development of this work. This work is also for my ever-beloved parents in heaven.

ABSTRACT

Construction of a concrete dam requires large volume of concrete. Due to the small surface area-to-volume ratio, concrete dams are often subjected to high potential of thermal cracking, caused by the heat generation from cement hydration. To reduce the thermal cracking and ensure dam structure safety, a concrete dam is often constructed with low heat-generating cement and separated blocks having relative thin lift thickness. In Korea, low heat Type IV has been mainly used to reduce the temperature rise. Although benefits of using supplementary cementitious materials (SCMs) in concrete have been recognized, the practice of SCMs in dam concrete is not very common due to a concern for safety. On the other hand, increasing lift thickness of concrete blocks to accelerate dam construction has always been a demand.

The purpose of this research is to explore the potential use of fly ash as Type IV cement replacement in Korea concrete dams and to determine the proper lift thickness of concrete blocks in dam construction. In the present study, the chemical compositions and fineness of cement and fly ash are characterized. The heat hydration of fly ash replacement for Type I cement and Type IV cement are studied and compared. The temperature distributions and thermal cracks of a concrete block having four different lift thicknesses (1.5m, 2m, 2.5m, 3m) are analyzed using FEM commercial software ANSYS.

The results indicate that 40% fly ash replacement for Type I cement shows a similar heat generation and compressive strength at 28 days with that of Type IV cement and also has cost savings of 25%. A lift thickness equal or less than 1.5m showed little potential for

thermal cracking. Construction placement with a lift thickness greater than 2m had high probability of thermal cracking.

CHAPTER 1. INTRODUCTION

1.1 General

The proper design and construction of mass concrete dams can help prevent disasters due to severe weather changes. In Korea, several concrete dam projects are actively planned or are in progress. To ensure safety and durability, mass concrete maintenances have attracted increasing attention in the structural design and construction.

The main difference between mass concrete dam construction and other typical concrete structure types is its thermal behavior. Depending on concrete block thickness, the temperature generated from the hydration of cement in mass concrete can reach a true adiabatic condition in the interior if large blocks prevent timely heat dissipation to the surroundings. At a high temperature, the interior concrete tends to expend, while at a low ambient temperature, the exterior concrete tends to shrink and resist interior concrete to expend, thus causing thermal stress. The high thermal gradient between the center and the surface may cause thermal cracks when the thermal stress in concrete exceeds its tensile strength. In other words, small concrete blocks and thin construction lift allows rapid heat dissipation, thus reducing thermal cracking.

Once cracks take place at the upstream side of a dam under high water pressure especially in flood season, the service life of the structure may be shortened or dam safety problems may occur in the long run.

Therefore, one of the challenges in mass concrete design and construction is the maximum thickness of the concrete lifts, which should be designed without creating

thermally-induced cracks as well as the time between the placements of the next layer. Major economic savings in large projects can be achieved when the size and placement of lifts are perfectly orchestrated (Mehta, 2002). Determining the maximum lift thickness of a concrete layer is among the most important considerations in concrete dam construction because it ultimately relates to saving time, effort, and money.

The control of heat generated from cement evolution is one of the most effective ways to reduce the temperature rise in mass concrete dams; methods include the use of low-heat-generating cement and the control of the amount of cement content by using the large size of aggregate. These methods have all been used in Korean dam construction.

Rate of cement hydration is closely related chemical composition of the cement. The use of supplementary cementitious materials (SCMs) such as fly ash in concrete generally reduces the heat of hydration and results in a lower concrete temperature. However, SCMs are rarely used in Korean dam construction.

Many thermal stress analyses in mass concrete have been performed by the finite element method (FEM). There are various approaches on how to use this method. In this thesis, commercial software ANSYS Ver. 12 is used. The software is a multipurpose finite element analysis package that can perform 2-D and 3-D analysis. The ANSYS/Structural and ANSYS/Thermal (steady state and transient thermal) packages are applied here. These components can accurately simulate the behavior of different kind of structures, from small structures to large and complex models (Kim, 2005).

1.2 Research Approach

The main objective of the thesis is to study thermally-induced stresses due to the heat of hydration generated in mass concrete dams. The study consists of two components, (1) to verify the possibility of using Type I portland cement with fly ash as an alternative of Type IV cement and, (2) to determine the proper lift thickness for dam concrete construction in order to avoid thermally-induced cracks in a mass concrete dam.

Fly ash can improve concrete workability, reduce the heat of hydration generated by portland cement and decrease concrete permeability. It is also cheaper than portland cement. However, the use of fly ash in Korean mass concrete dam construction is rare but if used, could have great economic benefits. Therefore, the objectives of this study are to evaluate the possibility of fly ash use in mass concrete dam and to investigate the effect of fly ash on hydration. The appropriate amount of fly ash replacement for Type I cement to produce similar heat of hydration characteristics as Type IV cement is also studied.

As mentioned before, thermal stress induced by cement hydration may cause thermal cracks. The bigger the concrete block or the thicker the lift thickness of each concrete construction layer, the higher the risk of thermal cracking. Knowing the thermal stress development in a mass concrete section, both its magnitude and its profile, is the key to determining the suitable lift thickness for dam concrete construction.

One thermocouple was installed in the center of one block of a mass concrete dam under construction in Korea. The measured data were used for verifying the analysis algorithm of the present study. The effect of thermal distribution corresponding to the

different lift thicknesses and the thermal stress analysis due to thermal loads were carried out to find out the proper lift thickness for mass concrete dams.

In the present study, FEM is used for the thermal analysis of a dam concrete structure constructed with different lift thicknesses. The thermal analysis is performed in several steps:

(1) Monitor temperature rise in concrete using adiabatic equipment

(2) Convert the temperature rise into heat of cement hydration

(3) Compute the temperature distribution in concrete block based on heat on hydration

(4) Verify the reliability of the FEM model by comparing with field temperature

(5) Estimate the maximum temperature and thermal cracks for a concrete block with different lift thickness.

1.3 Scope of the Thesis

The thesis is divided into six chapters including the literature review, experimental work, thermal distribution analysis, and thermal stress analysis.

Chapter 1 presents the overall subject of this research in terms of general background, research objective, the approach chosen, and the scope of the thesis.

Chapter 2 provides a literature review related to cement hydration factors, measurement of cement hydration, and thermal stress characteristics of mass concrete.

Chapter 3 discusses details of the experimental program, including materials properties, experiment tools used, and test results.

Chapter 4 provides a thermal analysis algorithm including its detailed procedure and parameters. All parameters are applied to match field conditions as closely as possible. Analysis of thermal distribution at each section of different lift thickness is also included in this chapter.

Chapter 5 covers the procedures for thermal stress due to the thermal loads developed in the chapter 4. The lift thickness effect is analyzed and the proper lift thickness to avoid thermal cracks is determined. The ANSYS software is also used to calculate the thermal distribution and thermal stress results of chapter 4 and chapter 5.

Chapter 6 provides overall conclusions of this study and recommendations for future work.

Several appendices provide supplementary information related to the thesis. Appendix A is an explanation of the internal heat of hydration of cement used as a load for thermal analysis. In Appendix B, the modulus of elasticity used in this study is included. Appendix C and Appendix D provide input data used for thermal distribution analysis and thermal stress analysis.

CHAPTER 2. LITERATURE REVIEW

2.1 Introduction

The temperature in mass concrete structures has an important effect on dam construction schedule and safety. The main factor contributing to temperature rise in mass concrete is heat evolution due to an exothermic reaction of cement. Understanding the mechanism of heat generation for cement is the key to controlling the temperature of mass concrete.

The first section of this chapter mainly describes the properties and hydration of cementitious materials. The second section discusses the methods used to measure cement hydration. This section describes the characteristics of heat generation in mass concrete.

2.2 Properties of Cementitious Materials

2.2.1 Ordinary Portland Cement (OPC)

OPC is mostly used in the production of concrete structures. It is hydraulic cement and composed primarily of alite (C_3S), belite (C_2S), aluminate (C_3A), and aluminoferrite (C_4AF). These four major compounds determine the hydraulic properties of cement because they account for over 90 % of Portland cement (Zhi Ge, 2005). The typical composition of OPC is listed in Table 2.1. The total percentage does not equal 100 because of the presence of impurities in the cement.

Chemical formulas of cement are commonly expressed as a function of sums of oxides. Most widely used abbreviations are listed in Table 2.2. The chemical composition of

OPC can be determined by many methods, with X-ray Florescence (XRF) Spectroscopy and chemical methods most commonly used. The results are reported as its oxide and can be converted to the chemical composition by the *Bogue calculation* (Bogue 1947). According to ASTM C 150, *Standard Specification for Portland Cement,* a simple *Bogue calculation* can be produced by Equations 2.1-2.8.

Table 2.1. Typical composition of portland cement (Mindess 2003)

Chemical Name	Chemical formula	Shorthand Notation	Weight percent
Tricalcium silicate(alite)	$3CaO·SiO_2$	C_3S	55
Dicalcium silicate (belite)	$2CaO·SiO_2$	C_2S	18
Tricalcium aluminate	$3CaO·Al_2O_3$	C_3A	10
Tetracalcium aluminoferrite	$4CaO·Al_2O_3·Fe_2O_3$	C_4AF	8
Calcium sulfate didydrate (Gypsum)	$CaSO_4·2H_2O$	$C\bar{S}H_2$	6

When A/F ≥ 0.64

$$C_3S = 4.071\ C - 7.600\ S - 6.781\ A - 1.430\ F - 2.852\bar{S} \tag{2.1}$$

$$C_2S = 2.867\ S - 0.7544\ C_3S \tag{2.2}$$

$$C_3A = 2.650\ A - 1.692\ F \tag{2.3}$$

$$C_4AF = 3.043\ F \tag{2.4}$$

When A/F < 0.64

$$C_3S = 4.071\ C - 7.600\ S - 4.479\ A - 2.859\ F - 2.852\ \bar{S} \tag{2.5}$$

$$C_2S = 2.867\ S - 0.7544\ C_3S \tag{2.6}$$

$$C_3A = 0 \tag{2.7}$$

$$C_4AF + C_2F = 2.100\ A + 1.702\ F \tag{2.8}$$

Table 2.2. Typical oxide composition of OPC (Mindess 2003)

Oxide	Shorthand Notation	Common Name	Weight percent
CaO	C	Lime	64.47
SiO_2	S	Silica	21.03
Al_2O_3	A	Alumina	6.16
Fe_2O_3	F	Ferric oxide	2.58
MgO	M	Magnesia	2.62
K_2O	K	Alkalis	0.61
Na_2O	N		0.34
SO_3	$\bar{S}$	Sulfur trioxide	2.03
CO_2	$\bar{C}$	Carbon dioxide	-
H_2O	H	Water	-

Among various cement chemical compositions, C_3S and C_2S mainly have an effect on the strength of concrete. C_3S affects most of the early strength and C_2S develops long term compressive strength. The two chemical compositions account for over 70% of the total cement composition.

Various types of portland cement have been developed to meet different physical and chemical requirements for specific construction conditions. These cement types are produced by adjusting the chemical composition and the fineness of cement. Usually, cement types are primarily classified according to ASTM C 150 into five classes:

Type I cement is general purpose cement suitable for all uses not requiring the special properties of other types. Examples include pavements, floors, reinforced concrete buildings, bridges, tanks, reservoirs, pipe, masonry units, and precast concrete products. Generally, it is more economical than type II cement.

Type II cement is used where relatively low heat generation is desired or where moderate sulfate attack may occur. The C_3A content increase of early heat in this cement is comparatively lower than that of other cement types

Type III cement provides more rapid development of strength at an early age after contact with water because of its higher surface area and increased C_3S content. It is used when high early strength is desirable.

Type IV cement is needed where heat generation from hydration should be minimized such as in mass concrete structures. It generates less heat at a slower rate than the other types because its C_2S content is higher and its C_3S content is lower. In addition, this cement has somewhat greater resistance to sulfate attack than for Type I or Type II, and has less rapid strength development with equal strength at advanced ages. This cement is rarely available in the United States where reduction methods of cement hydration using various cementitious materials are much preferred. However, it is commonly found in Korea, especially in mass concrete structures.

Type V cement is used where high sulfate resistance is desired such as in foundation and marine structures. The C_3A content of the cement is limited to less than 5 percent in the specification when a sulfate expansion test is not available.

Typical chemical composition and properties of portland cement for the five types is given in Table 2.3.

Table 2.3. Typical compound composition and properties of portland cement (Mindess 2003)

	Cement Type				
	I	II	III	IV	V
C_3S	55	55	55	42	55
C_2S	18	19	17	32	22
C_3A	10	6	10	4	4
C_4AF	8	11	8	15	12
Fineness (Blaine, m2/kg)	365	375	550	340	380
Compressive strength (1day, MPa)	15	14	24	4	12
Heat of hydration (7days, J/g)	350	265	370	235	310

2.2.2 Fly Ash

Fly ash is the most widely used as supplementary cementitious materials (SCMs), having been used in concrete for 50 years. According to ASTM C 618, *Standard Specification for Coal Fly Ash and Raw or Calcined Natural Pozzolan for Use in Concrete*, fly ash is the finely divided residue that results from the combustion of ground or powdered coal, and it is transported by flue gasses. It is sometimes called "pulverized fuel ash". It is approximately half the cost of portland cement and can be used at up to 50% replacement for

cement. Fly ash is classified into Class F and Class C types in the US and also is classified into two types in Korea.

Class F and Class C fly ashes are commonly used as pozzolanic admixtures for general purpose concrete. Class F fly ash is normally produced by burning anthracite or bituminous coal and has a low-calcium (less than 10% CaO) content. Conversely, class C fly ash is a high-calcium (10% to 30% CaO) material and typically has cementitious and pozzolanic properties. It is produced when subbituminous coal is burned

Most fly ash particles are spherical and are very fine. Particle size is between 10 and 100 μm, surface area is typically 300~500 m^2/kg, density is 540~ 860kg/ m^3, specific gravity is 2.2~2.4, and color ranges from off-white to light gray.

The spherical particle of fly ash improves the workability of concrete because its shape acts like ball bearing. Fly ash has features of pozzolanic reaction which increases amount of C-S-H at the expense of calcium hydroxide (Ca(OH)$_2$) at later and fills up large capillary space in cement. This pozzolanic reaction increases the long-term strength of concrete and reduces the permeability of concrete.

2.3 Hydration of Portland Cement

Chemical reactions and physical processes of cement after contact with water determine the setting and hardening properties of concrete. Heat of hydration of cement and its rate play key roles in determining concrete strength and durability. This section discusses the process of hydration of portland cement and factors that influence this process.

2.3.1 Portland Cement Hydration

There are two types of reaction underlying the hydration process: through-solution hydration and solid-state hydration. Through-solution hydration involves dissolution of anhydrous compounds to their ionic constituents, formation of hydrates in the solution, and eventual precipitation of hydrates. Solid-state hydration takes place directly at the surface of the anhydrous cement compounds without the compounds going into solution. (Mehta et al. 2006)

As noted in section 2.2.1, ordinary portland cement is composed largely of four types of minerals: alite (C_3S), belite (C_2S), aluminate (C_3A), and aluminoferrite (C_4AF). When these minerals and water are mixed together, hydration products are formulated. Calcium silicates consist of tricalcium silicate and dicalcium silicate. The two calcium silicates induce very similar hydration reactions. Equations 2.9 and 2.10 describe the hydration reaction of calcium silicates. The principal hydration product is calcium silicate hydrate (C-S-H) and calcium hydroxide. C-S-H gel plays the role of a binder of the cement paste and eventually has an effect on the strength and durability of concrete. C_2S and C_3S produce a C-S-H gel of about 82 percent and 61 percent, respectively. The ultimate strength and durability of a high-C_2S cement would be higher than for one with a high proportion of C_3S.

$$2C_3S + 11H \rightarrow C_3S_2H_8 \text{ (C-S-H)} + 3CH \text{ (calcium hydroxide)} \qquad 2.9$$

$$2C_2S + 9H \rightarrow C_3S_2H_8 \text{ (C-S-H)} + CH \text{ (calcium hydroxide)} \qquad 2.10$$
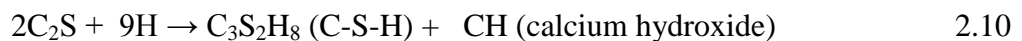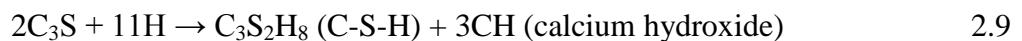
Tricalcium aluminate (C_3A) reacts immediately with water. The rapid hydration of C_3A can be slowed down by the addition of gypsum. Therefore, the final hydration products vary with the gypsum content. The hydration products of C_3A are commonly formed of ettringite in the first stage and monosulfoaluminate later (Equation 2.11). The precipitation of ettringite contributes to stiffening, setting, and early strength development. After the depletion of sulfate, ettringit becomes unstable and is gradually converted into monosulfoaluminate (Equation 2.12). If a new source of sulfate is added, monosulfoaluminate can convert back to ettringite again. Tricalcium aluminate (C_3A) contributes little to the strength of cement paste.

$$C_3A + 3C\bar{S}H_2 + 26H \rightarrow C_6A\bar{S}_3H_{32} \text{ (ettringite)} \qquad \qquad 2.11$$

$$C_3A + C_6A\bar{S}_3H_{32} + 4H \rightarrow 3C_4A\bar{S}H_{12} \text{ (monosulfoaluminate)} \qquad \qquad 2.12$$
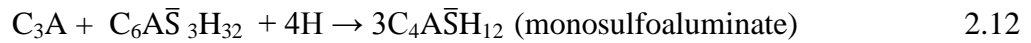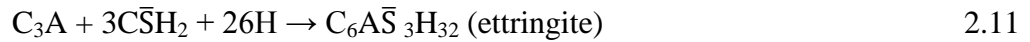
The hydration of tetracalcium aluminoferrite (C_4AF) is similar to hydration products of C_3A. The hydration reactions are slower and involve less heat. Two possible hydrates can form depending on the availability of gypsum (Equations 2.13 and 2.14).

$$C_4AF + 3C\bar{S}H_2 + 21H \rightarrow C_6(A,F)\bar{S}_3H_{32} + (F,A)H_3 \qquad \qquad 2.13$$

$$C_4AF + C_6(A,F)\bar{S}_3H_{32} + 7H \rightarrow 3C_4(A,F)\bar{S}H_{12} + (F,A)H_3 \qquad \qquad 2.14$$
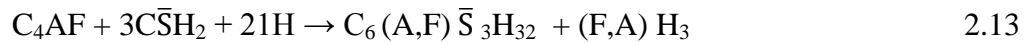
Over time, the cement hydration process due to the above minerals produces a unique heat release signature than can be monitored using an inductive isothermal calorimeter. The

heat sequence pattern can be commonly classified of five stages under normal conditions. A typical hydration process is shown in Figure 2.1 and the reaction sequence is briefly described in Table 2.4. The data from heat of hydration studies can be used for characterizing the setting and hardening behavior of cements, and for predicting the temperature rise. Lerch recorded the rate of heat evolution from cement pastes during the setting and early hardening period (Mehta, 2006).

In Stage I (the dissolution stage), the reaction occurs right after contact with water because ions dissolved in water react with C_3A and gypsum. The formation of ettringite produced after initial hydration reactions sharply reduces the rate of the reaction in the latter part of State I. This stage has little an effect on concrete strength. The system then enters a dormant period (Stage II).

In Stage II (the induction [dormant] period), the concentration of ions in the solution gradually increases along with the solution of solid phase. Cement concrete remains in the plastic state. This stage does not develop concrete strength. However, it is important for workability and transportation of concrete because this stage allows concrete to be transported to a job site.

In Stage III (the acceleration stage), the alite (C_3S) and belite (C_2S) in the cement start to hydration and release heat. In this stage concrete setting begins and heat generation is rapidly accelerated. The silicate reaches a high rate of hydration at the end of the Stage III. Concrete strength is developed in this stage in which final setting has been finished and early hardening has begun. Therefore, the acceleration stage is a very important characteristic in concrete.

In stage IV (the deceleration stage), the rate of heat generation again decreases and shifts to a diffusion-controlled process. In this phase, the thickness of hydrated particles increases and the surface area of the unhydrated parts decreases. The layer of cement hydrates acts as a diffusion area to govern the permeability of the water and dissolved ions. Ettringite is converted to monosulfate phase which is sometimes noted as the heat contribution of C_3A hydration (calorimeter results for cement typically may be show a shoulder).

In stage V (the steady stage), the thicker layer of hydrates around the cement particles reduces the rate of hydration remarkably. It is difficult in this stage for hydrates to be precipitated because the space originally filled by water is covered with hydrated cement. The hydration is completely controlled by the diffusion process.
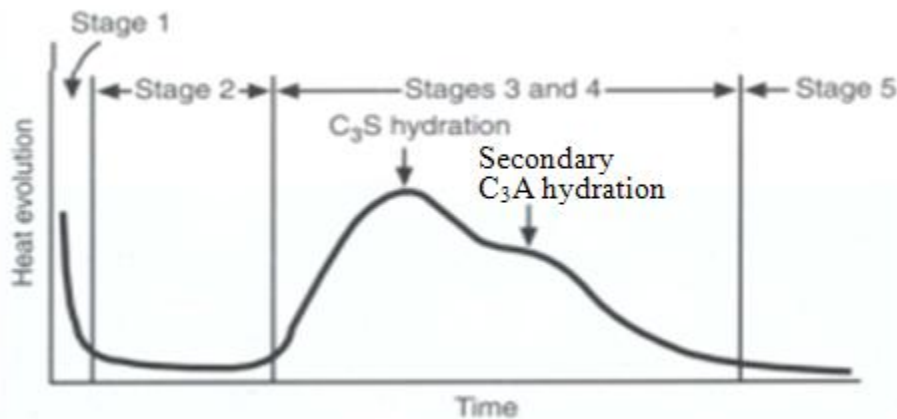
**Figure 2.1. Rate of heat evolution during hydration of portland cement
(Adapted from PCA 2006)**

Table 2.4. Typical hydration process of cement (Mindess 2003)

Reaction Stage	Kinetics of Reaction	Chemical Processes
1 Initial hydrolysis	Chemical control; **rapid**	Dissolution of ions
2 Induction period	Nucleation control; **slow**	Continued dissolution of ions
3 Acceleration	Chemical control; **rapid**	Initial formation of hydration products
4 Deceleration	Chemical and diffusion control; **slow**	Continued formation of hydration products
5 Steady state	Diffusion control; **slow**	Slow formation of hydration products

2.3.2 Factors that Influence Cement Hydration

The rate and amount of the heat liberated greatly depends on the cement type, the chemical composition and physical properties of the cement, the water/cement ratio, and supplementary cementitious materials (SCM) such as fly ash, chemical admixtures, and curing conditions.

2.3.2.1 Chemical Composition of Cement

The rate and amount of heat liberated for a givne chemical composition of cement depends on the temperature rise of the concrete. The rate of hydration for a cement compound can be found by evaluating the individual compound and its percentage in the cement. The hydration characteristics of cement compounds are listed in Table 2.5. The order of the rate of hydration during the first few days is approximately $C_3A > C_3S > C_4AF > C_2S$

as shown in Figure 2.2. This table and graph show that Aluminate (C_3A) and Alite (C_3S) are

the most reactive compounds, whereas belite (C_2S) reacts much more slowly.

Table 2.5. Characteristics of hydration cement compound (Mindess 2003)

Compounds	Reaction rate	Amount of Heat Liberated	Contribution to Cement Heat Liberation
C_3S	Moderate	Moderate	High
C_2S	Slow	Low	Low
$C_3A + C\bar{S}H_2$	Fast	Very High	Very High
$C_4AF + C\bar{S}H_2$	Moderate	Moderate	Moderate
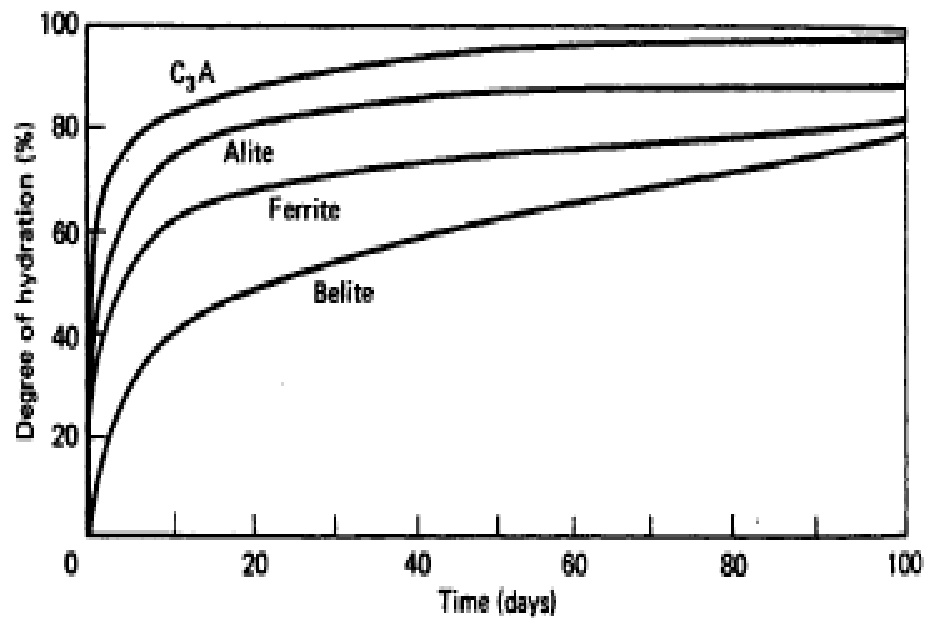
Figure 2.2. Hydration rate of the cement compound in a Type I cement paste (Adapted from Mindess and Young 2003)

The portland cement types classified by ASTM C 150 are also correlated with the amount of cement compound as stated above. Figure 2.3 shows that the heat generation rates for different types of cement under adiabatic conditions are different. This figure clearly expresses why Type IV cement is generally used in mass concrete structures. The difference in heat evolution rates for different cements is due to the chemical composition and fineness of cement.
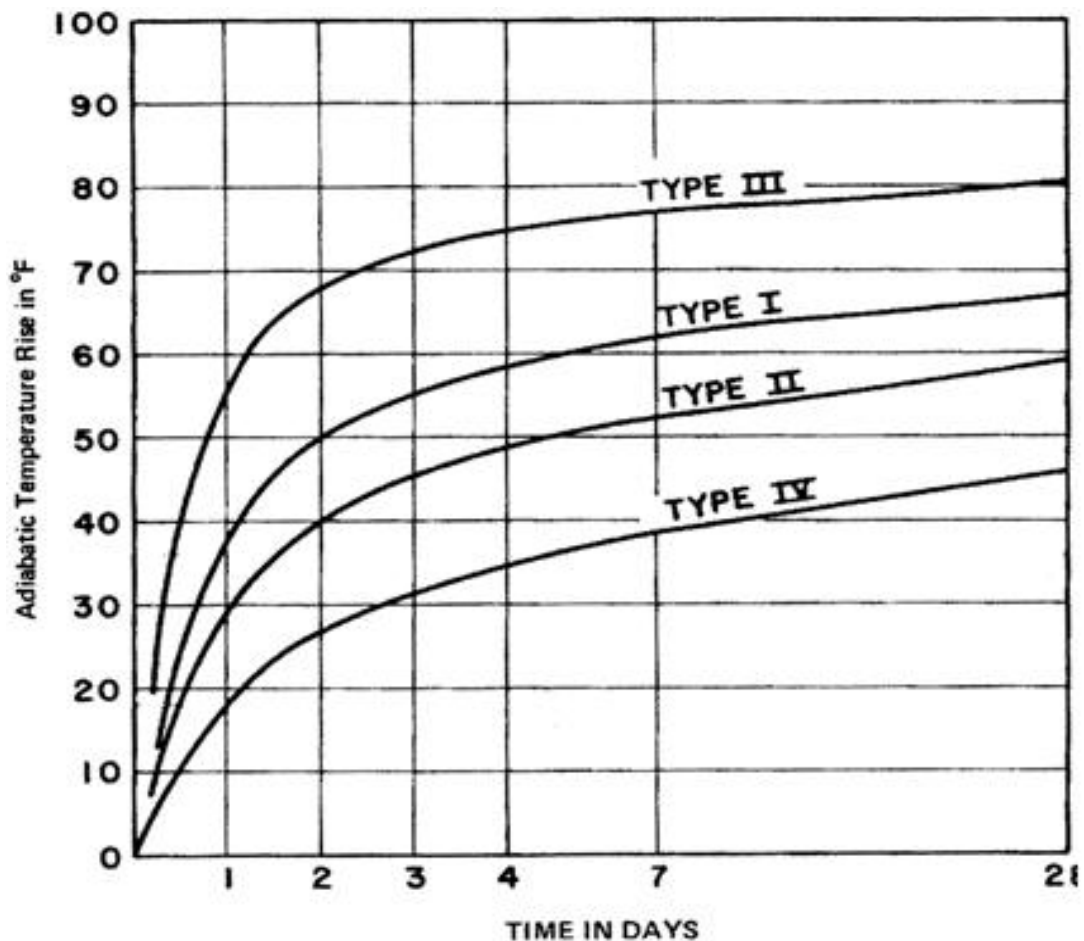
**Figure 2.3. Temperature rise of mass concrete under adiabatic condition
(Adapted from ACI 2007.2R-07)**

2.3.2.2 Sulfate Content

A small amount of gypsum is used to control the early reaction of tricalcium aluminate (C_3A). Cement with a low or over dosage of sulfate will exhibit either a false or a flash set. Therefore, it is necessary to consider the proper amount of sulfate required for cement because it varies with the composition and the fineness of the cement. The effect of gypsum on hydration was studied by Lerch (1946). He found that an increase of SO_3 reduced the heat of hydration (Figure 2.4) because alumina is less soluble in a lime-gysum solution.
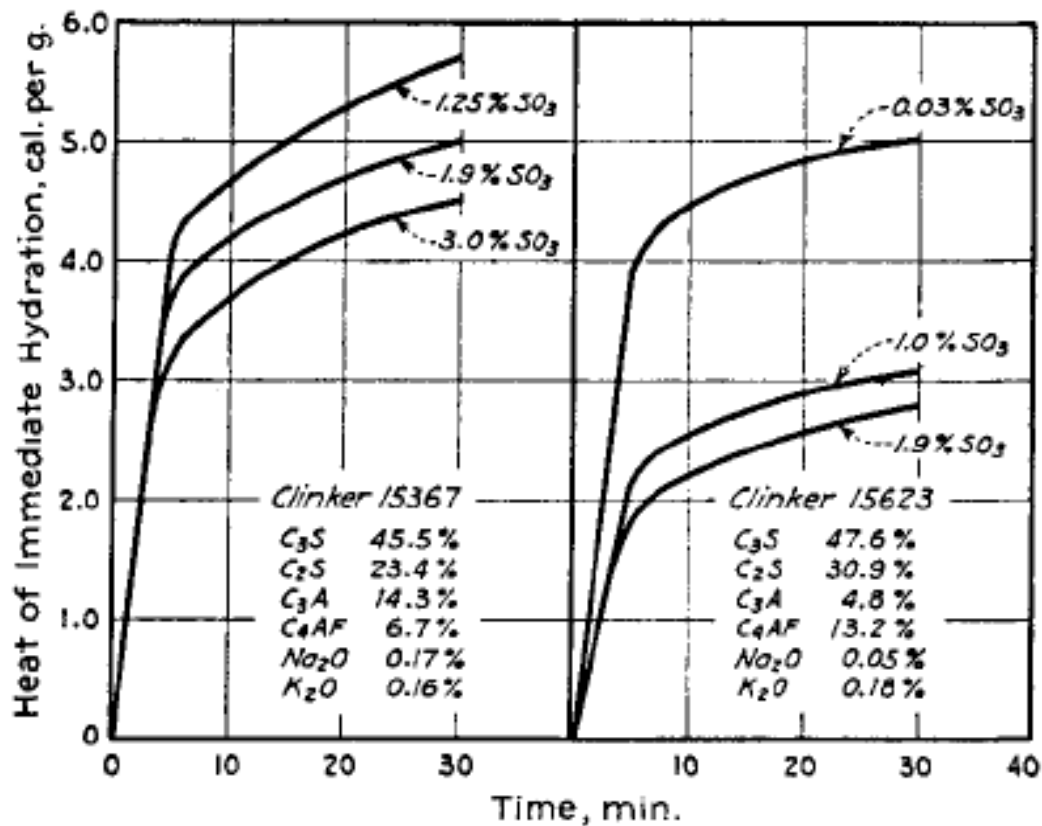
Figure 2.4. Heat of immediate hydration with SO_3 varied
(Adapted from Lerch et al. 1946)

2.3.2.3 Fineness

The fineness is defined as the overall particle size distribution of cement by describing the specific surface area (m^2/kg). Fineness of cement is commonly determined by two method; Wagner Turbidimeter test and Baine air-permeability test. The fineness of cement has a considerable effect on the placeability, workability, and water content of concrete.

The amount of hydration depends on the fineness of the cement because hydration starts at the surface of the cement particles. It represents the material available for making contact with water and therefore hydrating. Higher fineness provides a greater surface area to be wetted, resulting in an acceleration of the reaction between cement and water. This increases the rate of heat liberation at early ages, but may not influence the total amount of heat developed over several weeks. Figure 2.5 shows how the fineness influences for the rate of heat of hydration for a given cement. A high fineness quickly increases the heat of hydration at an early age.
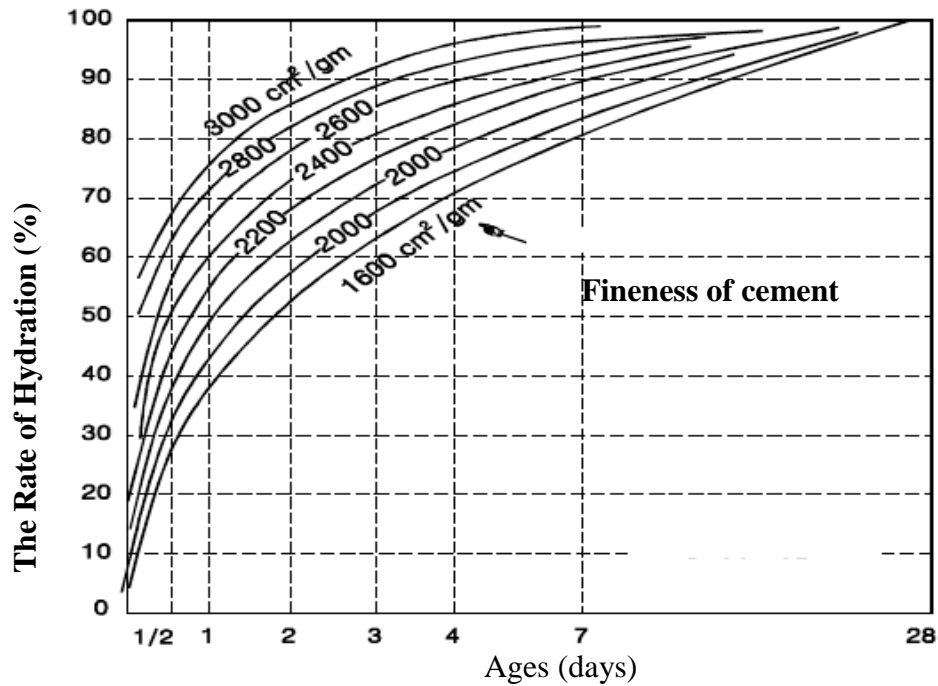
Figure 2.5. The rate of hydration as affected by fineness of cement
(Adapted ACI 207.2R-07)

2.3.2.4 Water/Cement Ratio

The space initially taken up by water is partially or completely replaced by hydration production as hydration reactions precede. Hydration products are produced by a reaction of between cement and water. If the w/c ratio is low, complete hydration is not possible because there is insufficient space for the hydration products. Conversely, if available water exists in cement, hydration will progress continuously and the available space within the paste will be completely filled. Complete hydration of cement is generally assumed to require a water/cement ratio of about 0.4 and a minimum w/c ratio of 0.42 (Mindess et al. 2003). The heat evolution rate starts to decrease as the w/c ratio decreases after a certain time (Byfors 1980). Figure 2.6 shows that the total heat liberated is affected by the w/c ratio.
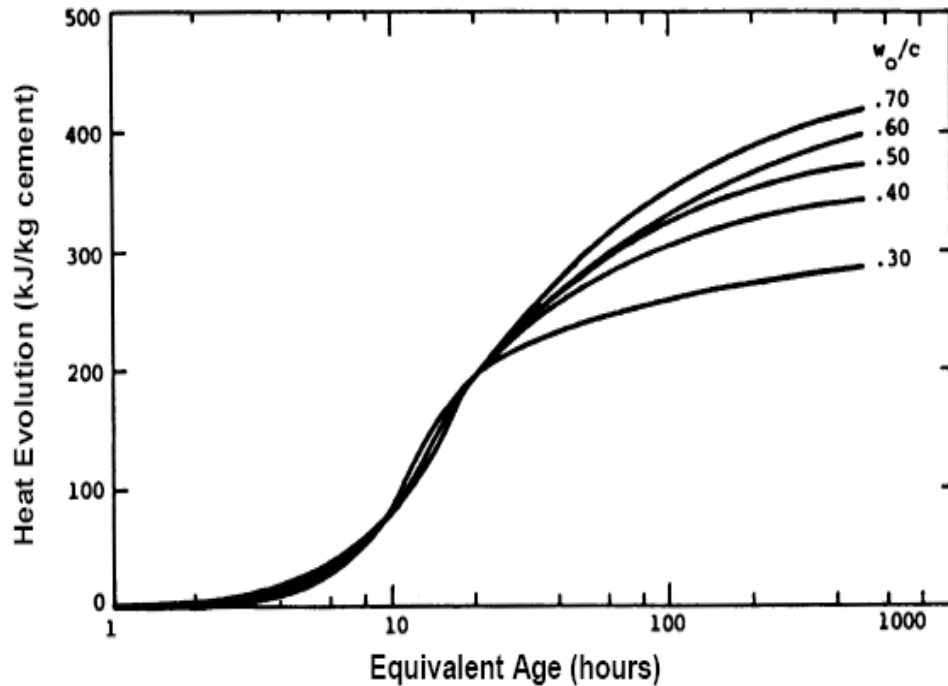
Figure 2.6. Effect of W/C ratio on the heat evolution (RILEM 42-CEA 1981)

2.3.2.5 Initial Temperature

The environmental temperature is also important in determining heat of hydration. Cement hydration at higher environmental temperature is accelerated at early ages, but decelerated later on. The heat of hydration of cement is faster when the ambient temperature is increasing because the rate of heat reaction increases. Figure 2.7 shows the relationship describing different heat evolution with curing temperature with respect to time. The concrete placement seasoning due to heat hydration as influenced by the curing temperature is important for mass concrete structures that are generally constructed over an interval of several years.
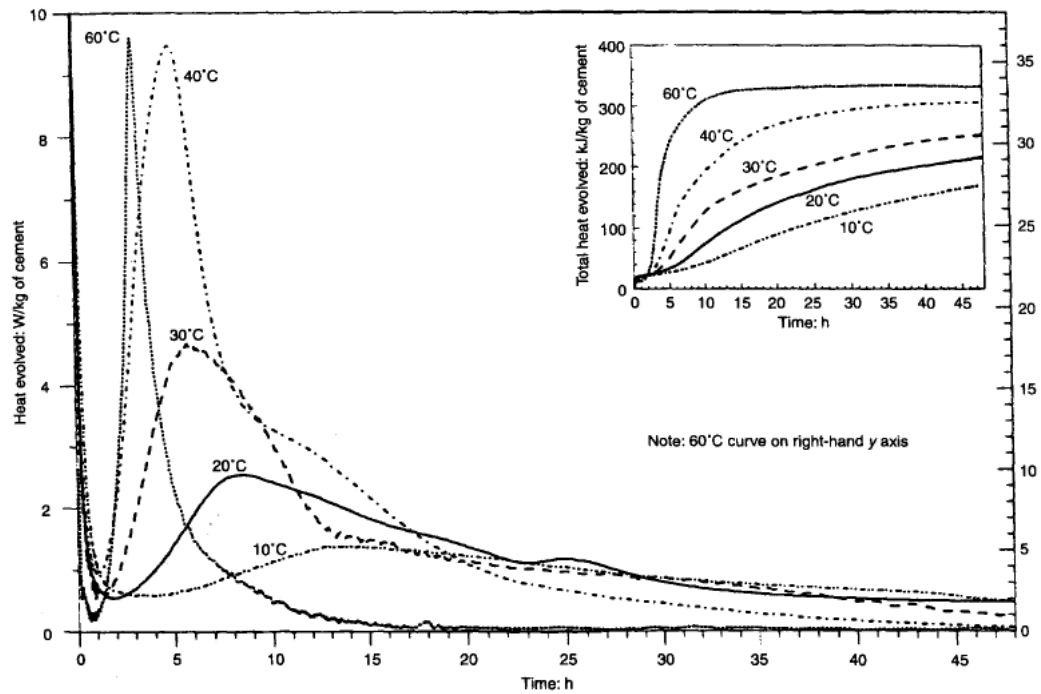
**Figure 2.7. Effect of curing temperature on hydration
(Adapted from Escalante-Garcia et al. 2000)**

2.3.2.6 Supplemental Cementitious Materials (SCMs)

SCMs, such as pozzolanic (e.g., flay ash) are widely used as partial replacements for portland cement. The proper use of SCMs has the advantages of the reduction of heat of hydration, economy, and workability. The properties of SCMs concrete are described through a pozzolanic reaction (Equation 2.15) between a pozzolan and calcium hydroxide. The Pozzolanic reaction generates less heat than ordinary portland cement because the reaction is similar to a C_2S reaction.
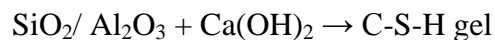
$$SiO_2/ Al_2O_3 + Ca(OH)_2 \rightarrow \text{C-S-H gel} \qquad\qquad 2.15$$

Fly ash

In generally, fly ash retards the hydration of portland cement, especially at an early stage, and increases the dormant period. The early-age heat contribution of fly ash may conservatively be estimated to range between 15 and 35% of the heat contribution from the same weight of cement (ACI 207.2R-07). The total heat of hydration of fly ash mainly depends on the lime (CaO) content. Aluminum ions on the fly ash surface depress Ca^{2+} ion concentration in pore solution when cement is mixed with fly ash. The depression of Ca^{2+} ion concentration retards the formation of CH and C-SH gel. (Langan et al. 2002). This means that heat evolution from portland cement generates slowly in a fly ash concrete. In addition, the pozzolanic reaction produces little heat. Figure 2.8 shows the influence of fly ash on the rate of heat generation of the mortar. As the replacement level of fly ash increases, the maximum heat generation decreases and the peak of hydration is delayed. Compressive strengths of concrete using fly ash are low during the first 28days, while long-term strengths are satisfactory. This illustrates that fly ash can use for mass concrete structures where high early strengths are not needed.
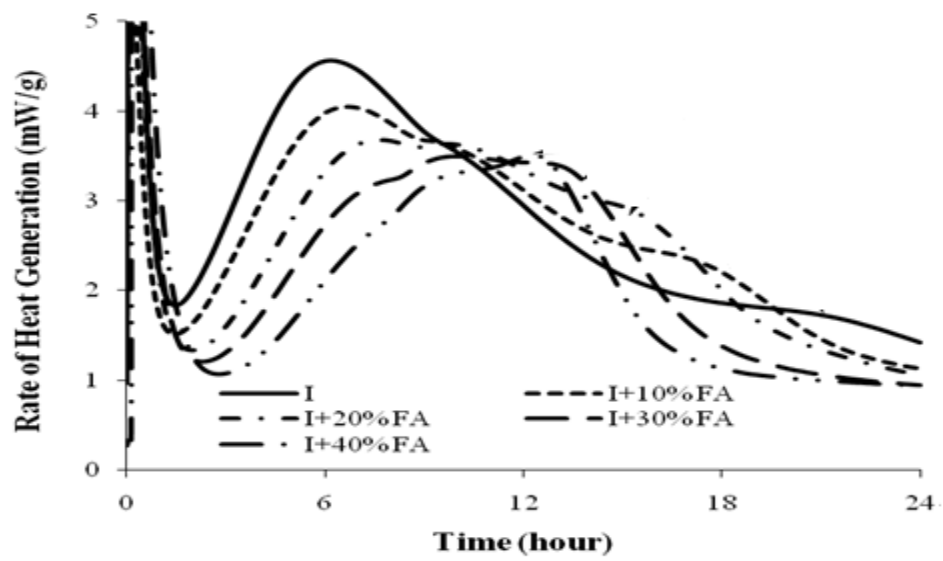
Figure 2.8. Effect of fly ash replacement level on heat generation
(Adapted from Zhi Ge 2009)

2.4 Measurements for Cement Hydration

Cement hydration is a highly exothermic and thermally activated reaction. Heat of hydration can be used for characterizing the setting and hardening behavior of cement, and for predicting the temperature rise. It is essential to measure different aspects of cement and concrete hydration, particularly in the case of major projects such as dams, foundations of large structures, etc. Various means for determination of the heat of hydration have been developed. Recently, the calorimeter test methods with monitoring heat of hydration over time are more commonly used. Calorimetry tests can be classified into three types: adiabatic (no gain or heat loss through system), semi-adiabatic (known heat loss through system), and isothermal calorimetry (constant temperature in system).

The adiabatic calorimeter measures the heat of hydration of samples in an insulated condition with no heat loss. It is performed by measuring the temperature of samples, and changing the temperature of the surrounding medium to match. Although a small amount of heat actually escapes from the system, the calorimeter is generally considered to be adiabatic as long as the temperature loss of the sample is not greater than 0.02 K/h. Most adiabatic calorimeters use a combination of water, air and/or oil circulation around the sample to reduce the heat loss. Since the apparatus is heavily insulated, adiabatic calorimeters give a good estimate of the adiabatic rise of a concrete temperature. However, high set-up costs and the large sample size could perhaps make the testing apparatus less practical than a semi-adiabatic calorimeter.

A semi-adiabatic calorimeter similar to the adiabatic calorimeter except it permits a certain amount of heat loss to the environment. The heat evolution in this test is lower than

that of the sample in the adiabatic test due to heat loss. The maximum heat loss is limited to less than 100 J/(h·K). The temperature measured by the semi-adiabatic calorimeter is typically 2%-3% below the results from the adiabatic tests (Springenschmid, 1998). This means that the semi-adiabatic calorimeter can predict the adiabatic temperature based on the activation energy, total heat of hydration, and calibrated heat loss. This test is often simpler and cheaper to run because insulation or control systems are much simpler than those of the adiabatic calorimeter. However, the semi-adiabatic calorimetry test has no established standard test method, so the sensitivity of the test results to instrument bias, calibration procedure, within batch and batch-to-batch variation is unknown (Poole et al, 2007)

An isothermal calorimeter measures the rate of heat of hydration generated from samples while both the specimen and the surrounding environment temperature are kept almost equal. The calorimeter is controlled to remain at a fixed temperature and sometimes involves measurement of the energy required to maintain that temperature. This may be one disadvantage, that is, temperature variations in the field is not taken into account. However, these data provide useful, controlled information about hydration kinetics of the system. The specimen's rate of heat evolution is monitored and determined by summing the measured heat over time. The shape of the curve plotted in units of specific power (rate of energy transfer per unit mass) versus time describes the hydration kinetics of the mortar or paste. This test is suitable for testing paste samples over a relatively short period, and it is commonly used for mortar or paste samples. These three calorimeter types are compared in Figure 2.9 and Table 2.6.

<Adiabatic calorimeter>

<Semi- adiabatic calorimeter>

<Isothermal calorimeter>
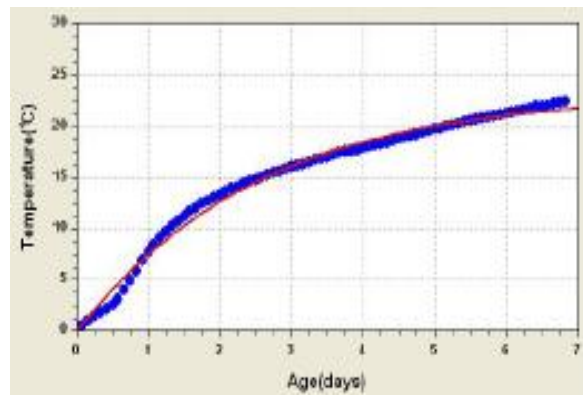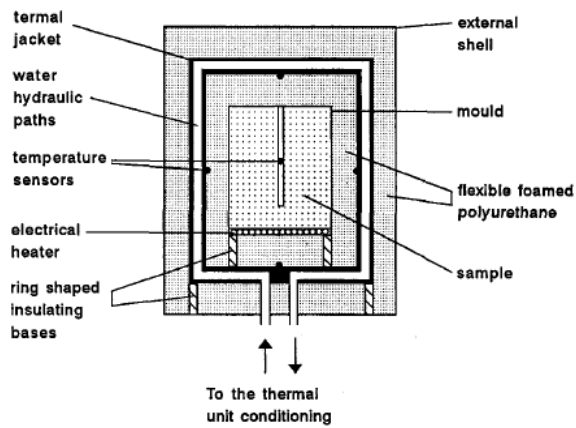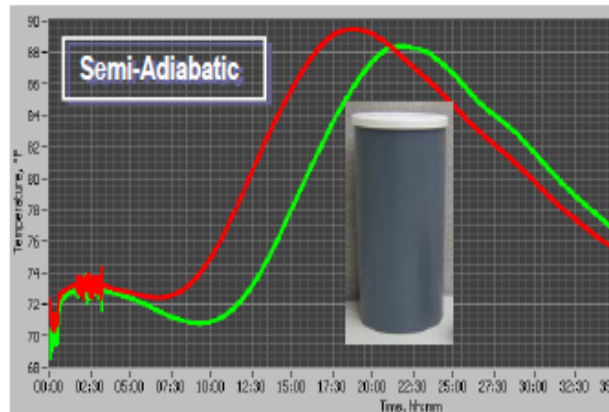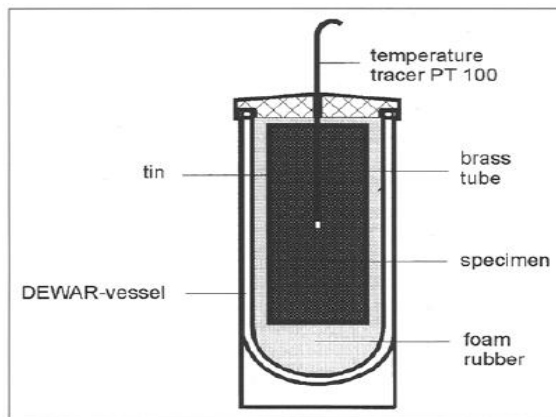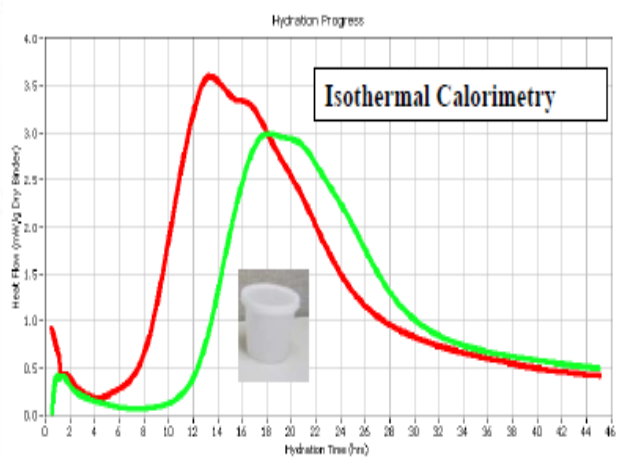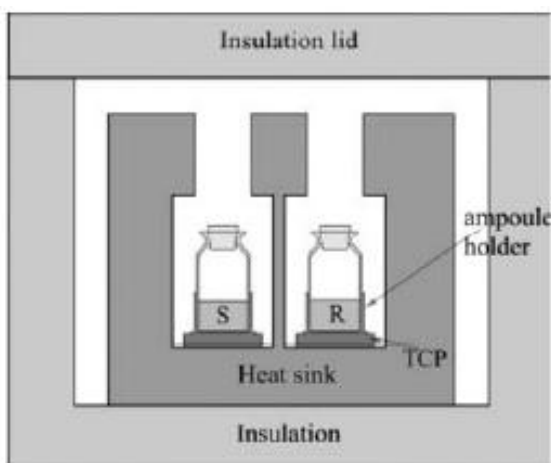
Figure 2.9. Comparison of equipment and result data for calorimeter types

Table 2.6. Comparison of calorimeter types (Radjy 2007)

	Adiabatic	Semi-adiabatic	Isothermal
Principle	Measure the adiabatic temperature increase and compute hydration heat.	Measure both rate of heat loss and sample temperature.	Measure rate of heat loss at constant sample temperature and integrate to compute heat
Sample type	Large concrete sample for mass placements such as dam. Suitable for low heat mixtures	Concrete or mortar	Cement or cement mortar
Sample size	Hundreds of pounds and 9" to 12" or more in diameter	Standar cylinder sizes; 2"x4", 4"x8", or 6"x12"	Few grams; 0.5 to 1 inch diameter
Field usability	Not field usable. Requires precision controlled temperature & its measurement to 0.001 dC or better	Can be used in a job-site trailer. Does not require a lab environment	Not field usable. Requires closely controlled temperature bath & lab environment
Advantage	Can be extremely high precision	Does not require a high level of skill to operate	Run test at different temperature to estimate hydration activation energy
Disadvantage	Very expensive	Can not measure very early hydration hdeat during the first 15 minutes after mixing	Can not run full size concrete or mortar sample tests

2.5 Mass Concrete

2.5.1 Definition

The significant characteristic of mass concrete distinguishing it from other general concrete structures is thermal behavior. Mass concrete structures produce significant temperature difference between the interior and the outside surface of the structures. This may result in cracks due to volume-change differentials and restraint conditions. The accurate understanding of mass can effectively control temperatures and ultimately save time, effort, and money. The definition of mass concrete is a little different in each country as described below:

Korea: the dimension of mass concrete depends on the type of structures, materials used, and construction conditions, but in the concrete standard specifications the thickness of a slab is larger than about 80cm~100cm and the wall thickness of a restrained foundation is larger than 50cm. Also, according to architecture standard specifications, the size of structures is larger than 100cm.

Japan: The thickness of a slab is about larger than approximately 80cm~100cm and the wall thickness of a restrained foundation is larger than 50cm in the civil society concrete standard specifications. According to the architect society construction standard specifications, the smallest cross member is larger than 80cm, and the internal and external temperature different due to heat of hydration is over 25℃.

USA: according to ACI 116R, mass concrete is defined as any volume of concrete with dimensions large enough to require that measures be taken to cope with generation of heat from hydration of the cement and attendant volume change to minimize cracking.

2.5.2 Restraint and Thermal Stress

If concrete element is free or move, tensile strain or stress caused by restraint would not develop. However, movements of concrete mass are restrained to some degree by the supporting elements or by different parts of the element itself. These restraints induce tensile and compressive stresses commonly due to temperature different. Tensile stresses in concrete can lead to cracking because concrete has the ability to withstand compressive stresses. There are internal restraint and external restraint. Both types are interrelated and usually exist to some degrees in all concrete elements (ACI 207.2R-07).

2.5.2.1 Internal Restraint

When concrete is placed, the internal temperature rapidly increases due to heat of hydration and the internal volume expands, but the deformation of concrete surface is small and surface volume contracts due to ambient temperature such as in shown Figure 2.10. The temperature different in young concrete between the core and the surfaces of concrete volume can induce thermal stress and thermal cracks when the tensile stress is greater than the tensile strength. The thermal cracks usually generate when the maximum temperature reaches within 1-5 days after concrete pouring (Korea Standard Specification for concrete, 2003).
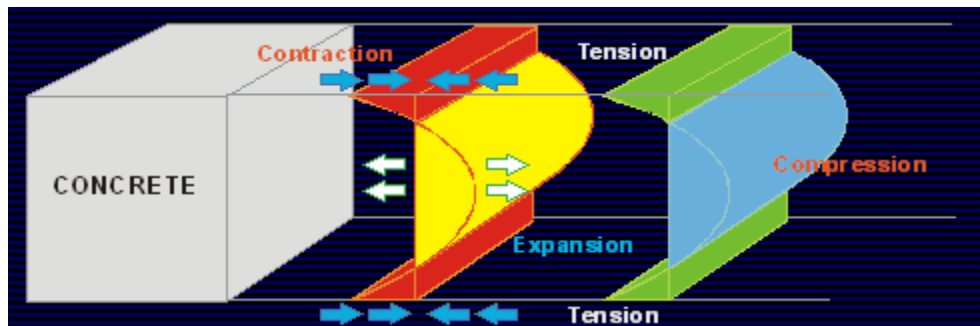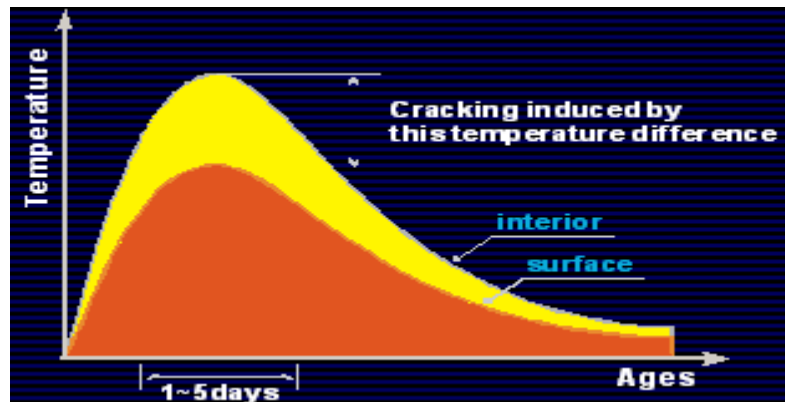
**Figure 2.10. The crack formation mechanism due to internal restraint
(Adapted from Cha. 2009)**

2.5.2.2 External Restraint

At some later time, an internal section of concrete enters a cooling phase controlled by the same ambient temperature after the peak temperature has been reached. This temperature decrease induces a contraction of concrete volume, but rigid structures such as a foundation or adjoining older concrete elements not experiencing temperature changes constrain moving. This mechanism known as an external restraint results in cracks in shown Figure 2.11. The external restraint develops compressive stress at early age and tensile stress later.

Cracking mainly depends on the amount or the extend of the degree of restraint. This degree of restraint varies between 0 and 100% depending on the physical boundary conditions and on the geometry of the structure (Muhammad, 2008). The degree of restraint depends primarily on the relative dimensions, strength, and modulus of elasticity of the concrete and restraining material (ACI 207.2R-07).
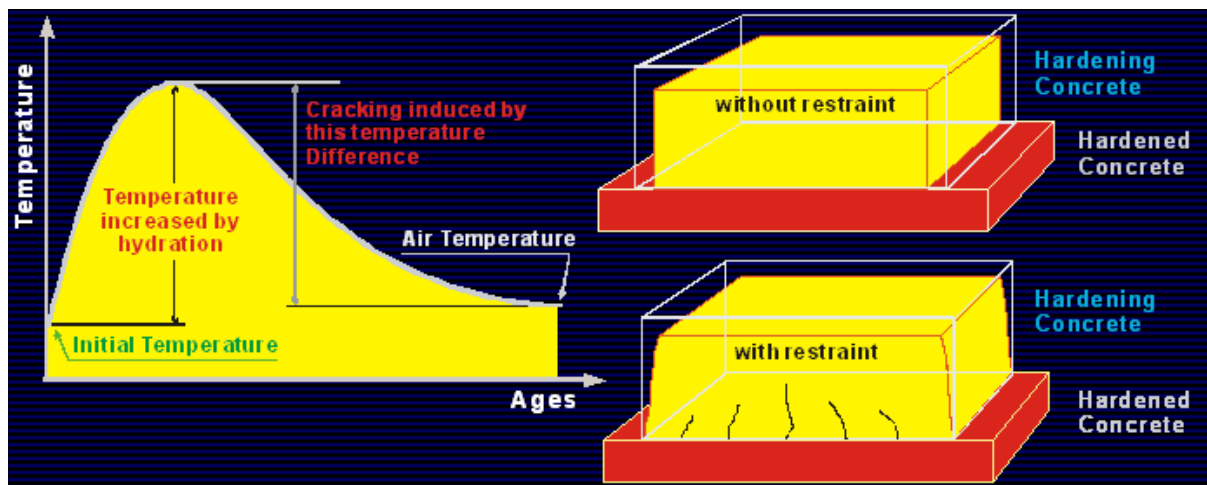
**Figure 2.11. The crack formation mechanism due to external restraint
(Adapted from Cha. 2009)**

2.5.2.3 Thermal Stress

A large amount of studies on thermal stress have been carried out to control and minimize early-age cracks in mass concrete. Many finite element methods have been also used to determine the thermal distribution and thermal stress in mass concrete. However, several finite element analyses were carried out using data obtained from a field for mass

concrete dam. The pertinent factors affecting thermal cracking and presented a step-by-step guide for computing the crack spacing, width and locations using manual and desktop computational methods were performed by Tatro and Schrader (1992). Noorzaei et al. (2005) analyzed the thermal and structural analysis of RCC dam using a two-dimensional finite element code. Jaafart et al. (2004) presented a finite element based analytical technique for evaluating the temperature within the RCC dam body using the two-dimensional FE method based on the Glerkin formulation. Ishikawa (1991) carried out a thermal analysis for a gravity-type concrete dam using the finite element program ADIAN software.

2.5.3 Temperature Control

There are generally specified temperature limits in mass concrete to prevent thermal cracking and durability problems. Temperature limits are commonly specified to maximum allowable concrete temper of 135° F (57 °C) and to maximum allowable concrete temperature difference between the center and surface of the mass concrete section of and 35° F (19°C) (John, 2002). In many cases, however, the specified limits are arbitrarily determined by each project. There are many methods, ranging from simple to complex and from cheap to costly, for controlling the temperature rise.

The control of cement amount is the largest direct influence for thermal stress. When cement completely reacts to water, the heat generated by exothermic chemical reaction is about 120cal/g (500 J/g). The heat of hydration induces the internal temperature of concrete rise because the heat conductivity of concrete is relatively small, and it acts somewhat like an insulator. Generally, amount of cement 10 kg/m^3 can elevate temperature in the middle area

of concrete approximately 0.7℃ ~ 1.1℃, and can control the temperature difference between internal and external to 0.3℃~0.4℃ (Korea Standard Specification, 2003).

The use of low-heat cement or a supplementary such as fly ash is one way to minimize the temperature rise because pozzolanic reaction between portland cement and fly ash does not produce significant heat of hydration. Different types of cement generate different amounts of heat evolution. Among all choices, Type IV cement or fly ash has been primarily used for temperature control. Figures 2.12-2.13 indicate the typical heats of hydration for different cements and also the effect of fly ash. In mass concrete such as that in a dam, Type IV cement is commonly used in Korea, but it is rarely available in the US. Conversely, fly ash is rarely used in Korea while widely available in the US.
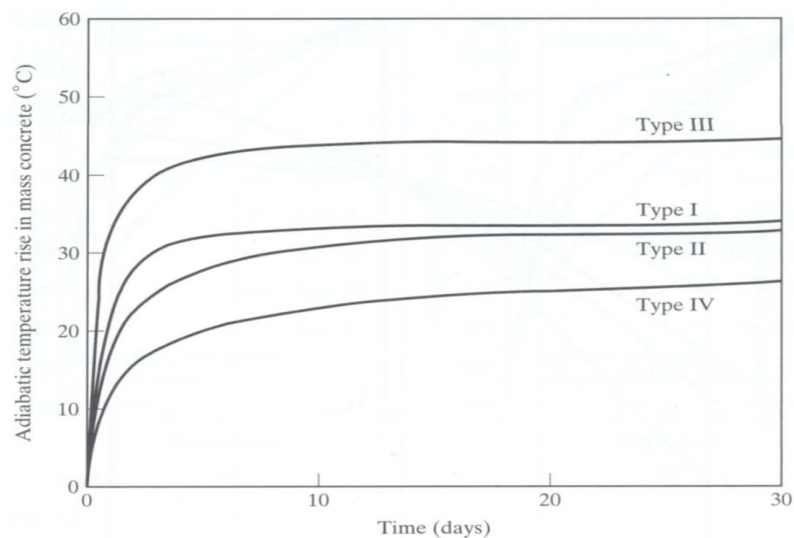
Figure 2.12. Temperature rise of mass concrete for typical cements
(Adapted from Mindness et al. 2003)
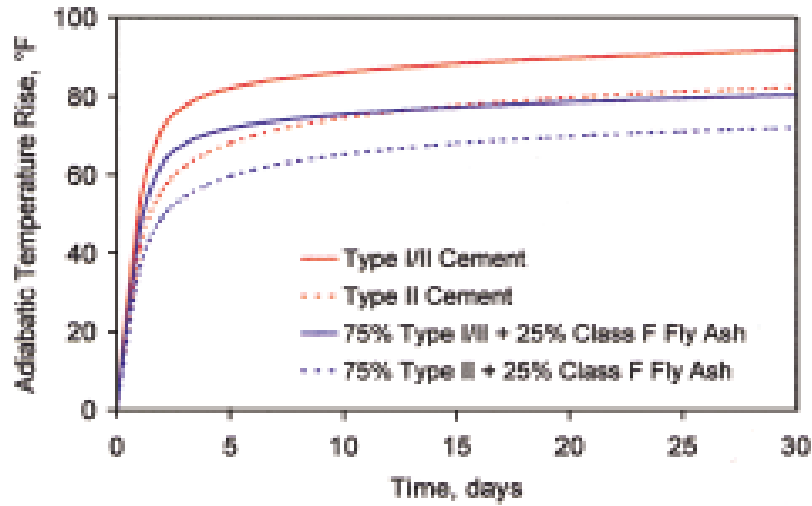
**Figure 2.13. Temperature rise for cementitious materials
(Adapted from John 2002)**

Reducing the temperature of concrete placement, known as pre-cooling, can also control concrete temperature rise. Typically, for every 0.6° C reduction or increase in the initial concrete temperature, the maximum concrete temperature is changed by approximately 0.6° C (Jonh 2002). As shown by Equation 2.16, use of chilled mix water and cooling aggregates can decrease the temperature. Among the various choices, cooling aggregates have the most effects on the concrete temperature because they comprise of 70-85% of the weight of concrete. Liquid nitrogen can also be used for pre-cooling concrete.

$$T = \frac{C_s\,(T_a W_a + T_c W_c) + T_w W_w}{C_s(W_a W_c) + W_w} \qquad\qquad 2.16$$

Where,

T : concrete temperature

F, W : the mass of ingredient per unit volume of concrete

a, c, w : the suffixes for aggregate, cement, and water respectively

In post-cooling, cooling pipes are used to quickly reduce interior concrete temperatures. However, this method is expensive and sometimes it is difficult to properly select the cooling pipe size, spacing, amount of cooling water, and cooling temperature.

2.5.4 Crack Index

At early ages, the temperature-based assessment of cracks in mass concrete due to heat of hydration has been used. However, the assessment provisions for the thermal cracking vary considerably. In the U.S., the ACI guides do not have any specific provisions for cracking induced by the heat of hydration except imposing for some limits for temperature drop in cold weather concreting (Jeon, 2008). In the Korea standard specifications for concrete, crack index is adopted. The crack index is defined by Equation 2.17. The crack index can be obtained from a thermal stress analysis.

$$\text{Icr (t)} = \frac{f_{sp}(t)}{f_t(t)} \qquad\qquad 2.17$$

Where,

$f_{sp}(t)$: the tensile strength of concrete at day (t)

$f_t(t)$: the maximum thermal stress at day (t)

The cracking tendency can be assessed by using the crack index on based on previous experience. The crack probability relationship is related to crack index in shown Figure 2.14

and crack criteria are listed in Table 2.7. This table explains that the crack index exceeds 1.2 at least to limit cracks. This index should be determined by depending on the structure important, economy, construction environment, etc.
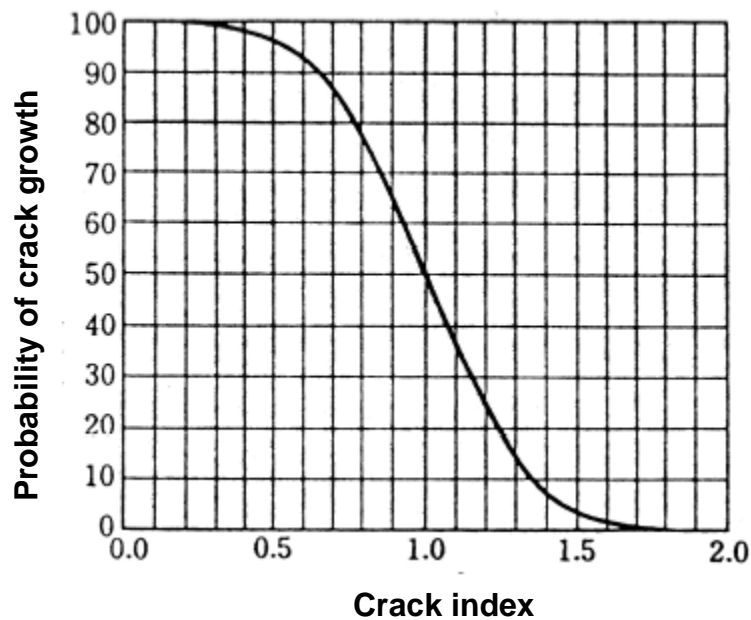
Figure 2.14. The relationship probability of crack growth and crack index
(Adapted from Korea standard specification for concrete 2003)

Table 2.7. Thermal crack criteria (Korea standard specification for concrete 2003)

Criteria	Thermal crack index (I_{cr})
To prevent cracks	$I_{cr} \geq 1.5$
To limit cracks	$1.2 \leq I_{cr} < 1.5$
To limit harmful cracks	$0.7 \leq I_{cr} < 1.2$

2.5.5 Fly Ash Use in Concrete Dam

Development of fly ash as a constituent of Portland cement concrete was initiated in the US during the early 1930s. According to work at the University of California in 1937, fly ashes can be used with technical benefit and economy to replace 20 to 50% of the amount of Portland cement that otherwise would be required to produce concrete of specific strength and durability (Kim et.al, 1990). Fly ash modified the properties of concrete in both fresh and hardened state including workability, strength and shrinkage. Furthermore, using fly ash in concrete reduces bleeding, heat of hydration, permeability and porosity of concrete. It increases abrasion resistance of concrete, and reduces alkali.

Replacing 35–50% of cement with fly ash, there was 5–7% reduction in the water requirement for obtaining the designated slump, and the rate and volume of the bleeding water was either higher or about the same compared with the control mixture (Ravina and Mehta, 1986). Malhotra and colleagues reported that concrete containing high volume of Class F fly ash exhibited excellent mechanical properties, good durability with regard to repeated freezing and thawing, very low permeability to chloride ions and showed no adverse expansion when reactive aggregates were incorporated into concrete

The current annual production of fly ash world-wide is estimated around 500 million tones, the world average only amounts to 16% of the total ash is used. Fly ash in the cement industry is used by three applications; (1) replacement of cement in Portland cement concrete (2) pozzolanic material in the production of pozzolanic cements, and (3) set retardant ingredient with cement as a replacement of gypsum (Ahmaruzzaman, 2010).

Since Hungry Horse Concrete Dam used fly ash was first constructed in Montana by U.S. Bureau of Reclamation, The application and performance of concrete containing fly ash has been increased in mass concrete. Recently, Roller compacted concrete (ROCC) application showed that usage of fly ash in ROCC production was a wide spread practice, such as, dams, and large floor construction (Ahmaruzzaman, 2010).

In China, the research of fly ash started in the 1950s and it was reported that fly ash used in Sanmen Gorges Project dam successfully prevented a high release of hydration heat. The compressive strengths of dam concrete with 50% of fly ash in 90 days are higher than those with 30% of fly ash or without fly ash. Fly ash may decrease the deformation of dam concrete with 50% of fly ash, and the shrinkage and expansive strain was reduced significantly-about 33% and 40% less than the specimens without fly ash, respectively (Gao Pei-wei et al, 2007).

Most of all fly ash in Korea have less than 10 percent CaO, therefore it is similar ASTM Class F fly ash in the USA. Studying and application for fly ash in mass concrete dam have rarely progressed because of a limited specification, quality variation due to indiscriminate fly ash replacement. However, recently studies and application using fly ash have been increasing to reduce the CO_2 emotion and reuse resources. K-water is also planning for use fly ash in RCC dam.

2.5.6 Dam Construction

The characteristics of concrete dam are the use of low heat cement to reduce temperature rise, the maximum size of aggregate to save in the amount of cement, proper size of construction block, and different thermal distribution on the sections. Generally, concrete

in concrete dam construction is placed with blocks and is joined by a vertically zigzag bonded contact to prevent the thermal cracking generated by cement hydration in concrete shown in Figure 2.15. It is important to choose a proper size of concrete block to prevent thermally-induced cracks and the minimum time between the placements of the next layer to allow for completion of thermal effects. The length of concrete block is related to the tensile stresses and its length is generally 15m according to U.S. Department of the interior and dam design criterion of Korea water resources association. Lift thickness of the concrete block is usually 1.5m according to dam design criterion of Korea water resources association.

The joints used in concrete dams are classified into contraction, expansion, and construction joints. Contraction and expansion joints are used to accommodate volumetric changes generated in the structures after concrete placement. Construction joint occurs at the surface between previously placed concrete and newly placed concrete according to construction plans and construction conditions. To prevent water leakage through a construction joint in concrete dam, PVC or metal waterstop can be installed at the surface of dam upstream.

To obtain the bond of concrete blocks between the old and new concretes, all laitance and inferior surface concrete are removed from the old surface using air and water jets, or wet sandblasting.

Construction specifications of concrete dam are different within each country and even within each company. The compressive strengths of a concrete dam operated by K-Water (Korea Water Resources Corporation in Korea) are in listed Table 2.8.

Table 2.8. The construction specification of concrete dam (K-water 1997)

Dam Structures	Compressive strength (91 days, MPa)	Maximum size of aggregate(mm)	Slump (mm)
Interior structures	11.8	150	30±10
Spillway	17.6	150	30±10
Surrounding structures	17.6	40	60±10
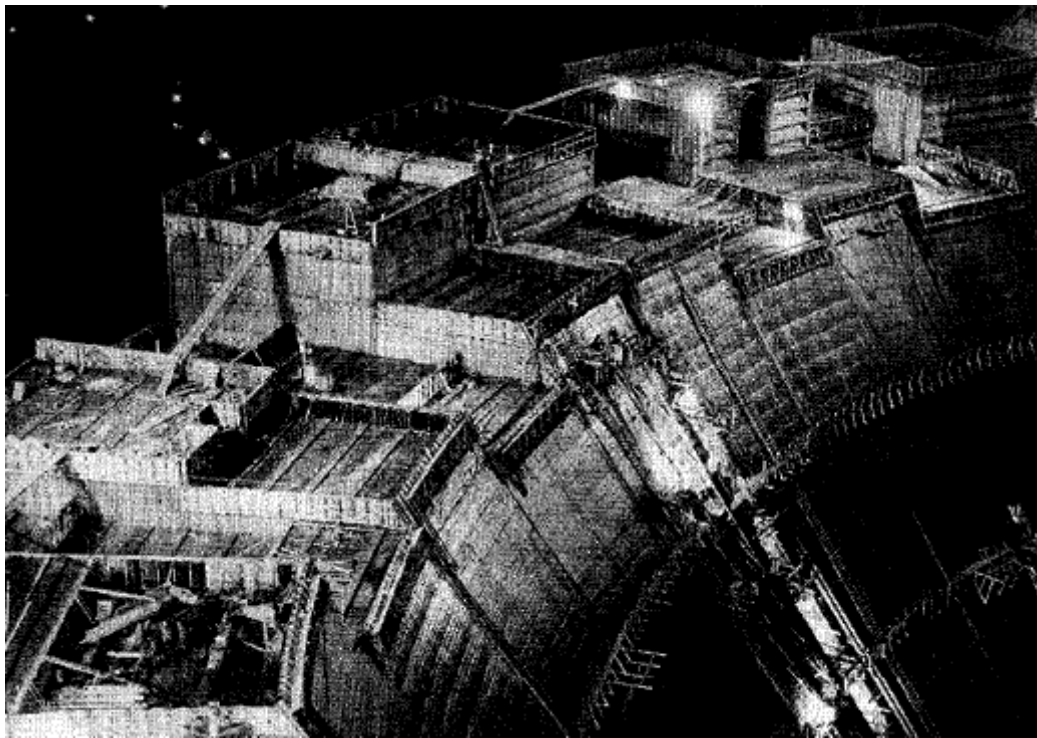
**Figure 2.15. The concrete block placement of Hoover dam
(Adapted from Dunar and McBride, 1993)**

CHAPTER 3. EXPERIMENTAL PROGRAM

The purpose of the experiment is to determine the amount of heat and rate of heat generation for several cement types and one type of fly ash. Blaine test and X-ray fluorescence (XRF) were performed to determine the fineness chemical composition of cements. An isothermal calorimeter test was also carried out to investigating the rate and heat evolution of cement. In this experiment, Type I cement from Korea and US, and Type IV cement and fly ash from Korea were used.

Experimental results include heat effects for each cement type, the effect of fly ash replacement for Type I cement, the suitable fly ash replacement levels equal to the rate of heat generation of Type IV cement, and cost comparison relating to the use of fly ash use.

3.1 Material and Mix Proportions

The cement materials used were a fly ash and three types of portland cement: Type I cement from the Holcim plant at Mason City, Iowa, US, another Type I, Type IV, and fly ash from SSanyon, Youngwol, Gangwon-do, Korea. The fine aggregate was natural river sand from Ames, Iowa, and it has a specific gravity of 2.6 and absorption of 0.7%. The water reducing admixtures (FLOWM1X 900SA) from Dong Nam Industry in Korea was used.

The mortar mixture was the same as that used in the Seongdeok dam in Korea. The water-to-cement (w/c) ratio was 0.66 and the fine aggregate-to-cement material ratio (s/c) was 4.33. Fly ash replacement levels (10%, 20%, 30%, 40%) for Type I cement from Korea were used for three curing temperatures (10°C, 20°C, 30°C)

3.2 Test and Procedures

3.2.1 Blaine and XRF Test

The Blaine test was performed to measure the fineness of all cement. The measurements were done according to ASTM C 204, *Standard Test Method for Fineness of Hydraulic Cement by Air-Permeability Apparatus*. This method is based on the relationship between the surface area of the cement particles in a porous bed and the rate of fluid through the bed. This apparatus is consisted of permeability cell, disk, plunger, U-tube manometer, and manometer liquid including a scale as shown Fig 3.1
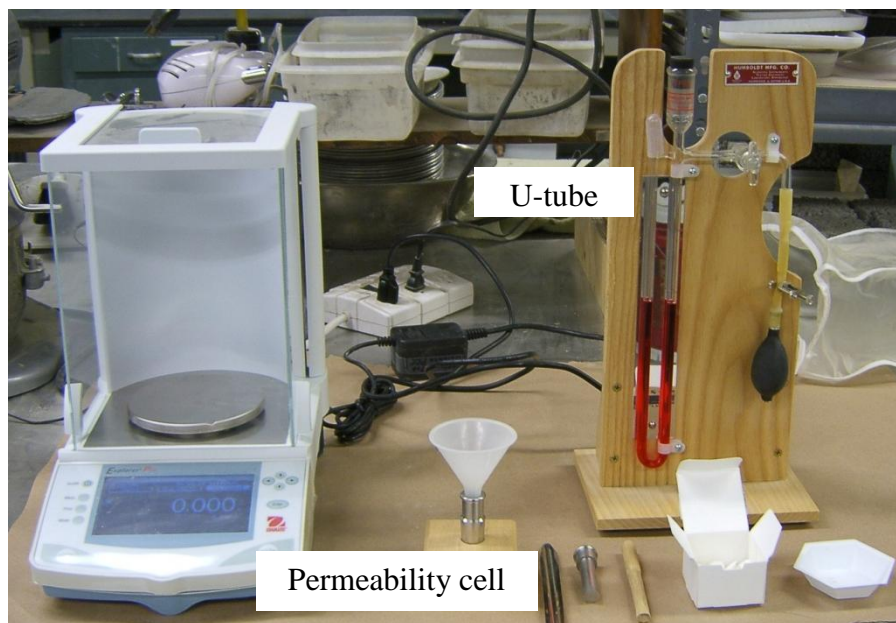
Figure 3.1. Blaine air-permeability apparatus

Mass of sample was calculated using Equation 3.1 and was weighted using scale. The sample is then placed into permeability cell. The permeability cell is inserted to the top of the manometer tube. Air is slowly evacuated in the one arm of the manometer U-tube until the

liquid reaches the top mark, after which the valve is closed tightly to prevent the liquid from falling. With a timer ready, the valve is opened and the time the liquid reaches calibrated marks (middle and bottom) on the manometer are recorded. Specific surface values were calculated using Equation. 3.2.

$$W = \rho V (1 - \epsilon) \hspace{3cm} 3.1$$

Where, W: grams of sample required

ρ: density of test sample

V: bulk volume of bed of cement (cm^3)

ϵ : desired porosity of bed of cement (0.5)

$$S = \frac{S_s \sqrt{T}}{\sqrt{T_s}} \hspace{3cm} 3.2$$

Where, S: specific surface of the test sample (m^2/kg)

S_s : specific surface of the standard sample used in calibration of apparatus, (m^2/kg)

T : measured time interval, s, of manometer drop for test sample

T_S: measured time interval

The X-ray Fluorescence (XRF) tests were conducted to obtain chemistry of three cements and one fly ash in the Material Analysis Research Laboratory in Iowa State University. The principle of XRF is as following (Sibilia, 1996):

3.2.2 Isothermal Calorimeter Test

Mortar samples were prepared for isothermal calorimeter tests. The samples were mixed according to ASTM C 305, *Standard Practice for Mechanical Mixing of Hydraulic Cement Pastes and Mortars of Plastic Consistency*.

An isothermal calorimeter manufactured by Thermometric was used for measuring for the rate of heat generation. This instrument can simultaneously measure the heat of eight samples during a test using eight separate channels as shown in Figure 3.2.
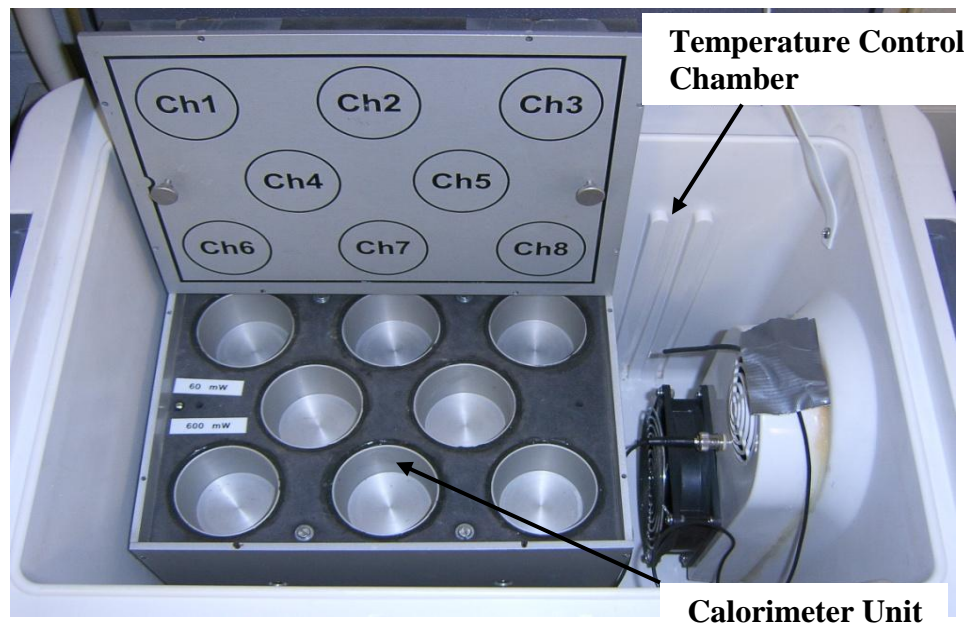
Figure 3.2. Calorimeter unit

The isothermal calorimeter consists of a heat sink with has two heat flow detectors and a sample holder attached to each sensor. The sample holder is placed in a container in contact with common heat sink and a reference 129-gram aluminum block is placed in contact with the same heat sink as shown in Figure 3.3. When a sample is placed in the unit, heat created by any physical and chemical reaction in the sample will flow rapidly to its

surroundings. The output from the calorimeter is the difference between the outputs from the sample heat flow sensor and the inert heat flow sensor. This difference creates a voltage signal proportional to the heat flow. This voltage is converted to the rate of heat evolution by applying a calibration factor.
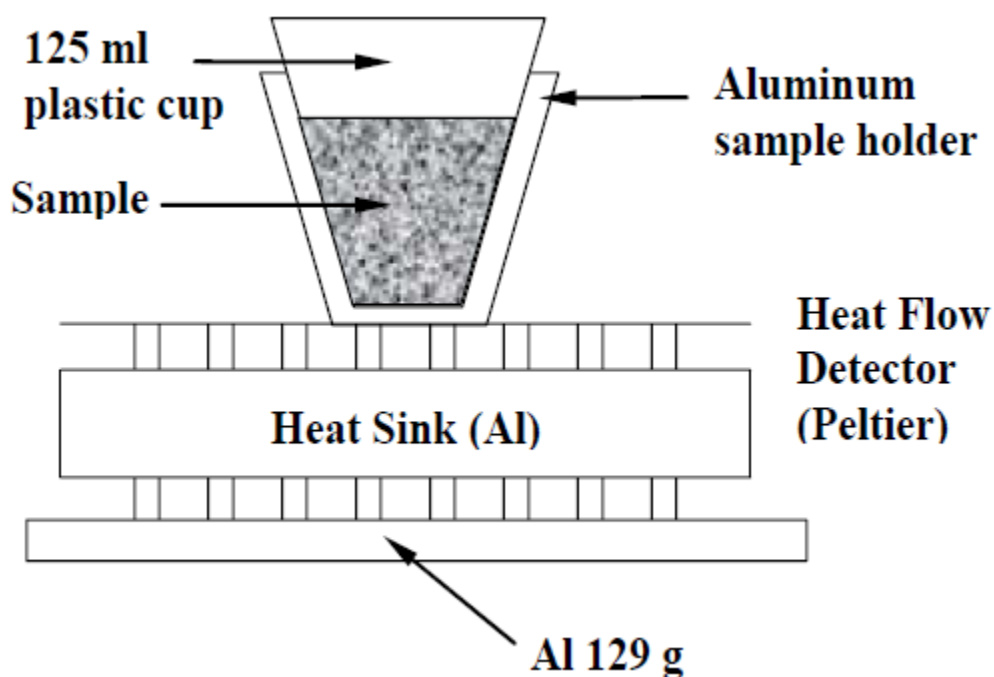
Figure 3.3. Configuration of the calorimeter module
(Adapted from Zhi Ge. 2009)

Before used in formal tests, the calorimeter equipment was calibrated for each of eight calorimetric channels because the voltage values might vary depending on the influence of environment over time. The calibration procedure may be described as follows. First, the environmental chamber set to the desired temperature and the calibration units are positioned in the calorimeter. Reading of the calorimeter occurred at 30-second intervals. After the

reading (baseline) was stable, the voltage generator was turned on and kept constant until a steady-state reading (Unsteady) was achieved. The voltage generator was then turned down. When the reading was stable again, the test was terminated. The calibration factor was calculated using Equation 3.3 with the calibration process shown in Figure 3.4.
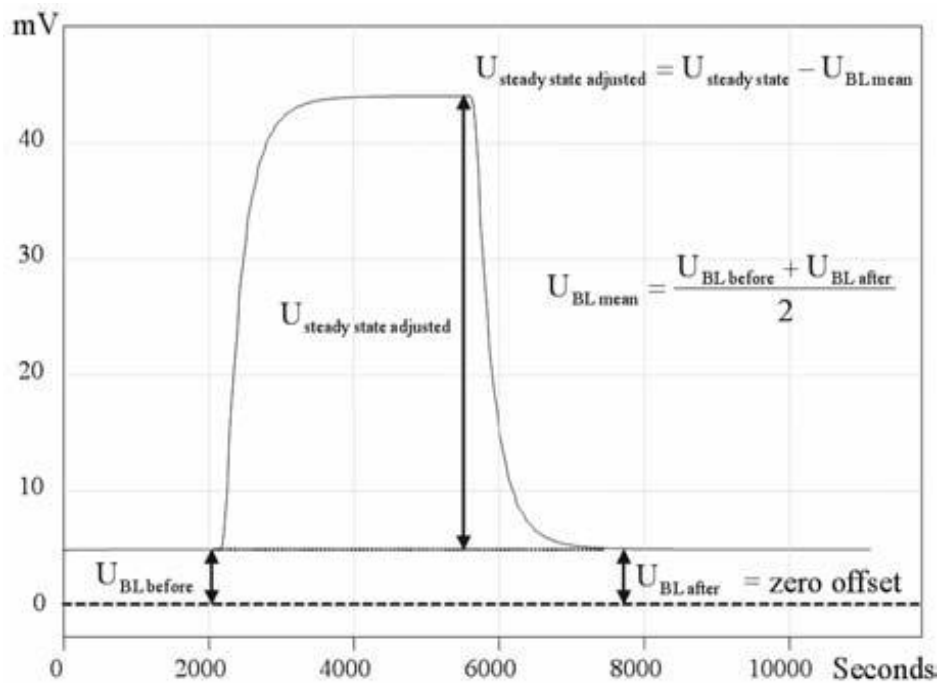
Figure 3.4. Calibration process
(Adapted from Isothermal calorimeter manual)

$$CF = \frac{P}{U_{steady\ adjusted}}$$
<div align="right">3.3</div>

Where, CF : calibration Factor

P : calculated rate of heat production

After calorimeter calibration tests, about 100 grams of just-mixed mortar samples were placed into each sample holder of the calorimeter with a preset temperature, because cement hydration starts immediately after mixing. The measurement for rate of heat generation in the calorimeter was performed every 30 seconds and continued for 48 hours. The rate of heat generation per gram of cement (mW/g) was calculated using Equation 3.4. The rate of heat hydration was also monitored by a personal computer. For each mix, four samples were tested to minimize variability in the test results and average values of these four samples were used.

$$Q = \frac{(R-B) \times CF}{ws/(1+\frac{S}{C}+\frac{W}{C})} \qquad \qquad 3.4$$

Where, R : the data reading (mV)

B : the calibrated base line (mV)

ws : the weight of sample (g)

S : the weight of f sand (g)

C : the weight of cement (g)

W : the weight of water (g)

In this study, the total heat values generated by each cement at different curing temperatures (10°C, 20°C, 30°C) are presented. The isothermal test was performed for 48 hours because the sample showed no appreciable variations in the heat evolution of cement.

3.3 Test Results

3.3.1 Chemical Composition and Fineness of Cement

Chemical and physical properties of the materials used in this experiment are summarized in Table 3.1. Cement phases were determined from XRF analyses. The four main cement chemical compositions described in Figure 2.2.1 were calculated based on the Bogue reference.

For fineness, The US Type I cement has the highest specific surface area (405 m^2/kg) and the Korea Type IV cement has the lowest specific surface area (347 m^2/kg). US Type I cement contains 50% C_3S, 23% C_2S, and 10% C_3A, Korea Type I cement contains 52% C_3S, 22% C_2S, and 7% C_3A, and Korea Type IV cement contains 38% C_3S, 43% C_2S, and 1% C_3A.

US Type I cement has the highest content for C_3S, C_3A, and fineness which impact fast early age hydration of cement. Korea Type IV cement has the lowest content for C_3S, C_3A and fineness, while has the highest C_2S that causes slow early age hydration of cement.

For fly ash, CaO content is 1.8% and the SO_3 content is 0.09 %. This is less than the maximum content defined by ASTM C 618. Fly ash used in this study is similar to the kind of Class F fly ash used in the US because the content of CaO is less than 10% and the sum of $SiO_2+Al_2O_3+Fe_2O_3$ is greater than 70%. To reduce the heat of hydration, this material can be used as a partial replacement for portland cement because of a pozzolanic reaction.

Table 3.1. Chemical composition and fineness of cement

Chemical Composition (%)	Type I (US)	Type I (Korea)	Type IV (Korea)	Fly Ash (Korea)
CaO	63.5	63.03	63.03	1.85
SiO_2	21.1	21.41	25.13	67.16
Al_2O_3	5.4	4.59	2.51	18.99
Fe_2O_3	2.2	3.24	3.48	3.75
MgO	3.1	1.88	1.66	0.89
K_2O	0.43	1.04	0.64	1.06
Na_2O	0.25	0.05	0.04	
SO_3	3.2	2.2	2.05	0.09
BaO	-	-	-	0.09
C_3S	50	52	38	-
C_2S	23	22	43	-
C_3A	10	7	1	-
C_4AF	7	10	11	-
Loss on Ignition	2.5	1.89	1.25	3.24
Fineness (m^2/kg)	405	367	347	362

3.3.2 Isothermal Calorimeter Test and Compressive Strength Test

Among the five stages of cement hydration process noted in section 2.3.1, the first stage (initial hydrolysis) is commonly not captured by this calorimeter test because of its short reaction time. Results based on the heat rate curves, effect of cement types, effect of fly ash replacement, curing temperature, and effect of Type I + fly ash replacement for Type IV are presented following sections.

3.3.2.1 Effect of Cement Type on Hydration

As given in Table 2.5, the rate of cement compound hydration is in the order $C_3A > C_3S > C_2S$. Figures 3.5-3.7 present the rate of heat generation for mortar made with the three different types of cement at environmental temperature of 10°C, 20°C, and 30°C. Among all the samples, the mortar made with Type IV cement shows the lowest the rate of heat of hydration because of its low C_3S and C_3A content.

Since finer cement has a larger specific surface area to contact and react with water, and C_3A and C_3S hydrate fast, US Type I cement displays a higher rate of heat evolution during hydration. This illustrates that fineness of cement has an effect on heat evolution.
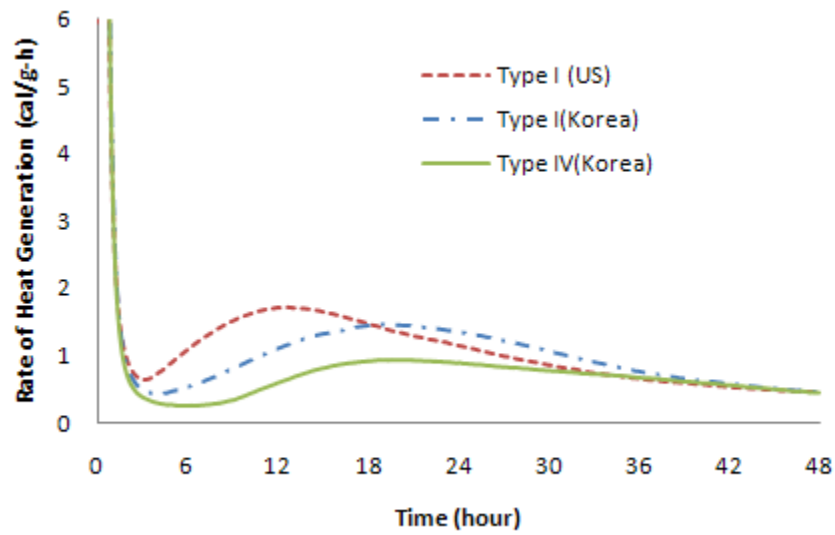
Figure 3.5. Effect of cement types on heat of hydration at 10°C
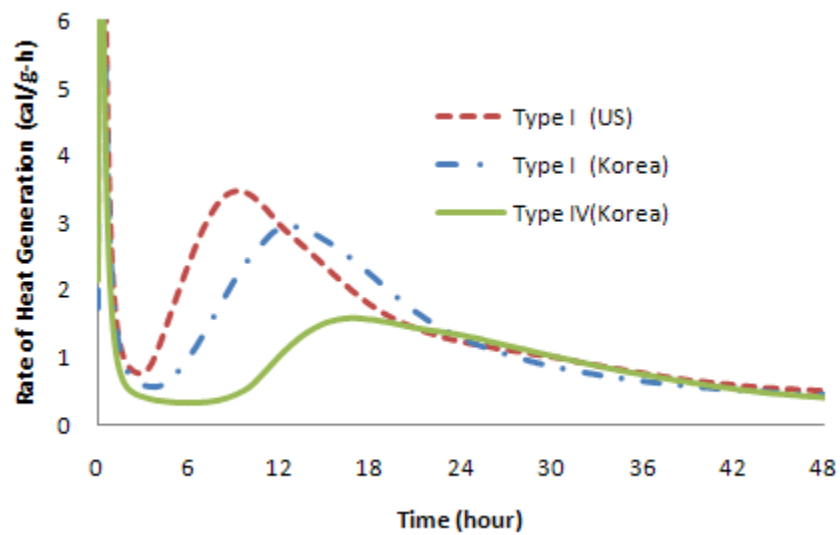
Figure 3.6. Effect of cement types on heat of hydration at 20°C
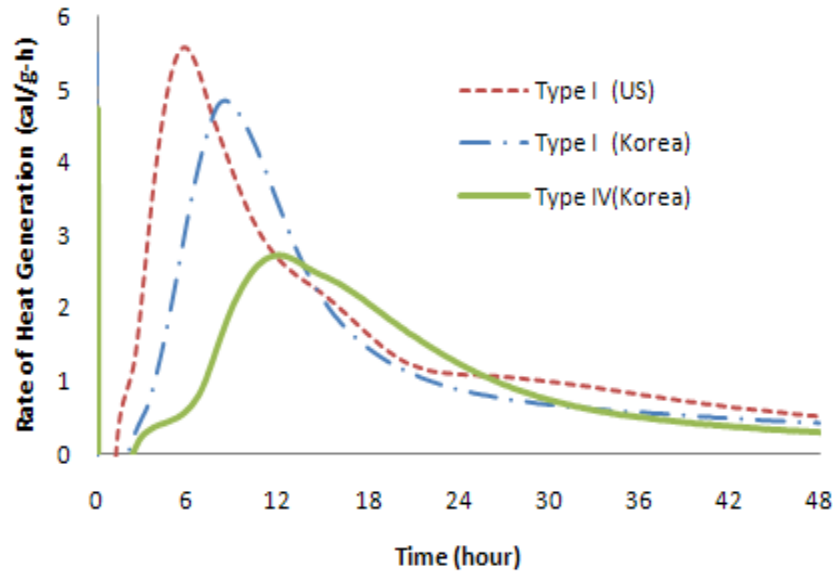
Figure 3.7. Effect of cement types on heat of hydration at 30°C

3.3.2.2 Effect of Curing Temperature on Hydration

Curing temperature has a significant effect on the hydration process. Figures 3.8-3.10 present typical effects of curing temperature on the cement hydration process for three different types of cement at 10°C, 20°C and 30°C. When the curing temperature is higher, mortar has a greater peak heat evolution and a smaller time to peak. The main peak might be primarily attributed to C_3S hydration. Cement hydration reactions progress faster at early ages with an increase of curing temperature. However, at the end of the measurement period, the rate of hydration is almost the same without this increased temperature. This result illustrates that temperature plays an important role of mass concrete.
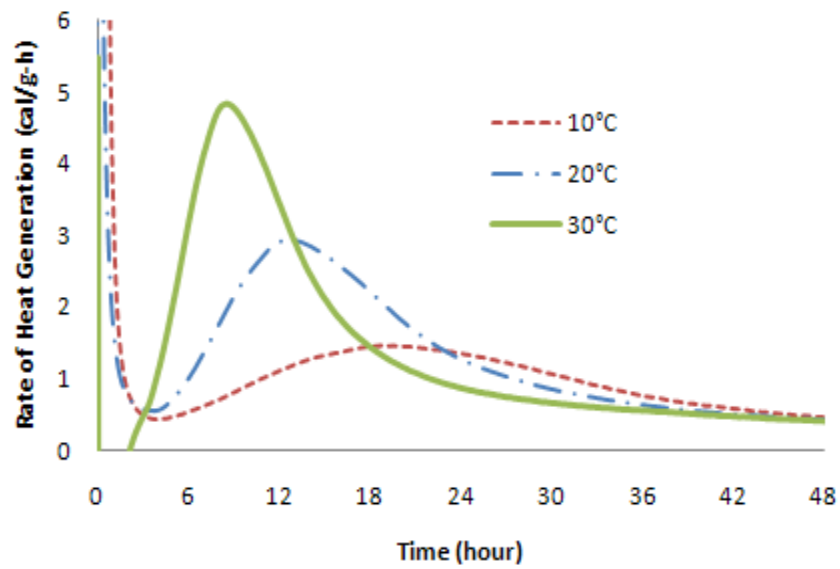
Figure 3.8. Effect of curing temperature on heat of hydration for Type I (US)
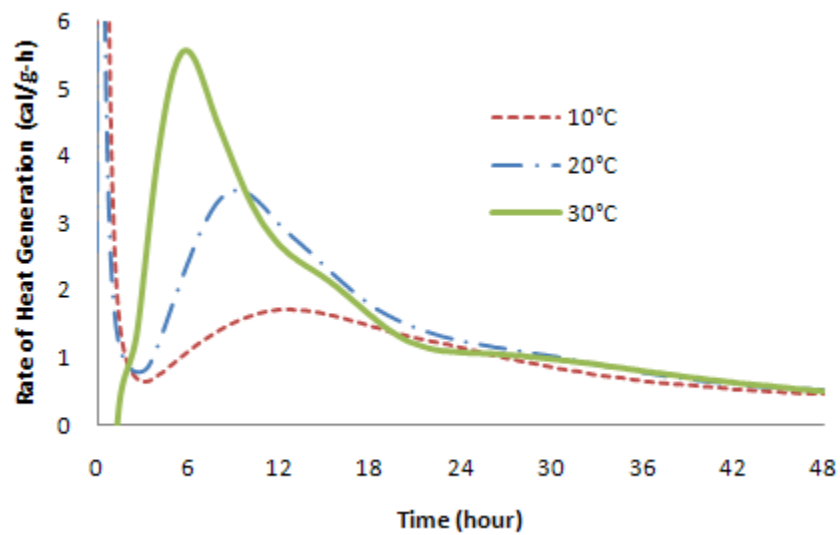
Figure 3.9. Effect of curing temperature on heat of hydration for Type I (Korea)
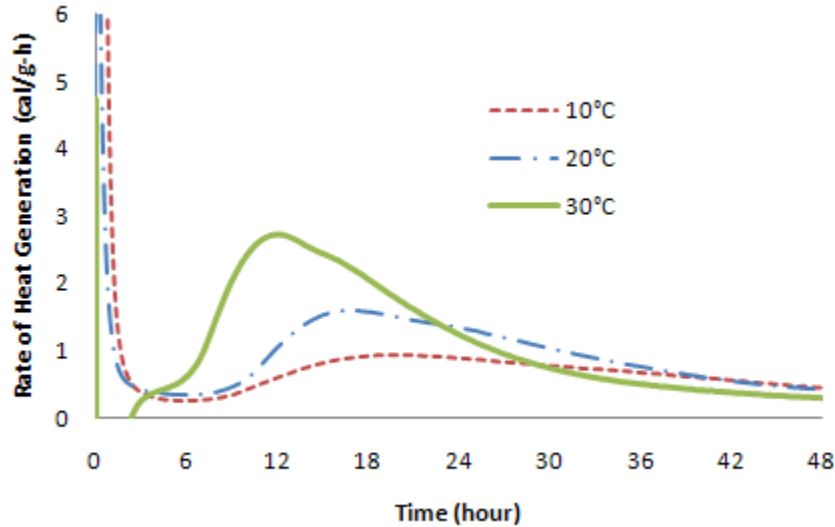
Figure 3.10. Effect of curing temperature on heat of hydration for Type IV(Korea)

3.3.2.3 Effect of Fly Ash Replacement on Hydration

Figures 3.11-3.13 show the effect on the rate of heat generation of fly ash replacement in amounts of 10%, 20%, 30%, and 40%, for Type I cement from Korea. When fly ash replacements for cement increase in each curing temperature, the peak of heat hydration is lowered and the time of occurrence is retarded due to pozzolanic reaction. That is, the fly ash delays the onset of the acceleration stage and produced a prolonged induction period. This illustrates that use of fly ash can take advantage of retarding the heat reaction and reducing the heat evolution. A blended cement of fly ash and Type I cement may be also used as a replacement material for Type IV cement.
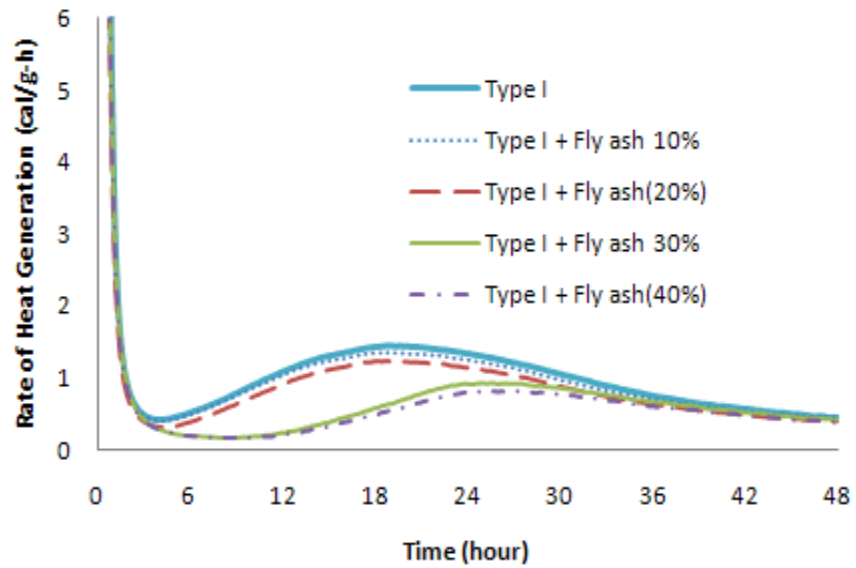
Figure 3.11. Effect of fly ash replacement level on heat of hydration at 10°C
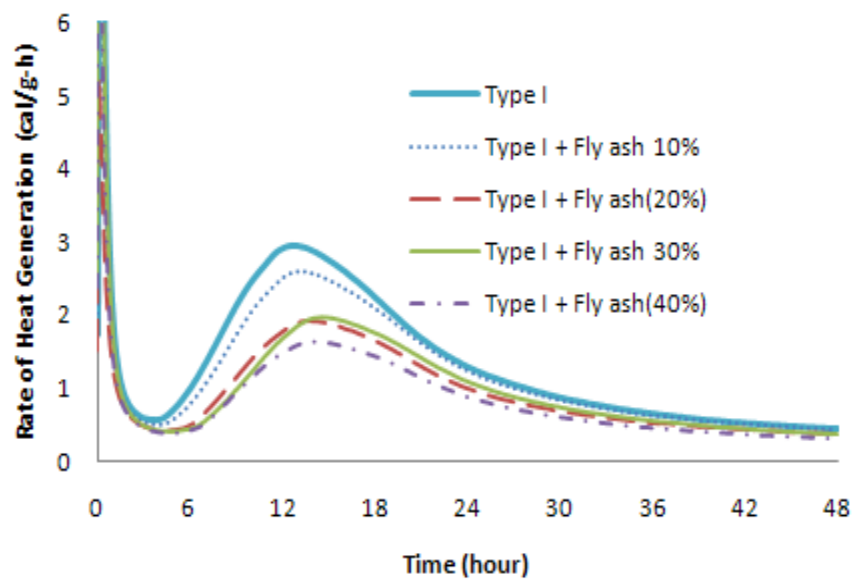
Figure 3.12. Effect of fly ash replacement level on heat of hydration at 20°C
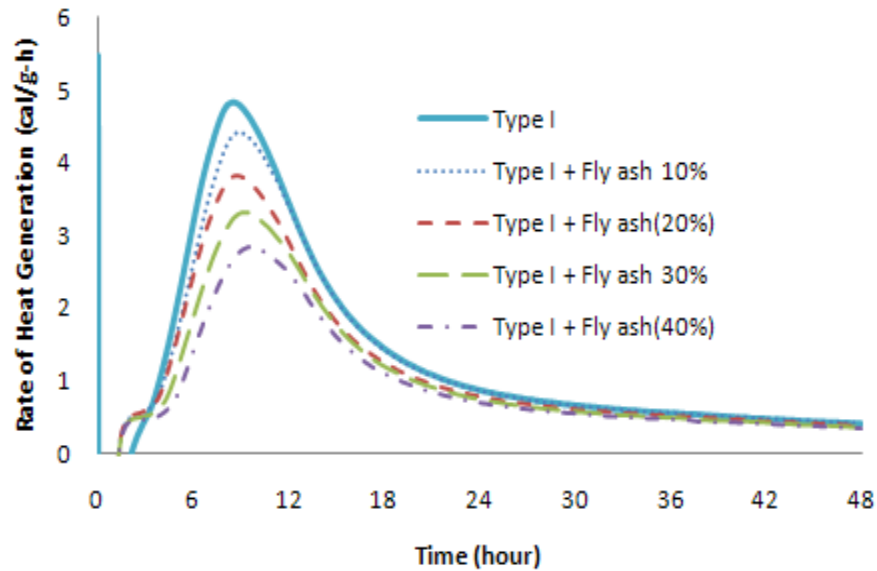
Figure 3.13. Effect of fly ash replacement level on heat of hydration at 30°C

3.3.2.4 Comparison Type I+Fly Ash Replacement and Type IV on Hydration

Figures 3.14-3.16 show the correlation with heat evolution of fly ash replacement for Type I and Type IV materials. At a curing temperate of 10°C, shown in Figure 3.14, the rate of heat generation of fly ash replacement and Type IV do not have show similar behavior. However, Figures 3.15-3.16 show that fly ash replacement of 40% has a similar heat generation with Type IV cement at a curing temperate at 20°C and 30°C. These results indicate that a replacement level of 40% for Type I cement may possibly be used as a binder material in a mass concrete dam.
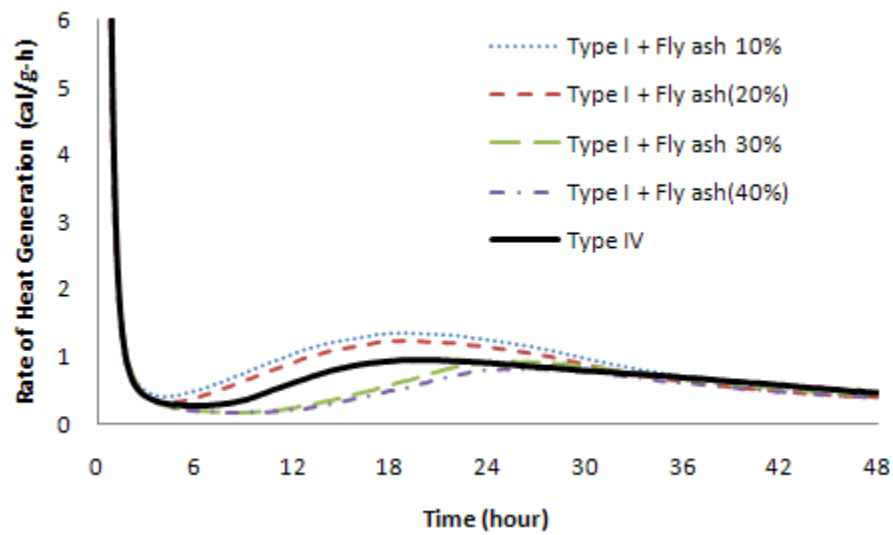
Figure 3.14. The rate of heat generation for Type IV and fly ash replacement at 10°C
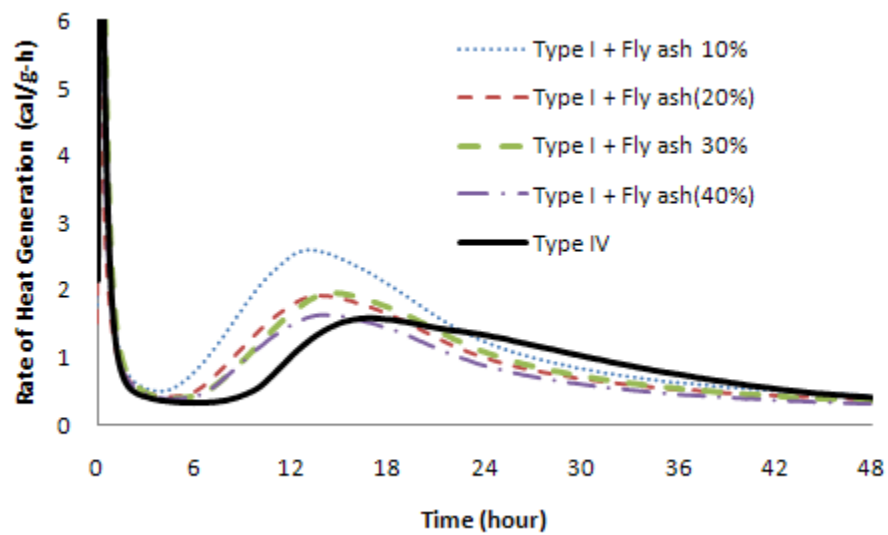
Figure 3.15. The rate of heat generation for Type IV and fly ash replacement at 20°C
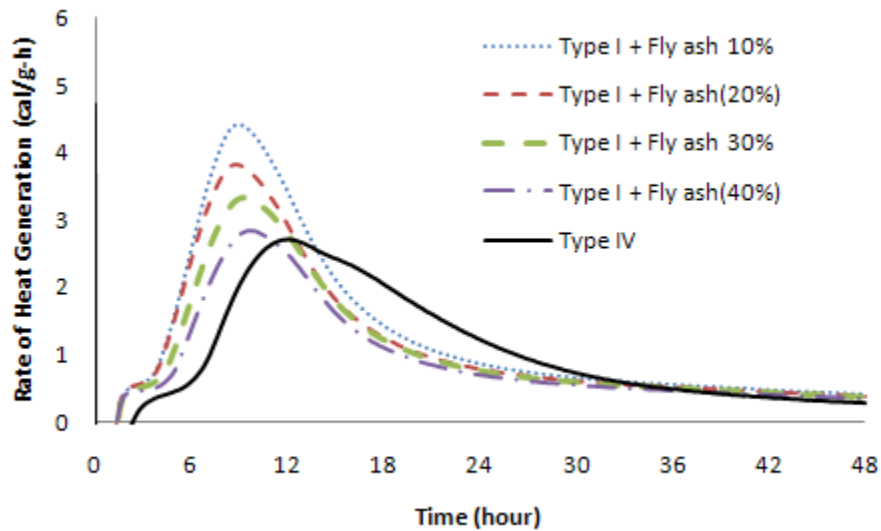
Figure 3.16. The rate of heat generation for Type IV and fly ash replacement at 30°C

3.3.2.5 Compressive Strength Test

Besides the effect of the heat generation of 40% fly ash replacement for Type I cement according the results in chapter 3.3.2.4, compressive strength tests were also performed for mortar made with three different cement types and 40% fly ash replacement for Korea Type I cement. Water-to-cementitious ratio was also 0.66 with the same as that used in the Seongdeok dam in Korea. Figure 3.17 shows the compressive strength result for three different cement mortars and 40% fly ash replacement mortar for Type I cement at 7 days and 28 days. At 7 days, the strength compressive of 40% fly ash replacement for Type I cement is a little greater than that Type IV cement. At 28 days, the compressive strengths of above two types are almost similar values. These results also indicates that fly ash 40% replacement for Type I cement may possibly be used in the material of concrete dam in Korea.
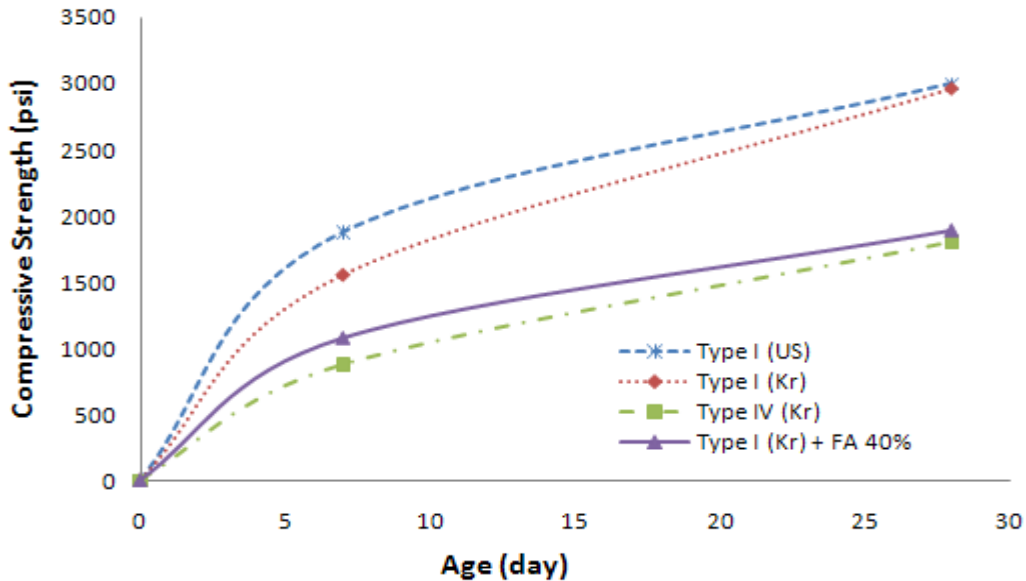
Figure 3.17. Effect of fly ash replacement on strength development (w/b = 0.66)

3.3.2.6 Cost Comparison of Type IV and Type I + 40% Fly Ash Replacement

In spite of the typically small price difference for these two materials, the overall savings for a large concrete dam may be worthy of consideration. Table 3.2 shows a material cost comparison between Type IV and fly ash replacement 40% for Type I. If fly ash replacement 40% for Type I are substituted for Type IV cement, the saving is about 25%. For example, if the cost comparison will apply for Seongdeok dam (used cement 74 million lb), we might save $6 million.

Tabel 3.2. Cost compare with Type IV and Type I + Fly ash 40%

Type I	Fly Ash	Type I + Fly Ash 40%	Type IV	Saving Ratio
3.179	1.434	2.481	3.295	25%

*Unit : $/100 lb

CHAPTER 4. THERMAL ANALYSIS

4.1 Introduction

The maximum hydration temperature in mass concrete structures has a great influence on determining the lift thickness which impacts economic savings and construction period. Large lift thickness speed up construction and obtain the economic benefits but can lead to thermal cracking which results in reducing concrete durability. To deal with this problem, thermal analysis was performed to determine the thermal distribution changes according to varying placement lift thicknesses in mass concrete dam. The concrete temperatures of a concrete dam construction in Korea were predicted using a finite element analysis program.

The finite element program ANSYS was used for thermal analysis. A concrete block having 4m (width) x 15m (length) x 1.5m (lift thickness) such as the same field placement condition was considered. First, analysis values of 1.5m lift thickness were compared to actual concrete temperatures. Finally, temperature analysis of different lift thicknesses (2.0m, 2.5m, 3.0m) was carried out.

The input parameters for the thermal analysis were mainly convection coefficients, ambient temperature, lift placement thickness, internal heat generation rate of concrete, material properties, and thermal boundary conditions.

The temperature distribution in mass concrete is commonly a transient thermal processes because the temperature of mass concrete changes with time. The heat generated by hydration of cement and change of ambient temperature significantly affects the thermal

distribution in mass concrete. The analysis was performed for the first 5days (120hours) which are the same field condition as placing one block concrete.

4.2 The Heat Balance Equation

The basis for thermal analysis is the heat balance equation or governing heat transfer equation based on the principle of energy conservation. The governing heat transfer equation in the global Cartesian system can be described by the Fourier equation expressed by Equation 4.1 (Heat transfer analysis, 2006)

$$\rho c_p \frac{\partial T}{\partial t} = q + \frac{\partial}{\partial x}\left(k_x \frac{\partial T}{\partial x}\right) + \frac{\partial}{\partial y}\left(k_y \frac{\partial T}{\partial y}\right) + \frac{\partial}{\partial z}(k_z \frac{\partial T}{\partial z}) \qquad 4.1$$

Where:

ρ : concrete density, (Kg/m^3)

c_p: specific heat of concrete, (Kcal/Kg·°C)

T : temperature T=T(x, y, z, t), (°C)

t : time

q : rate of internal heat generation rate per unit volume, (Kcal/m^3·°h)

k_x, k_y, k_z : thermal conductivity in x, y, and z direction, (Kcal/m·hr·°C)

Equation 4.1 can be solved for the temperature distribution inside the cross section of the concrete. In this thesis, the boundary conditions are the same for all models' analyses. The boundary conditions used for thermal analysis are bottom surface S$_1$ in contact with previously concrete block and all other surface S$_2$ in contact with air. Equation 4.1 can be expressed in matrix form:

$$[C]\{\dot{T}\} + [\bar{K}]\{T\} = \{Q\} \qquad\qquad 4.2$$

Where,

[C] : specific heat matrix

[$\bar{K}$] : heat conductivity matrix (conduction, convection)

{Q} : total heat flux vector for internal hydration and heat convection

{T} : nodal temperature vector

$\{\dot{T}\}$: time derivative vector of above nodal temperatures ({T})

The relationship between the temperature at a given time and at the next successive time is applied here using the implicit trapezoidal rule (Fig 4.1) as a time-stepping integration scheme for the heat transport equation, as shown in Equation 4.3:
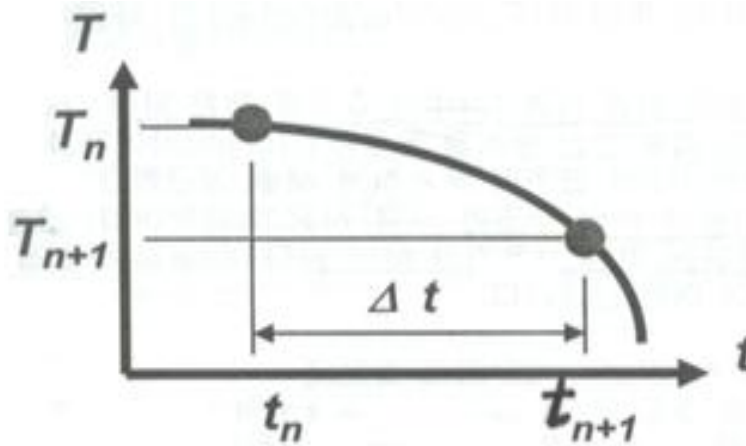
**Figure 4.1. Generalized trapezoidal rule with time
(Adapted from Heat transfer analysis 2005)**

$${T_{n+1}} = {T_n} + (1 - \theta)\Delta t{\dot{T}_n} + \theta\Delta t{\dot{T}_{n+1}} \qquad 4.3$$

Where,

$\quad$ ${T_n}$ $\quad$: temperature at a given time

$\quad$ ${T_{n+1}}$: temperature at next successive time

$\quad\quad$ Δt $\quad$: time interval

Equation 4.4 is acquired by numerically solving Equation 4.2 and Equation 4.3 in the time domain numerically.

$$\left\{\frac{1}{\Delta t} [C] + \theta[K]\right\}{T_{n+1}} = \left[\frac{1}{\Delta t} [C] - (1 - \theta)[K]\right]{T_n} + (1 - \theta){Q_n} + \theta{Q_{n+1}} \qquad 4.4$$

Where θ is equal to ½ in Crank-Nicolson method. Then Equation 4.4 can take the following general form:

$$[A_G]{\Delta T} = {Q_G} \qquad 4.5$$

Where,

$$[A_G] = \frac{1}{\Delta t}[C] + \frac{1}{2} [K]$$

$$\{Q_G\} = \frac{1}{2} (\{Q_n\} + \{Q_{n+1}\} - 2[K]\{T_n\})$$

Where $\{\Delta T\}$ represents temperature changes at the nodal point with respect to time Δt, which is used to calculate temperature at the next time stage using the following equation;

$$\{T_{n+1}\} = \{T_n\} + \frac{1}{2}\{\Delta T\} \qquad 4.6$$

The value of the [C] and [K] in the above equation are also constant over each element because conductivity, density, and specific heat are constants. This means that the matrix $[A_G]$ for each element has a constant value for each time interval. Therefore, the nodal temperature changes are only based on the value of the heat flux vector $\{Q_G\}$. In other words, the temperature changes as a function of time are be calculated for variable values of concrete hydration rate and the ambient temperature. The temperature computation of a mass concrete can be described by the following steps:

Step 1 : divide construction time into several time increments in units of hours

Step 2 : calculate temperature changes $\{\Delta T\}$ using Eq. (4.5)

Step 3 : accumulate the changes of temperature vector $\{\Delta T\}$ using Eq. (4.6)

Step 4 : the temperature of the ith time increment $\{T_i\}$vector becomes the initial

temperature for next time increment Δt_{i+1}

Step 5 : repeat steps 1-4 until the solution for the concrete block is completed

4.3 Analysis Algorithm

The thermal distribution analysis was performed by the finite element method widely used in many fields of engineering. This method is a powerful numerical technique. It discretizes the structure into elements and then assembles the elements at "nodes" as if nodes were pins or drops of glue that hold elements together. The analysis procedure followed in the finite element method for this model is shown in Fig. 4.2.
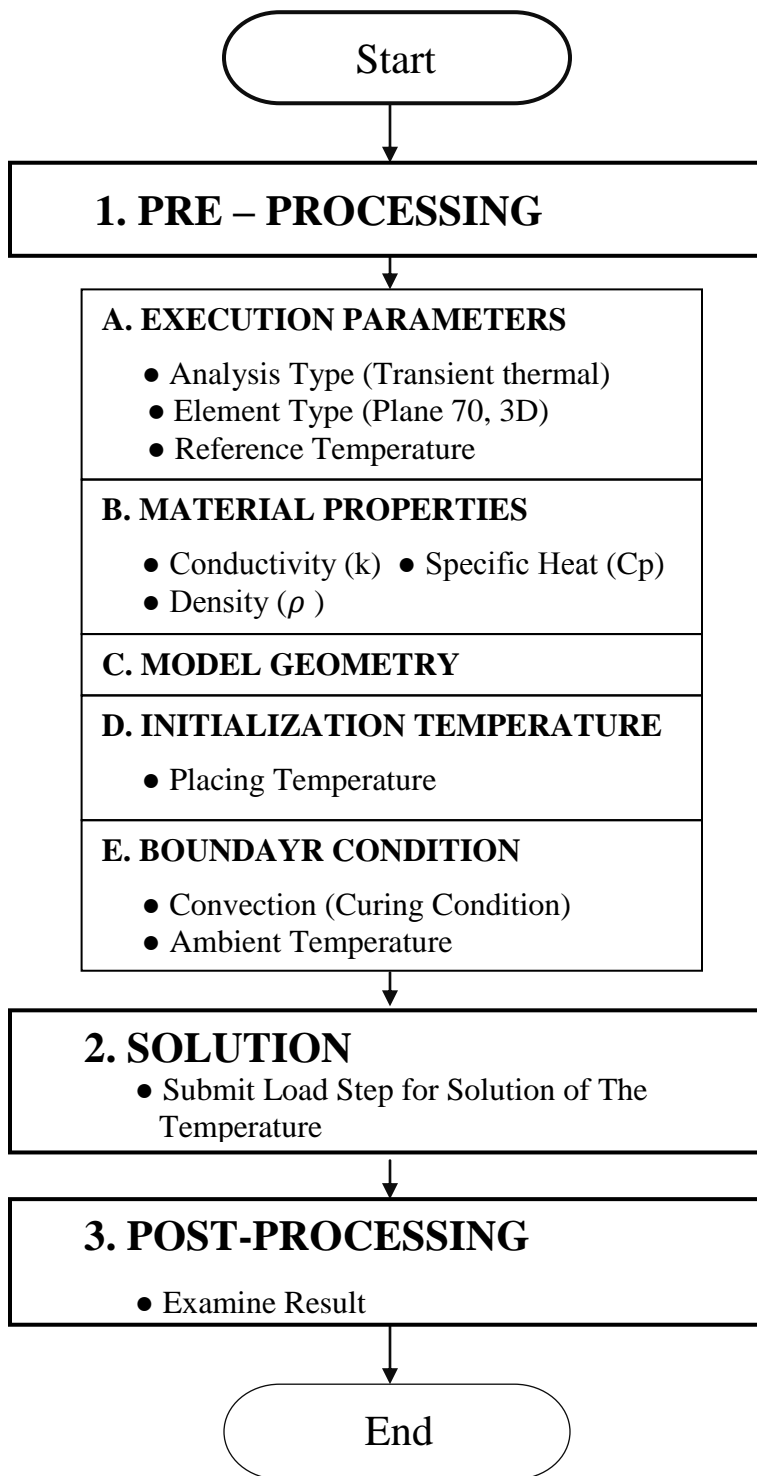
Figure 4.2. Finite element modeling algorithm for thermal analysis

4.3.1 Execution Parameters

Execution parameters are composed of the analysis type, the element type, and reference temperature. The analysis type is transient thermal that considers changes of loads and boundary conditions with time. The thermal quantities of mass concrete are calculated by this type of analysis. The principally needed quantities are temperature field, thermal flux, and thermal gradient. The thermal gradient can be defined in terms of temperature changes along a particular path or through a section of a structure. These results act as loads for later stress analysis. As stated above, thermal quantities are transferred by elements with thermal properties. These elements are comprised of nodes. A three-dimensional solid element was used for thermal analysis, as shown in Figure 4.3. This element is a three-dimensional, isoperimetric, and eight-node solid element, with a single degree of freedom temperature at each node. Such an element is called a PLANE 70 – 3D Thermal Solid in ANSYS.

Transient analysis requires the reference or initial temperature because this affects the next temperature change with time. The reference temperature is the temperature of the concrete at its moment of placing in a formwork.
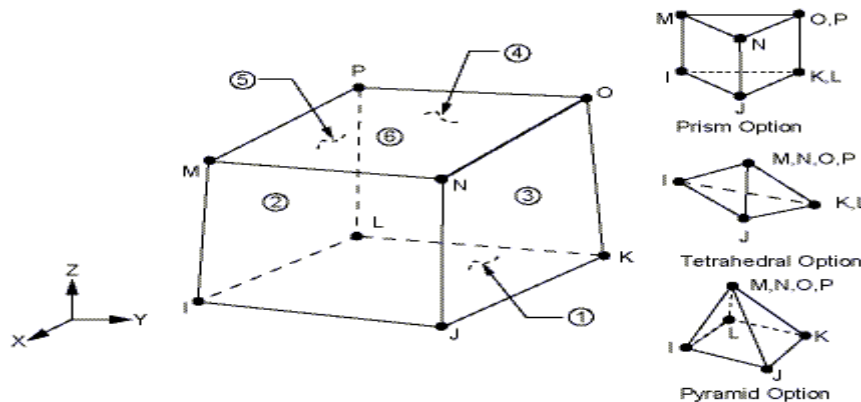
Figure 4.3. Finite element SOLID 70 (Adapted from ANSYS manual 2009)

4.3.2 Thermal Properties of Concrete

Thermal properties used to determine concrete temperature are thermal conductivity, density, specific heat, and convective heat transfer coefficients. These properties depend on age of the concrete and temperature, cement type, w/c, aggregate type and unit weight. It may be difficult to determine these values because the variations of these properties are large and the test methods for acquiring them are also very complex. The values of thermal properties of concretes adopted in this analysis are determined with reference which will be discussed later.

4.3.2.1 Thermal Conductivity

Thermal conductivity is defined as a uniform flow of heat through a unit thickness of material between two faces subjected to a unit temperature difference during a unit time. It is displayed as the ratio of the rate of heat flow to the temperature. It is widely influenced by a unit weight of concrete, type of aggregates used and a moisture content of concrete. Generally, a typical value of thermal conductivity of concrete is in the range 2.15-2.51 kcal/m·h·℃ according to Korean standard specification, and in the range 1.7-2.53 kcal/ m· h·℃ according to ACI 207.2R-07. The value of thermal conductivity adopted in this analysis is 2.3 kcal/m·h·℃ and is assumed to be temperature-independent during the analysis.

4.3.2.2 Specific Heat

The specific heat is the main parameter affecting the heat capacity. It is the amount of heat needed to change the temperature of 1g of material by 1℃. The specific heat of concrete depends on the specific heat of the constituent materials. Since the specific heats of rocks do

not change much with mineralogical type, the type of aggregate has little effect on the specific heat. The main factors that influence the specific heat are porosity of cement paste, water content, and specimen temperature characteristics. The common range of specific heat values for concrete is 0.27-0.31 kcal/kg·℃ according to JCI, and 0.22-0.24 kcal/kg·℃ according to ACI 207.2R-07. The specific values adopted in this analysis are 0.23 kcal/kg·℃.

4.3.3 Model Geometry

As a case study, one block of a concrete cofferdam in Korea was used to analyze the heat evolution because the thermocouple was inserted into this block to check the concrete temperature. This block was located at a 4.5m height in the cofferdam. The concrete gravity cofferdam is 10.6 m in total height, 4.0m in top width, and 102m long. During the construction period of a concrete cofferdam, the dimension of one block is 1.5m (height), 15m (length), and 4m (width). The total amount of concrete is 3,866 m^3. After 5days curing, the forms were removed in accordance with the construction schedule.

The temperature in mass concrete varies with time and locations. The size and shape of the model have an important role in achieving convergence and accurate results. The target concrete block for this analysis was divided into 15 cm height divisions to produce accurate results. The typical block was discretized by three-dimensional isoparmetric cubic elements. The model of a target block was composed by 1200 elements and 1584 nodes. Other blocks were treated as a coarse mesh to reduce analysis time because these previously-placed blocks have a little effect on the heat evolution of the target block. The selected geometrical layout is shown in Figure 4.4 and input data is listed in Table 4.1

Model Block

Plane of symmetry
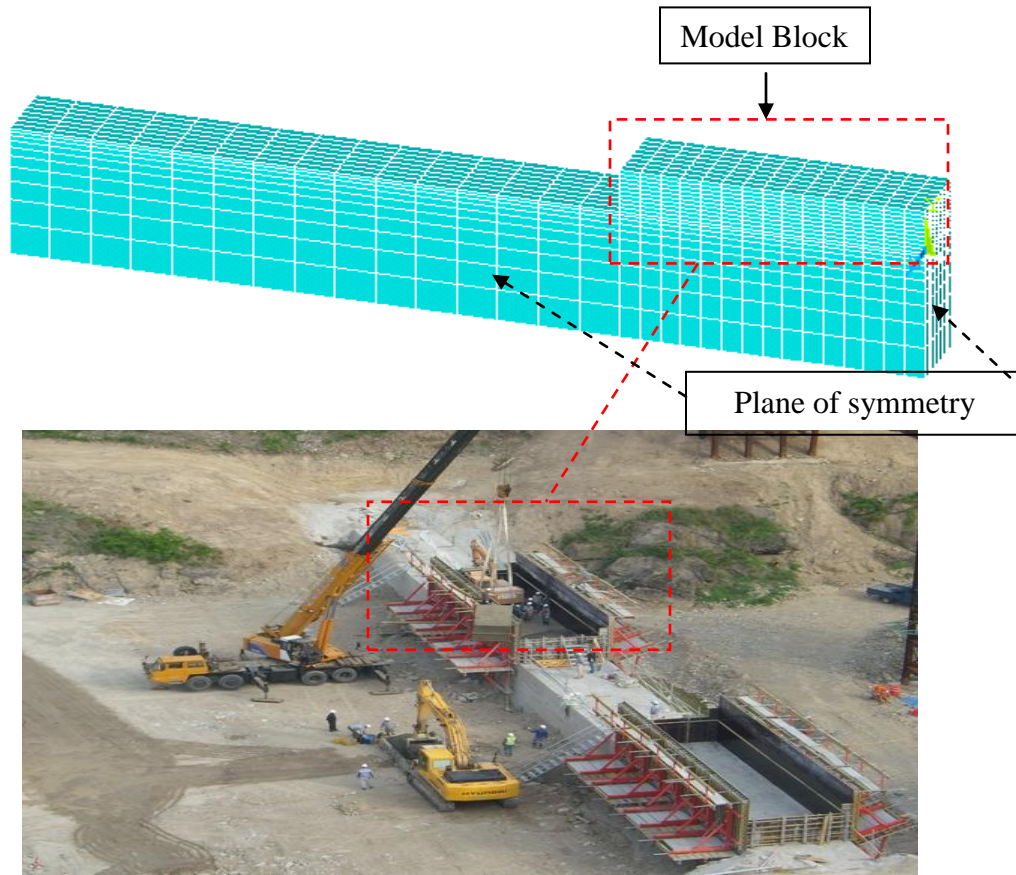
Figure 4.4. Layout of finite element mesh

Table 4.1. The input values used for thermal analysis and thermal stress analysis

Items	Unit	Value
Conductivity	kcal/m·h/°C	2.3
Specific heat	kcal/kg/°C	0.23
Density	Kg/m^3	2400
Placement temperature	°C	16.5
Convection (Steel form)	kcal/m^2·h·°C	12
Analysis time	hr	120
Thermal expansion	/°C	1 x 10^{-6}
Poisson's ratio		0.18

4.3.4 Fresh Concrete Placing Temperature

Fresh concrete placement temperature has a significant effect on temperature rise in a mass concrete dam. The higher is the initial placement temperature, the greater is the rate of hydration because the cement hydration reacts fast with temperature increase. If it is difficult to control material temperature, post-cooling methods such as pipe cooling can be applied. This method did not be applied in this analysis. The fresh concrete placement temperature in this analysis was 16.5℃ which was measured in the field.

4.3.5 Boundary Condition

Boundaries in our transient thermal analysis are composed of the thermal transfer boundary, insulation boundary and fixed thermal boundary. Because the thermal transfer boundary mostly affects the surface of concrete structures, in this model convection is applied.

Convection is heat transfer by mass motion of a fluid such as air or water in which the heated fluid is moved away from the source of heat, and carries heat with it. Convection depends on types and setting period of the formwork, curing methods, and wind speed. The overall effect of convection is described by Newton's law of cooling as following:

$$q = h \cdot A \cdot (Ts - Ta) \qquad\qquad 4.7$$

Where,

q : heat flow (kcal/h)

h : convection heat transfer coefficient (kcal/m$^2 \cdot$ h $\cdot$℃)

A : area (m^2)

Ts : surface temperature (℃)

Ta : air temperature (℃)

Convection can be determined using Equation 4.7, but this value can be typically used by the reference values of Korea standard specification for concrete listed in Table 4.2. The convection value of the formwork and surface of mass concrete applied in this analysis was 12 kcal/m^{2}h°C. The ambient temperature in our analysis was used as the temperature for 5 days which are the period from concrete placement to curing time.

Table 4.2. The reference value of convection (Korea standard specification 2003)

No	Curing methods	Convection value(kcal/ m^2 h °C)
1	Steel form, water	12
2	Straw bag	7
3	Plywood	7
4	Sheet	7
5	Curing mat	4.5
6	Stropore	1.5
7	Air	4.3

4.3.6 Internal Heat Generation Rates of Concrete

The temperature distribution in concrete produced by the heat of hydration is analyzed using boundary conditions, initial conditions, and internal heat generation acquired by Equation 4.1. The internal heat rate due to cement hydration is calculated for each interval of the analysis algorithm. These values are obtained from time after concrete placement temperature because the heat generation pattern depends only on time.

Internal heat generation can be calculated by the adiabatic temperature rise Equation (4.8) because the temperature near the center of the mass concrete is almost equal to the adiabatic temperature. The magnitude of the adiabatic temperature rise and the shape of the curve can vary significantly depending on the particular concrete mixture. The adiabatic temperature rise equation is displayed as an exponential function suggested by Sukiyaki from Japan.

$$T(t) = K\,(1 - e^{-\alpha t})\qquad\qquad 4.8$$

Where,

T is amount of adiabatic temperature rise at time (°C)

α is the coefficient of temperature rise (reaction rate)

K is final amount of adiabatic temperature rise acquired by test (°C)

t is a time (day)

The total amount of heat generation per unit volume can be obtained from the equation:

$$Q(t) = C_p \rho T(t) = K C_p \rho (1 - e^{-\alpha t})\qquad\qquad 4.9$$

By differentiating Equation 4.9 with respect to time, the heat generation per unit volume and unit time can be calculated as:

$$q(t) = \frac{\partial Q}{\partial t} = \frac{K C_p \rho\, e^{-\alpha t/24}}{24} \qquad\qquad 4.10$$

On this basis, the internal heat generation was acquired by the adiabatic temperature test measured in the field laboratory. The results of the regression analysis for the adiabatic temperature rise curve fit well as shown in Figure 4.5. This regression analysis does not include the initial 10 hours comprising the retarding of heat at the time of concrete production, concrete transfer to the field, and placement time in the field. The R^2 values for adiabatic temperature (measured) and regression equation (calculated) are 0.988, meaning that over 95% of the variation of the regressively determined internal heat generation values can be explained by the proposed model. The internal heat generation Equation 4.11 in this model was used for thermal distribution analysis.

$$Q\,(t) = 27.6592\left(1 - e^{-0.5428\,(t-0.3229)^{0.5203}}\right) \qquad\qquad 4.11$$
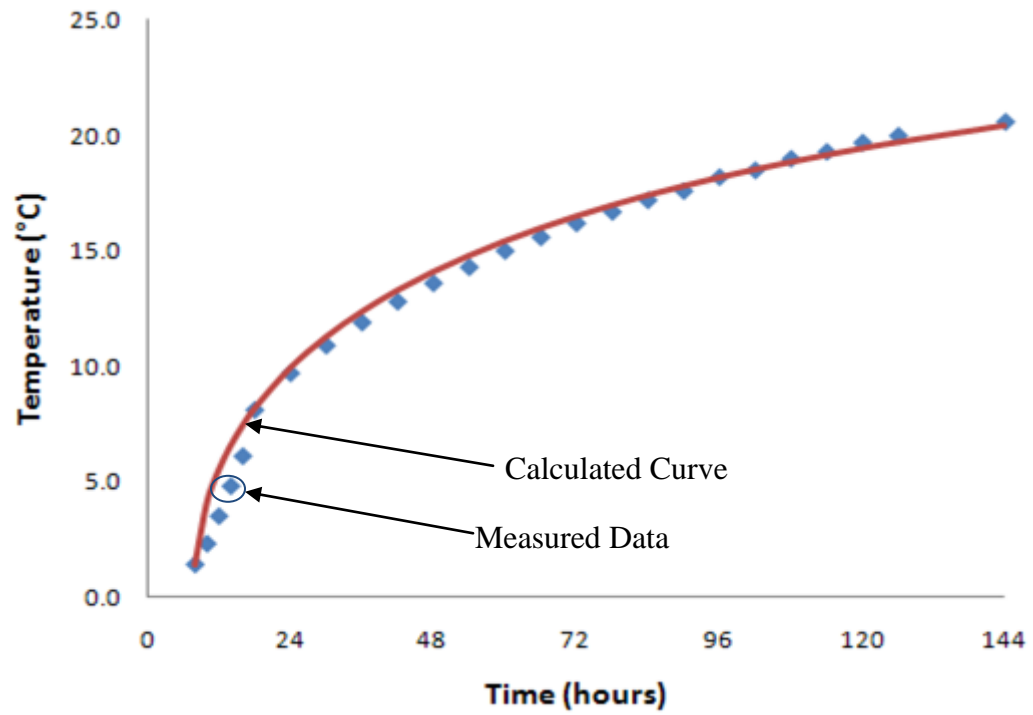
Figure 4.5. The results of adiabatic temperature rise and regressive analysis

4.4 Model Verification

To verify the model reliability, the temperatures obtained from FEM analysis (ANSYS) were compared with the temperature measured from the center of one block concrete in the concrete dam. As shown in Figure 4.6, one temperature sensor was located at the center (width 2m, length 7.5m, lift 0.75m) of one block concrete (width 4m, length 15m, lift 1.5m). The R^2 values of regression are 0.978. Figure 4.7 shows that the results of FEM analysis are in good agreement with the temperatures measured from the field. It is clear that this model can be well applied for analysis of different lift thicknesses
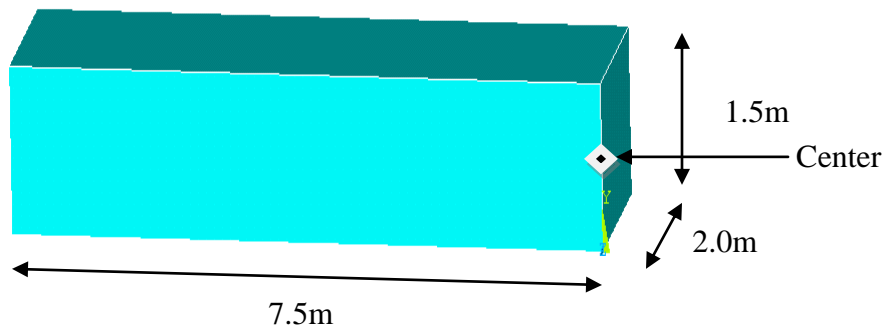
Figure 4.6. Temperature sensor at the center of one concrete block
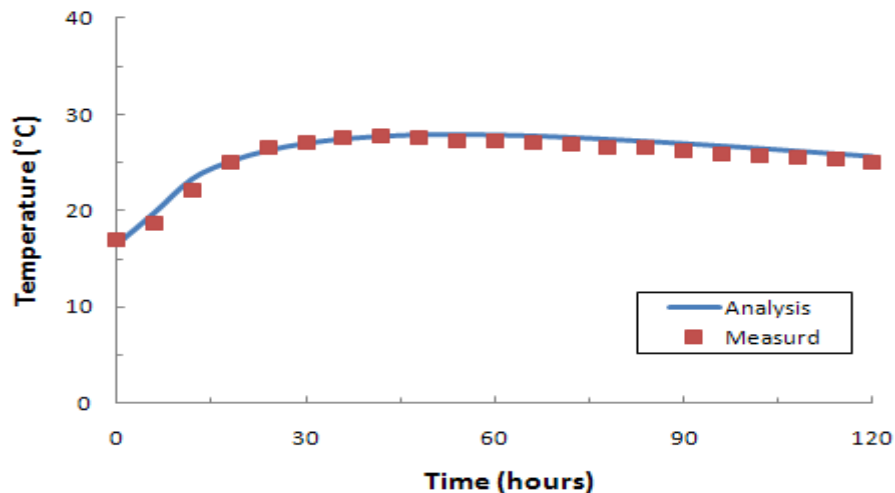
Figure 4.7. FEM analysis and field measurements comparison

4.5 Analysis Results

4.5.1 Temperature Distribution of Lift Thickness 1.5M

The Figure 4.8-9 show the temperature distribution at the top, middle, and bottom of the center of the concrete block having 4m (width) x 15m (length) x 1.5m (lift thickness). It can be seen that the temperature is the highest at the center and is the lowest at the surface contacting the atmospheric temperature. The highest temperature in the center is 27.9 °C and the lowest temperature at the surface is 18.5 °C at 54hours after concrete pouring. The temperature difference between the center and the surface is 9.4 °C. The results also illustrate that the temperature at the surface is significantly affected by atmospheric conditions, while the temperature at the center is almost unaffected by the ambient temperature.
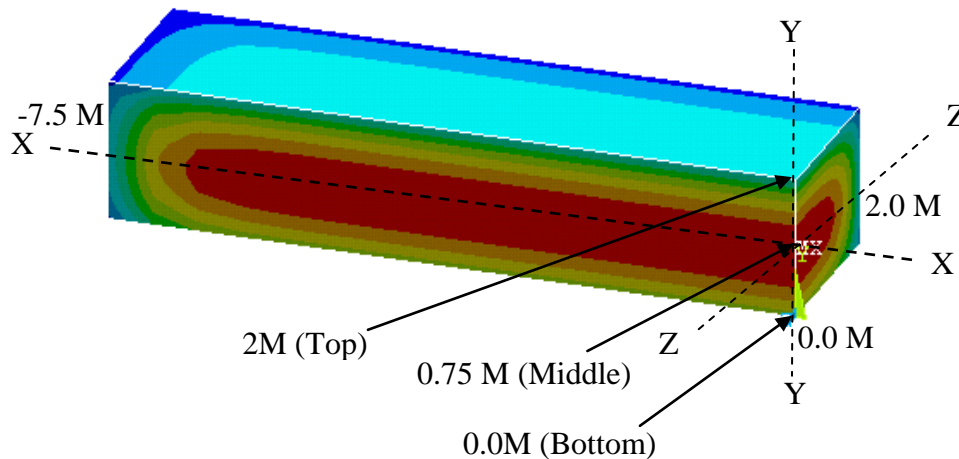
Figure 4.8. Temperature distribution at the center of 1.5m thickness
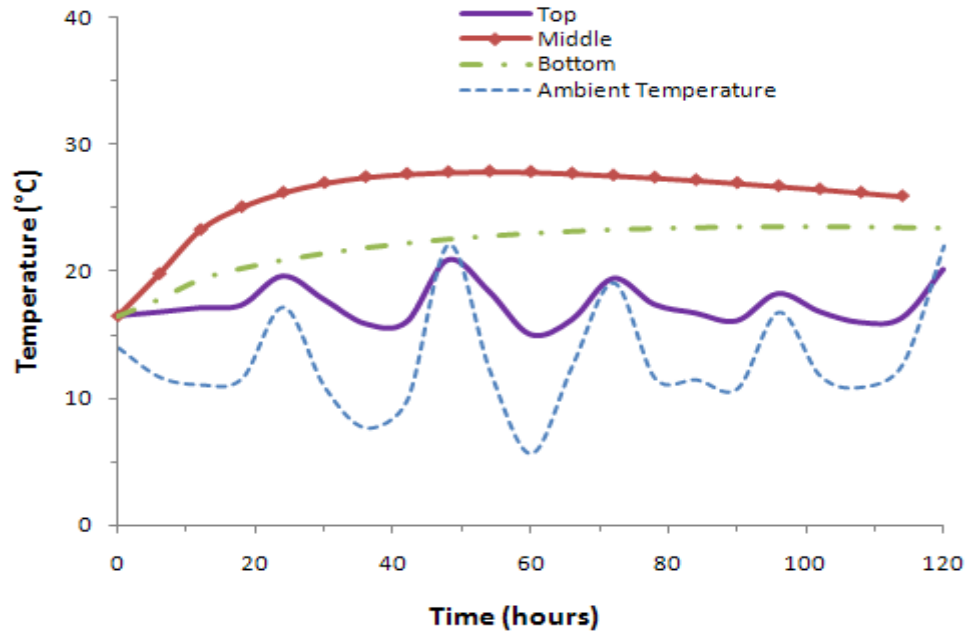
Figure 4.9. Temperature changes of lift thickness 1.5m

4.5.2 Temperature Distribution at Different Thicknesses

The temperature generated at a 1.5 m lift thickness was compared with that at the different lift thicknesses to study the possibility for increase of placement lift. Figure 4.10 shows the temperature development at the central point of different concrete thicknesses. The temperature also increases as the placement thickness increase due to heat produced by hydration. However, amount of temperature rise does not increase at the same rate as thickness increase because the concrete conductivity is low. The occurrence time of the maximum temperature is delayed as the placement thickness increase. The maximum temperature and its occurrence time are listed in Table 4.3. After maximum temperature, the block begins to cool down. It also predicts that the internal temperature of this block to drop to stable temperature takes a long time.
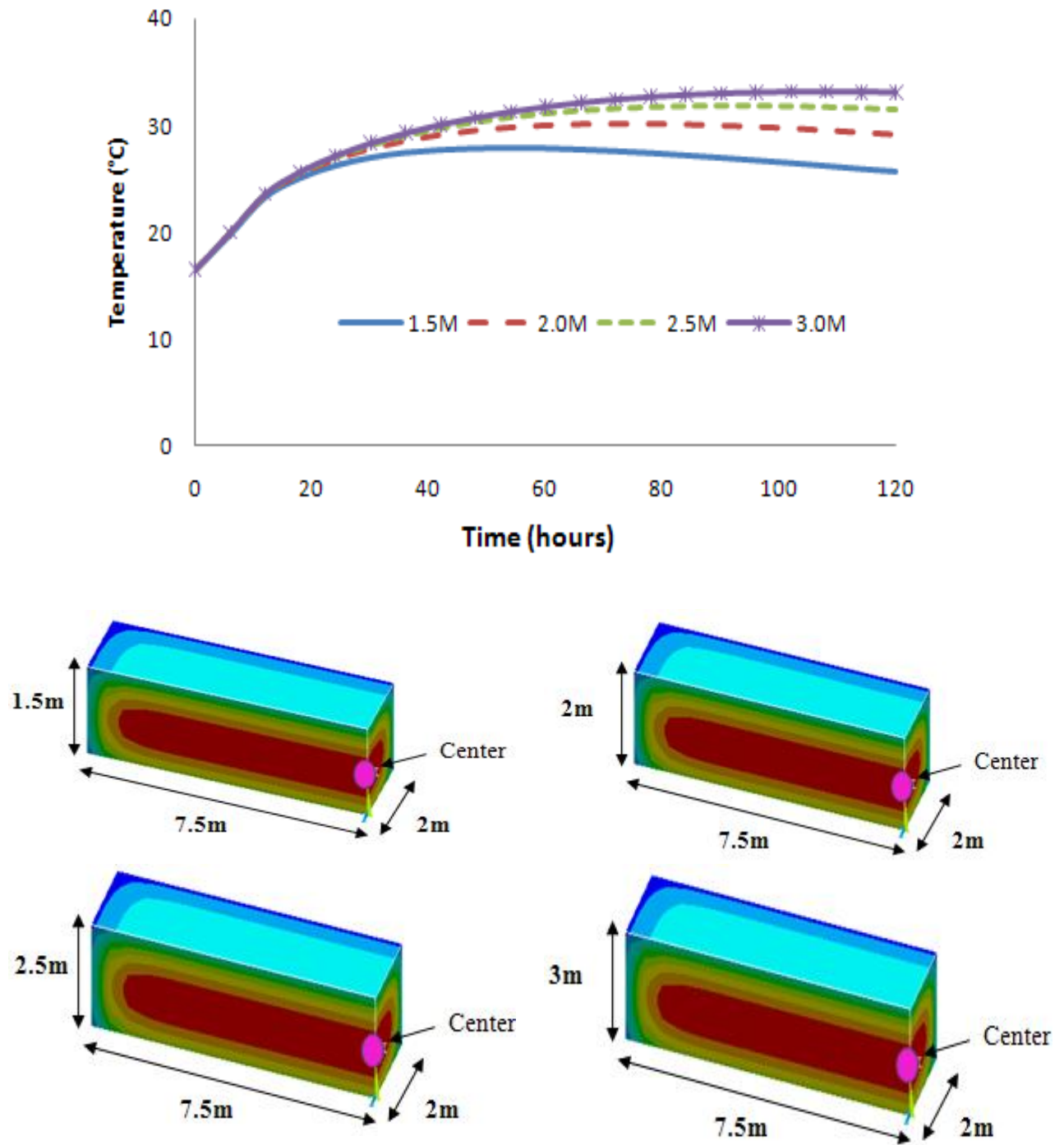
Figure 4.10. Temperature development at the center of different thicknesses

Table 4.3. The maximum temperature and its occurrence time at different thicknesses

	1.5m	2m	2.5m	3m
Maximum temperature (°C)	27.9	30.2	31.9	33.2
Maximum temperature occurrence time (hours)	54	72	84	96

CHAPTER 5. THERMAL STRESS ANALYSIS

5.1 Introduction

Thermal stress transients due to a hydration process may induce thermal cracks resulting in failure of concrete structures. To control this process, a study of thermal stress produced by thermal distribution is necessary. When the thermal stress is larger than the tensile strength of concrete, concrete cracks are generated at a time after concrete pouring. Such thermal cracks are mainly generated by internal restraint due to the temperature differences between the surface and the center of the concrete. Therefore, thermal analysis of the mass concrete dam would certainly play an important role in its design and construction schedule.

The purpose of this chapter is to investigate the thermal stress at different lift thicknesses for the thermal loads calculated in chapter 4 and to study the efficient lift thickness required to ensure dam safety. To calculate this thermal stress, we explored the mechanical properties of concrete using ANSYS for analysis.

5.2 Thermal Stress Analysis

5.2.1 Structural Analysis Algorithm

The process of stress analysis is similar to that for analyzing thermal distribution as a function of time. The mechanical properties of concrete, the analysis type, and the boundary conditions were changed. Thermal distributions acquired in Section 4 were applied as time

function to constitute a body load on the concrete. Figure 5.1 presents the finite element

modeling algorithm for thermally induced stresses on structure behavior of concrete.

```
                    ╭─────────────────╮
                    │      Start       │
                    ╰─────────────────╯
                              │
                              ▼
        ┌─────────────────────────────────────────┐
        │  1. PRE – PROCESSING                     │
        └─────────────────────────────────────────┘
                              │
                              ▼
        ┌─────────────────────────────────────────┐
        │  A. EXECUTION PARAMETERS                 │
        │                                          │
        │     ● Analysis Type (Structural)         │
        │     ● Element Type (Plane 45, 3D)        │
        ├─────────────────────────────────────────┤
        │  B. MATERIAL PROPERTIES                  │
        │                                          │
        │     ● Thermal Expansion (α) ● Density (ρ)│
        │     ● Elasticity Modulus (Ec)            │
        │     ● Poisson's ratio (υ)                │
        ├─────────────────────────────────────────┤
        │  C. MODEL GEOMETRY                       │
        ├─────────────────────────────────────────┤
        │  D. BOUNDAYR CONDITION                   │
        │                                          │
        │     ● Constrains at the Bottom, Formwork │
        └─────────────────────────────────────────┘
                              │
                              ▼
        ┌─────────────────────────────────────────┐
        │  2. SOLUTION                             │
        │                                          │
        │    A.  LOAD : THERMAL BODY               │
        │                                          │
        │   ● Define Analysis Option               │
        │   ● Apply Thermal Distribution in Section 4│
        │   ● Calculate Thermal Stress             │
        └─────────────────────────────────────────┘
                              │
                              ▼
        ┌─────────────────────────────────────────┐
        │  3. POST-PROCESSING                      │
        │                                          │
        │   ● Save Data                            │
        │   ● Examine Result                       │
        └─────────────────────────────────────────┘
                              │
                              ▼
                    ╭─────────────────╮
                    │       End        │
                    ╰─────────────────╯
```

Figure 5.1. Finite element modeling algorithm for thermal stress analysis

5.2.2 Analytical Formulation

Considering an energy principles, the internal strain work is equal to the external work, as can be represented by

$$\delta U = \delta V \qquad\qquad 5.1$$

Where,

U is strain energy (internal work)

V is external work

δ is variation operator

The internal work and external work can also be represented as follows (Heat Transfer Analysis, 2005):

$$\delta U = \{\delta_u\} \int_v \left([B]^T [D][B]dV\{u\} - \{\delta_u\}^T \int_A [B]^T [D]\{\varepsilon^{th}\} \right) dV \qquad 5.2$$

$$\delta V = \{\delta_u\}^T \{F_\varepsilon{}^{nd}\} \qquad\qquad 5.3$$

Where,

$\{\varepsilon\}$: strain vector $= \begin{bmatrix} \varepsilon_x & \varepsilon_y & \varepsilon_z & \varepsilon_{xy} & \varepsilon_{yz} & \varepsilon_{zx} \end{bmatrix}^T$

$\{\varepsilon^{th}\}$: the thermal strain vector $= \Delta T \begin{bmatrix} \sigma_x & \sigma_y & \sigma_z & 0 & 0 & 0 \end{bmatrix}$

$\{\sigma\}$: stress vector $= \begin{bmatrix} \sigma_x & \sigma_y & \sigma_z & \sigma_{xy} & \sigma_{yz} & \sigma_{zx} \end{bmatrix}^T$

[B] : strain-displacement matrix, based on the element shape functions

{u} : nodal displacement vector

$\{F_\varepsilon{}^{nd}\}$: generalized nodal point forces

The internal virtual work and external virtual work must be equal. After cancellation of $\{\delta_u\}^T$ term from both sides (eqn. 5.2 and eqn. 5.3), we can write the equation in the following form:

$$[K_e]\{u\} = \{F_e^{th}\} = \{F_e^{nd}\} \qquad 5.4$$

Where,

$[K_e] = \int_V [B^T][D][B]dV$ is the element stiffness matrix

$\{F_e^{th}\} = \int_V [B^T][D]\{\varepsilon^{th}\}dV$ is the element thermal load vector

After formation of the element stiffness matrix, the stiffness matrix can be formed by the systematic addition of element stiffness.

$$\{F\} = [K]\{u\} \qquad 5.5$$

Where,

$\{F\}$ is external nodal point load (known)

$\{u\}$ is the unknown nodal point displacements to be determined

Now, when nodal point displacement is known, the element stresses within each element can be found using the following equation:

$$\{\sigma\} = [D][B]\{u\} = [D](\{\varepsilon\} - \{\varepsilon^{th}\}) \qquad 5.6$$

The sign convention used for stress and strain is that tension is positive and compression is negative.

5.2.3 The Coefficient of Linear Thermal Expansion

The coefficient of thermal expansion is defined as the change in volume per degree of temperature. The expansion coefficient of concrete is that of a combination of hydrated cement and aggregate. The composition of aggregate and moisture in concrete have a big influence on the coefficient of linear thermal expansion. The coefficient of thermal expansion varies greatly depending on different aggregate type. Moisture content also influences the thermal expansion coefficient of cement paste. Moisture-based concretes exhibit an increase in the coefficient of thermal expansion with temperature rise. These may become critical factors for crack prevention in mass concrete. The coefficient for concrete is generally in the range 6-12 x 10^{-6} per °C (Mehta et al. 1993). The value of linear thermal expansion adopted in this thermal stress analysis is 1 x 10^{-6} /°C. The value of Poisson's ratio is 0.18.

5.2.4 Modulus of Elasticity

The modulus of elasticity is the one of the most important characteristics of concrete. The mechanical properties of concrete behavior depend on concrete age and concrete hardening process at early age because the modulus of elasticity changes until reaching the age of about 28 days. This modulus must be assumed to be variable to provide the most accurate analysis. Although concrete is not an elastic material, it is assumed to behave elastically in this analysis.

Many equations are required to determine the modulus of elasticity, and the method used may depend on the country involved. In the project, the modulus of elasticity was determined using the standard concrete specification of Korea.

(1) ACI Committee 318

$$E_c(t) = W^{1.5} \times 33\sqrt{f_c\acute{}(t)} \text{ (psi)} \qquad 5.7$$

$$f_c(t) = \frac{t}{a+bt} f_c\acute{} \qquad 5.8$$

Where,

W : the weight of concrete (lb/ft^3)

$f_c\acute{}(t)$: the compressive strength with age (lb/ft^2)

a : 0.05 to 9.25 in days and b : 0.67 to 0.98 depending on curing and cement type

t : time (day)

(2) CEB-FIP Model Code

$$E_c(t) = \exp\left[\frac{s}{2}\left(1 - \sqrt{\frac{28}{t}}\right)\right] E_{c,28} \text{(MPa)} \qquad 5.9$$

$$E_{c,28} = 10{,}000(f_{cm})^{1/3} \qquad 5.10$$

Where,

s : the coefficient, dependent of types of cement

$E_{c,28}$: elasticity modulus of concrete at 28 days (MPa)

f_{cm} : average compressive strength of concrete at 28 days (MPa)

t : time (days)

(3) Standard Concrete Specification of Korea

$$E_e(t) = \varphi(t) \times 4.7 \times 10^3 \times \sqrt{f_{cu}(t)} \qquad \text{5.11}$$

$$f_{cu}(t) = \frac{t}{a+bt} \, d(i)f_{ck} \qquad \text{5.12}$$

$$f_{sp}(t) = c\sqrt{f_{cu}(t)} \qquad \text{5.13}$$

Where,

$E_e(t)$: the effective elasticity modulus of concrete at age t (MPa)

$\varphi(t)$: correlation coefficient

at 3 days : $\varphi(t) = 0.73$

after 5 days : : $\varphi(t) = 1.0$

between 3 days and 5 days : interpolation

$f_{cu}(t)$: concrete compressive strength at age t (MPa)

$f_{sp}(t)$: concrete tensile strength at age t (MPa)

c : coefficient, 0.44

a,b,c,d : cement coefficient, here a=16.2, b=0.82, d=1

5.3 Results

Figures 5.3-6 present the results of thermal stress analysis at lift thicknesses of 1.5m, 2m, 2.5m, 3m. The crack index for the top section of each lift thickness is listed in Table 5.1. The maximum tensile stress due to thermal distribution occurs around the surface of all lifts, while the maximum compressive stress occurs at the center and bottom. The compressive stress at the center increases as the lift thickness increases. The stresses around the center and bottom vary with the age of concrete and these stresses may slowly decrease after cooling down. The stress changes around the surface are similar to the variation of ambient temperature and these stresses may also decrease after cooling down.

At lift thicknesses of 1.5m and 2m, the thermal cracks may not occur because the tensile stresses are less than the tensile strength of concrete. However, when the crack index is considered according to Figure 2.14 and Table 2.7, the occurrence probability of cracks with a lift thickness of 2m is about 23%. The smallest crack index to limit cracks is 1.2 shown in Figure 5.2. If concrete is placed at lift thickness 2m, the placement temperature must be strictly controlled to prevent cracking.

At lift thicknesses 2.5m and 3m, the thermal cracks may occur because the tensile stresses are much larger than the tensile strength of concrete. Considering the crack index, the occurrence probabilities of cracks at the surface block of these thicknesses are above 50% because the crack index is less than 1.2. The results above illustrate that concrete placement above a lift thickness 2m is not suitable.

As mentioned before, one objective of this study is to determine the maximum lift thickness with no thermal cracking. To simplify the analysis, a fixed width of concrete block

from Seongdeok dam was selected. Generally, the maximum lift thickness will change if other dimensions of concrete block (width and length) changes.

Table 5.1. The crack index at top section of different lift thicknesses

Lift thickness	1.5 m	2 m	2.5 m	3 m
The crack index	1.5	1.2	1.0	0.9
fsp(t) : tensile strength (MPa)	0.725	0.725	0.725	0.725
ft (t) : tensile stress (MPa)	0.485	0.611	0.728	0.833
Probability of crack occurrence (%)	4	23	50	68
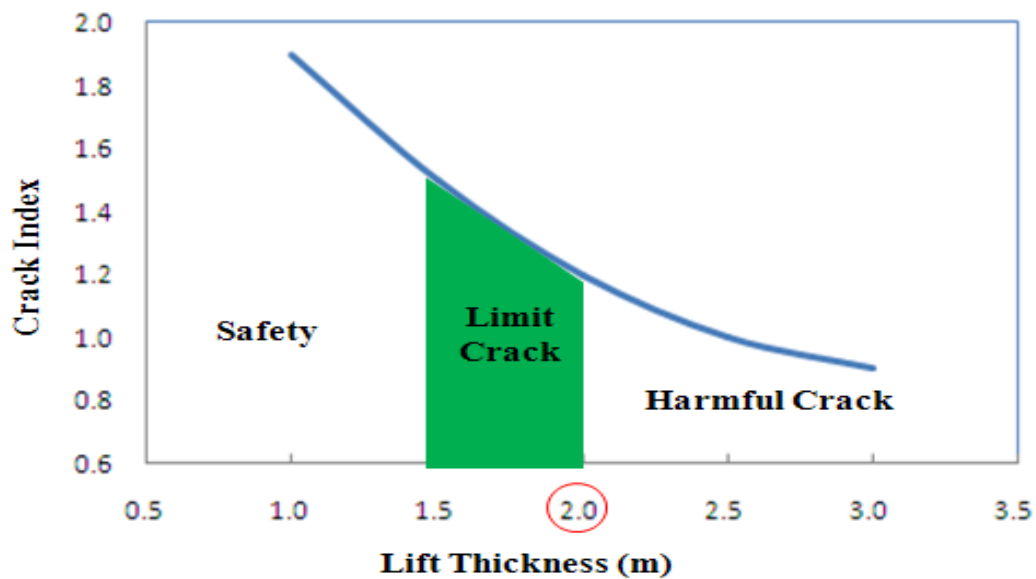
Figure 5.2. Compare crack index with lift thicknesses
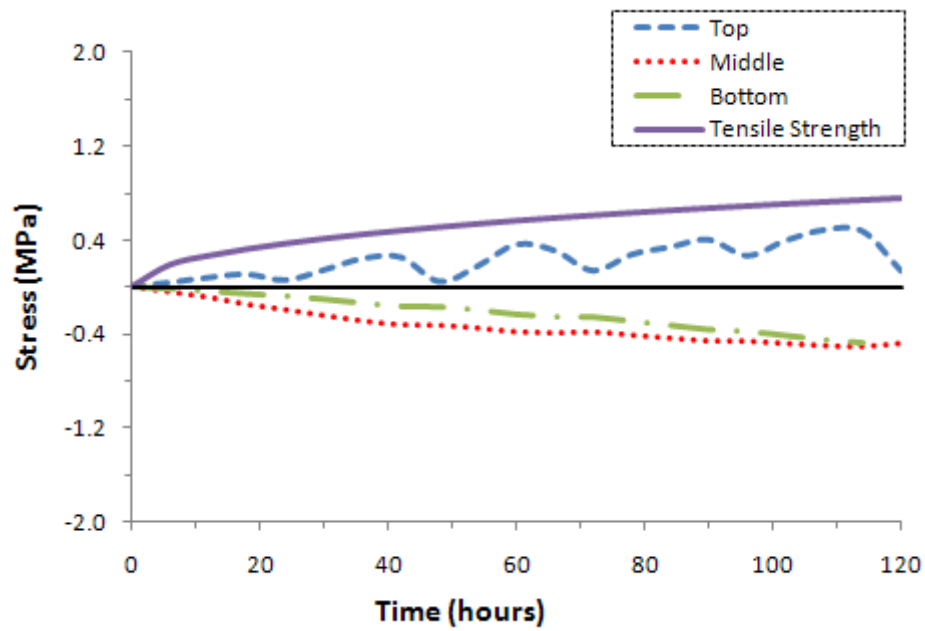
Figure 5.3. Thermal stress analysis at the lift thickness 1.5m
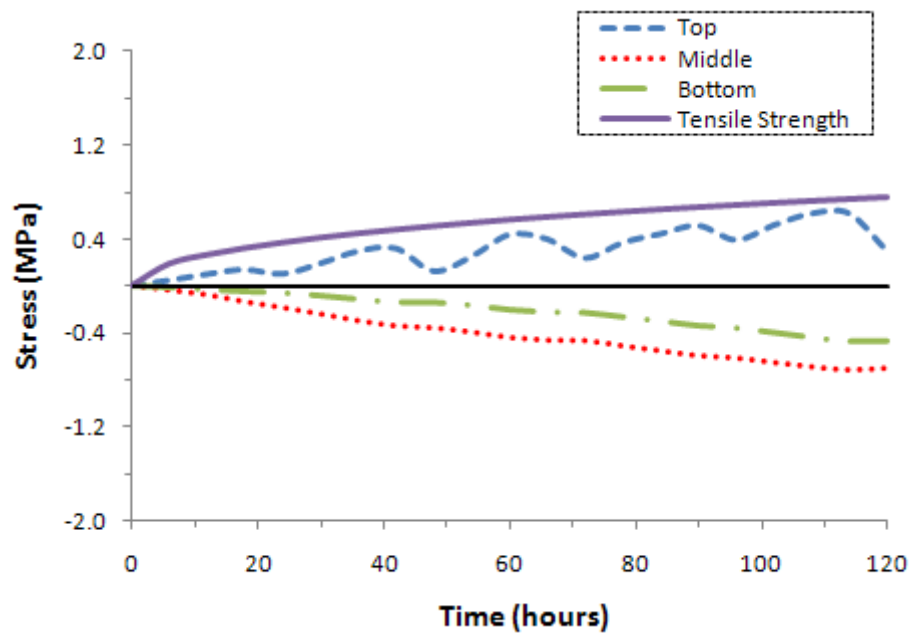
Figure 5.4. Thermal stress analysis at the lift thickness 2m
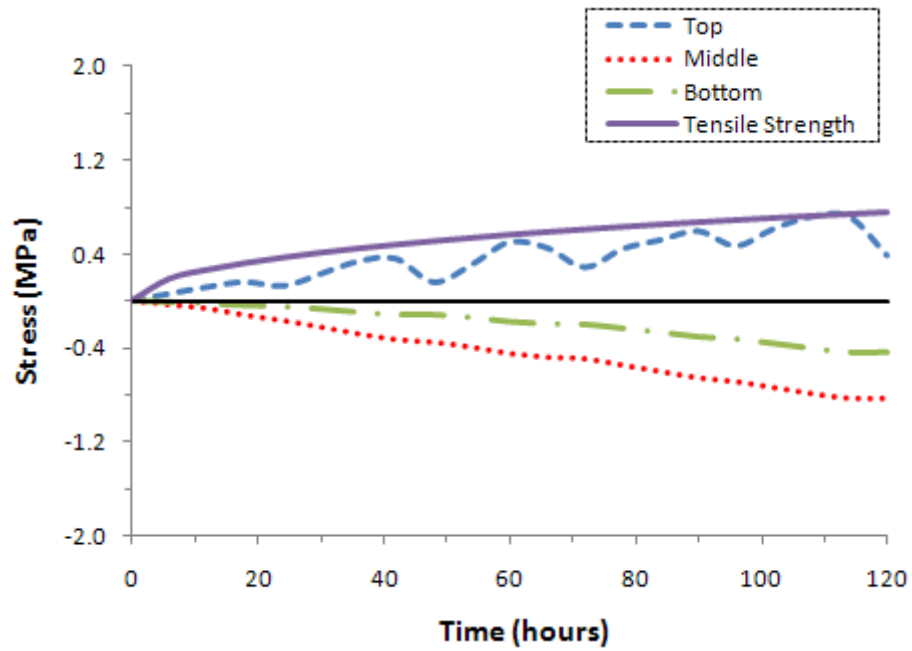
Figure 5.5. Thermal stress analysis at the lift thickness 2.5m
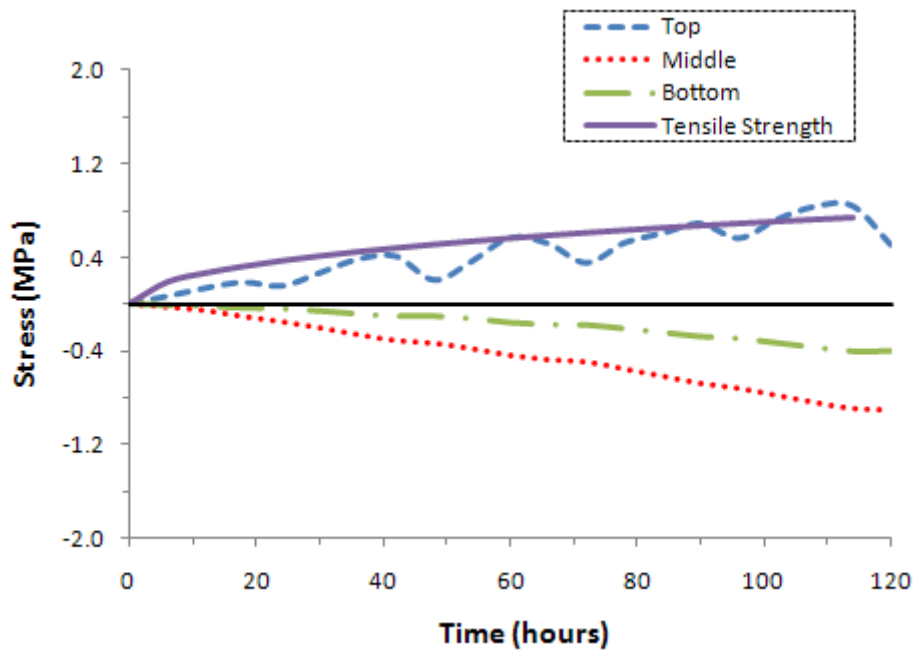
Figure 5.6. Thermal stress analysis at the lift thickness 3m

CHAPTER 6. CONCLUSIONS AND RECOMMENDATIONS

6.1 Conclusions

The objectives of this study are to verify the use of fly ash replacement for Type I cement instead of Type IV in concrete dam and to find out the proper lift thickness of mass concrete. The major findings obtained from chemical composition and fineness of cement, and heat evolution tests can be drawn as follows:

(1) US Type I cement has the highest content for C_3S, C_3A, and fineness, and Korea Type IV cement has the lowest content for C_3S, C_3A and fineness, while has the highest C_2S.

(2) Korea Type IV cement displays the lowest rate of heat evolution during hydration because it is C_3S, C_3A that impact fast early age hydration and C_2S than impacts slow early age hydration, and fineness

(3) Curing temperature has a significant effect on the hydration process. Cement hydration reactions progress faster at early ages with an increase of curing temperature.

(4) Fly ash replacement of 40% for Type I cement shows a similar heat generation and compressive strength at 28 days with that of Type IV cement. It shows that this blended cement can be used as an alternative of Type IV cement in a mass concrete dam. The cost-benefit obtained from the use of 40% fly ash replacement for Type I cement without Type IV cement is about 25%.

Based on the results obtained from thermal analysis, the following conclusions can be also drawn:

(1) The finite element modeling developed for this study is capable of simulating the thermal response of an actual concrete dam, which shows this modeling is effective and feasible.

(2) The maximum temperature and occurrence time increase with lift thickness increase.

(3) Considering Korea Standard Specification for concrete, crack index at the lift thickness 1.5m, 2.0m, 2.5m, 3.0 is 1.5, 1.2, 1.0 and 0.9, respectively. Cracks do not occur with a lift thickness of 1.5m. The occurrence probability of cracks with a lift thickness of 2.0m is about 23%, which need to be strict control to casting and curing conditions to prevent the cracking. Concrete placement above a lift thickness of 2m is not suitable because the occurrence probability of cracks is too high.

6.2 Recommendations

In this thesis, the use of fly ash replacement with Type I cement as an alternative to using Type IV cement was verified by fineness, chemical composition and rate of heat evolution. The proper lift thickness was also studied by modeling one concrete block in a dam construction. Therefore, the following recommendations are proposed for the further research:

(1) A study on the effects of fly ash replacement on permeability, porosity and elastic modulus of concrete and verify the results in literature and compared with concrete made with Type IV cement.

(2) The work of thermal analysis needs to be extended to the whole dam's body following construction schedules. Shrinkage, creep, and crack resistance of concrete should be considered in the future study

REFERENCES

ACI (2005). Building Code Requirements for Structural (ACI 318-05) Concrete and Commentary (ACI 318R-05). ACI Committee 318

ASTM C 150 (2002). Standard specification for Portland cement. *Annual Book of ASTM Standards*, 1, 4.02.

ASTM C 305 (2002). Standard practice for Mechanical Mixing of Hydraulic Cement Pastes and Mortars of Plastic Consistency. *Annual Book of ASTM*, l, 4.02.

ASTM C 204 (2002). Standard Test Method for Fineness of Hydraulic Cement by Air-Permeability Apparatus. *Annual Book of ASTM Standards*, l, 4.02.

Abdllah I. Husein Malkawi, et at. (2003). Thermal-Structural Modeling and Temperature Control of Roller Compacted Concrete Gravity Dam. *Journal of Performance of Consturcted Facilities*, 17(4), 177-187

Ahmaruzzaman.M. (2010). Progre. A review on the utilization of fly ash. *Progress in Energy and Combustion Science*, 36, 327-363

Broda M., Wirquin E., and Duthoit B. (2002). Conception of an isothermal calorimeter for concrete-Determination of the apparent activation energy. *Materials and Structures/Matdriaux et Constructions,* 35, 389-394

Baert G., Hoste S., et al. (2008). REACTIVITY OF FLY ASH IN CEMENT PASTE STUDIED BY MEANS OF THERMOGRAVIMETRY AND ISOTHERMAL CALORIMETRY. *Journal of Thermal Analysis and Calorimetry,* 94(2), 485–492

Ballim Y. and P.C. Graham. (2004). Early-age heat evolution of clinker cements in relation to microstructure and composition: implications for temperature development in large concrete elements. *Cement and Concrete Composition*, 26, 417-426.

Ballim Y. (2004). A numerical model and associated calorimeter for predicting temperature profiles in mass concrete. *Cement and Concrete Composition*, 26, 695-703.

CEB-FIP Mode Code, Comite Euro International du Beton, 1993

Cengiz Duran Atis. (2002). Heat evolution of high-volume fly ash concrete. *Cement and Concrete Research*, 32, 751–756

Dunar. Andrew J. and McBride Dennis. (1993). *Building Hoover Dam*. Twayne Publishers, New York, New York 10022.

Evju. (2003). INITIAL HYDRATION OF CEMENTITIOUS SYSTEMS USING A SIMPLE ISOTHERMAL CALORIMETER AND DYNAMIC CORRECTION. *Journal of Thermal Analysis and Calorimetry,* 71, 829–840

Eduardo M.R. Fairbair, et al. (2003). Optimization of mass concrete construction using genetic algorithms. *Computer and Structures*, 82, 281-299

Farmington Hills, Mich. (2000). Cement and Concrete Terminology. ACI 116R-00

Gao Pei-wei, et al. (2007). Effects of fly ash on the properties of environmentally friendly dam concrete. *Fuel*, 86, 1208-1211

Gibbon G.J., Ballim Y., and Grieve G.R.H. (1997). A Low-Cost, Computer-Controlled Adiabatic Calorimeter for Determining the Heat of Hydration of Concrete. *Journal of Testing and Evaluation,* 25(2), 261-266.

Jaafar.M.S, et al.(2007). Development of finite element computer code for thermal analysis of roller compacted concrete dams. *Advances in Engineering Software*, 38, 886-895.

Japan Society of Civil Engineers. (1999). *Standard Specification for Design and Construction of Concrete Structures*: Construction, Japan Society of Civil Engineers, Tokyo, Japan.

Jose Miltoen de Arauujo, Armando Miguel Awruch. (1998), CRACKING SAFTY EVALUATION ON GRAVITY CONCRETE DAMS DURING THE CONSTRUCTION PHASE. *Computer and Structures*, 66, 93-104.

Jiapeng Sun, and Liang Fang. (2009). Numerical simulation of concrete hollow bricks by the finite volume method. *International Journal of Heat and Mass Transfer*.

Jin Keun Kim, Kook Han Kim, and Joo Kyoung Yang (2001). Thermal analysis of hydration heat in concrete structures with pipe-cooling system. *Computers and Structures*, 79, 163-171.

John P. Sibilia. (1996). A Guide to Materials Characterization and Chemical Analysis. *2nd Edition, VCH Publishers, Inc*

John Gajda and Martha Vangeem (2002). Controlling Temperatures in Mass Concrete. *Concrete International*.

How-Jin Chen, Hsien-Sheng Peng, and Yi-Feng Chen. (2004). NUMERICAL ANALYSIS OF SHRINKAGE STRESSES IN A MASS CONCRETE. *Journal of the Chinese Institute of Engineers*, 27(3),357-365

Hong Wei Xie, and YaoLong Chen. (2005), Determination of the type and thickness for impervious layer in RCC dam. *Advances in Engineering Software*, 36, 561-566.

Ishikawa M. (1991). Thermal stress analysis of a concrete dam. *Journal of Computers and Structures*, 40(2), 347-352

Ivindra Pane, Will Hansen. (2005). Investigation of blended cement hydration by isothermal calorimetry and thermal analysis. *Cement and Concrete Research*. 35, 1155-1164.

Kejin Wang, Zhi Ge, et al,. (2007). Developing a Simple and Rapid Test for Monitoring the Heat Evolution of Concrete Mixtures for Both Laboratory and Field Applications. Phase II Report, FHWA DTF61-01-00042, Ctre, Iowa State University.

Kim, Ji young. (2005). Heat Transfer Analysis 4th Edition. *Tae Sung Software & Engineering. INC*.

Kim, Jin Keun, Park, Yong Dong, and Sung, Keun Yeol (1990). Strength and Workability Characteristics of High-Strength Fly Ash Concrete. Korea Concrete Institute, 2(2), 125-130

Kishi, T., and K. Maekawa. (1994). Thermal and mechanical modeling of young concrete based on hydration process of mutli-component cement minerals, In Thermal Cracking in concrete at Early Ages. *Proceeding of RILEM*, Edited by Springenschmid, R., 11-18.

Korea Concrete Institute. (2003). Standard Specification for Concrete. *Korea Concrete Institute*, Seoul, Korea

Korea Water Resources Association (2005), Dam Design Criteria, Korea Water Resources Association, Seoul, Korea

Langana B.W., Wengb K., and Warda M.A. (2002). Effect of silica fume and f ly ash on heat of hydration of Portland cement. *Cement and Concrete Research*, 32, 1045–1051

Leonhardt J., and Hugo P. (1997). COMPARISON OF THERMOKINETIC DATA OBTAINED BY ISOTHERMAL, ISOPERIBOLIC, ADIABATIC AND TEMPERATURE PROGRAMMED MEASUREMENTS. *Journal of Thermal Analysis*, 49, 1535-1551

Lien.H.P.,and Wittmann.F.H. (1995). Coupled heat and mass transfer in concrete elements at elevated temperatures. *Nuclear Engineering and Design*, 156, 109-119.

McCarthy M.J., Dhir R.K. (2005). Development of high volume fly ash cements for use in concrete construction, *FUEL*, 84, 1423-1432

Mehta. P.K., Ravina. D. (1986). Properties of fresh concrete containing large amounts of fly ash. *Cement and Concrete Research*, 16 (2), 227–238.

Metha, P.K., and Paulo J.M.Monteiro. (2006). Concrete, Microstructure, Properties, and Materials. *McGraw-Hill Company, Inc*.

Majoran, C.E., Zavarise, Z., Borsetto, M. (1990). Nonlinear Analysis of Thermal Stresses in Mass Concrete Castings. *Cement and Concrete Research*, 20, 559-578.

Milestone, N.B., and Rogers, D.E. (1981). Use of an Isothermal Calorimeter for Determining Heats of Hydration at Early Ages. *World Cement Technology*, 12(8), 374-380.

Muhammad Nasir Amin, et al. (2009). Simulation of the thermal stress in mass concrete using a thermal stress measuring device. *Cement and Concrete Research*, 139, 154-164.

Noorzaei.J., et al. (2006). Thermal and stress analysis of Kinta RCC dam. *Engineering Structures*, 28, 1795-1802

Neville, A.M. (1998). Properties of Concrete, Jonh Wiley & Sons, Inc.

Paine K. A., Zheng L., and Dhir R. K. (2005). Experimental study and modeling of heat evolution of blended cements. *Advances in Cement Research*, 17(3), 121–132

Polle.J.L., et al. (2007). Hydration Study of Cementitious Materials Using Semi-Adiabatic Calorimetry. *Concrete Heat Development Monitoring, Prediction, and Management, ACI, SP-241*.

Radjy. F.F. (2007). An Overview of Heat Signature Technology and its Application to Proposed Concrete In-Place Thermal Cracking Field Curing Indices. *Concrete Heat Development Monitoring, Prediction, and Management, ACI, SP-241*.

Rafat Siddique. (2004). Performance characteristics of high-volume Class F fly ash concrete. *Cement and Concrete Research*, 34, 487-493

Roman Lackner, and Herbert A.Mang. (2004), Chemoplastic material model for the simulation of early-age cracking: From the constitutive law to numerical analyses of massive concrete structures. *Cement & Concrete Composites*, 26, 551-562.

Sandberg.J.P. and Liberma.S. (2007). Monitoring and Evaluation of Cement Hydration by Semi-Adiabatic Field Calorimetry. *Concrete Heat Development Monitoring, Prediction, and Management, ACI, SP-241*.

Santurjian.O and Kolarow.L. (1996). A SPATIAL FEM MODEL OF THERMAL STRESS STATE OF CONCRETE BLOCKS WITH CREEP CONSIDERATION. *Computer & Structures*, 58(3), 563-574.

Se-Jin Jeon. (2008). Advanced Assessment of Cracking due to Heat of Hydration and Internal Restraint. *ACI Materials Journal*, July-August, 325-333

Sidney Mindess, J.Francis Young and Daivd Darwin. (2002). *Concrete*, Upper Saddle River, NJ : Pearson Education, Inc.

Taylor. H.F.W. (1997). Cement Chemistry. 2nd Edition, Thomas Telford Services Ltd.

Steven H. (2006). Design and Control of Concrete Mixtures. 14th Edition, PCA

United States Department of the Interior. (1976). *Design of Gravity Dams*, a Water Resources Technical Publication, Denver, Colorado.

Taylor. P and Gajda. J. (2007). What Can We Learn From Monitoring Concrete Temperature? *Concrete Heat Development Monitoring, Prediction, and Management, ACI, SP-24*.

Tatro S, Schrader E. (1992). Thermal analysis for RCC-a practical approach. In:Roller compacted concrete III. New York. *ASCE*, 389-406

Wang J.-C. and Yan P.-Y. (2006). INFLUENCE OF INITIAL CASTING TEMPERATURE AND DOSAGE OF FLY ASH ON HYDRATION HEAT EVOLUTION OF CONCRETE UNDER ADIABATIC CONDITION. *Journal of Thermal Analysis and Calorimetry*, 85(3), 755-760

Yaolong Chen, Changjiang Wang, et al. (2001). Simulation analysis of thermal stress of RCC dams using 3-D finite element relocating mesh method. *Advances in Engineering Software*, 32, 677-682

Yong Wu and Ronaldo Luna. (2001). Numerical implementation of temperature and creep in mass concrete. *Finite Elements in Analysis and Design*, 37, 97-106.

Zhi Ge and Kejin.W., Paul J., Sandberg and M. Ruiz. (2009). Characterization and Performance Prediction of Cement-Based Materials Using a Simple Isothermal Calorimeter. *Journal of Advanced Concrete Technology*, 7(3), 1-12.

Zhi Ge. (2005). Predicting temperature and strength development of the field concrete.

Zieying Zang, Daniel Cusson, et al. (2008). New perspectives on maturity method and approach for high performance concrete applications. *Cement and Concrete Research*, 38, 1438-1446.

Zhang Xiao-fei, Li Shou-yi, et al. (2009). The development and verification of relocationg mesh method for computation of temperature field of RCC dam. *Advances in Engineering Software*, 40, 1119-1123.

APPENDIX A. HEAT OF HYDRATION OF TYPE IV CEMENT

Time (day)	Time (hour)	$T(t)^{1)}$ (°C)	$Q(t)^{2)}$ (Kcal/m^3)	$q(t)^{3)}$ (Kcal/m^3·hr)
0.5	12	5.5	3284	359
0.75	18	8.2	4885	207
1	24	9.9	5941	151
1.25	30	11.3	6747	120
1.5	36	12.3	7404	100
1.75	42	13.3	7959	86
2	48	14.1	8439	75
2.25	54	14.8	8862	66
2.5	60	15.4	9240	60
2.75	66	16	9580	54
3	72	16.5	9889	49
3.25	78	17	10172	45
3.5	84	17.4	10432	42
3.75	90	17.8	10673	39
4	96	18.2	10896	36
4.25	102	18.5	11104	34
4.5	108	18.8	11299	31
4.75	114	19.1	11481	29
5	120	19.4	11653	28

[1] T(t) : Adiabatic temperature rise due to cement hydration heat

[2] Q(t) : Total amount of heat generated per unit volume

[3] q(t) : The rate of heat generation per unit volume and per time

APPENDIX B. MODULUS OF ELASTICITY WITH TIME

Time (day)	Time (hour)	$E^{1)}$ (MPa)	$fsp^{2)}$ (MPa)
0.5	12	2062	0.264
0.75	18	2510	0.322
1	24	2881	0.369
1.25	30	3202	0.411
1.5	36	3487	0.447
1.75	42	3744	0.480
2	48	3980	0.510
2.25	54	4197	0.538
2.5	60	4399	0.564
2.75	66	4588	0.588
3	72	4766	0.611
3.25	78	5161	0.633
3.5	84	5563	0.653
3.75	90	5970	0.672
4	96	6382	0.691
4.25	102	6799	0.708
4.5	108	7221	0.725
4.75	114	7649	0.741
5	120	8080	0.756

[1] E : Modulus of elastic

[2] fsp : Concrete Tensile strength

APPENDIX C. THERMAL DISTRIBUTION ANALYSIS MODEL

/title,Dam Thermal Distribution Analysis (Size 4M*15M*1.5M) : Cement Type IV

```
/FILNAM,THERM_1.5m
/PREP7
ET,1,SOLID70

!Material properties (kcal/m^3-hr)
!
mp,kxx,1,2.3   $mp,c,1,0.25   $mp,dens,1,2400            ! Concrete Properties
!
BLOCK,0,-7.5,0,1.5,0,-2
BLOCK,0,-7.5,0,-4.5,0,-2
BLOCK,-7.5,-22.5,0,-4.5,0,-2
VGLU,ALL
!
LSEL,S,,,1
LSEL,A,,,3
LSEL,A,,,6
LSEL,A,,,8
LESIZE,ALL,,,10              ! X DIRECTION OF UPPER BLOCK
  !
LSEL,S,,,25
LSEL,A,,,39
LSEL,A,,,38
LSEL,A,,,40
LSEL,A,,,39
LSEL,A,,,32
LESIZE,ALL,,,10,10  ! X DIRECTION OF UNDER BLOCK
  !
LSEL,S,,,2
LSEL,A,,,16,17
LSEL,A,,,7
LESIZE,ALL,,,15             ! Y DIRECTION OF 7.5M BLOCK
  !
LSEL,S,,,41
LSEL,A,,,43,44
LSEL,A,,,42
LESIZE,ALL,,,15             ! Y DIRECTION OF 15M BLOCK
  !
LSEL,S,,,11
```

```
LSEL,A,,,12
LSEL,A,,,10
LSEL,A,,,36
LSEL,A,,,22
LSEL,A,,,33
LESIZE,ALL,,,8                 ! X DIRECTION OF UNDER BLOCK
!
ALLSEL,ALL
VMESH,ALL

/SOLU
ANTYPE,TRANSIENT
TINTPR,,,,1.0
NROPT,1
CNVTOL,HEAT,,,,1.0E-10
 !
! Initial conditions
 !
TIMINT,OFF
 !
TIME,0.1
VSEL,S,,,1,,,1
D,ALL,TEMP,16.5              ! INITIAL TEMPERATURE OF UPPERE CONCRETE
 !
NSEL,S,LOC,Y,-0.11011,-4.5
NSEL,R,LOC,X,0,-7.51
D,ALL,TEMP,14               ! 7.5M UNDER CONCRETE BLOCK TEMPERTURE
  !
VSEL,S,,,5,,,1
D,ALL,TEMP,14               ! 15.0M UNDER CONCRETE BLOCK TEMPERTURE
 !
ALLSEL,ALL
!
SOLVE
!
!TRANSIENT PART
!
TIMINT,ON
KBC,1
DDELE,ALL,TEMP             ! DELETE INITIAL TEMPERATURES
!
SFA,1,,CONV,12,14  ! SURFACE LOAD OF FORMWORK
SFA,5,,CONV,12,14  ! SURFACE LOAD OF FORMWORK
!
```

```
SFA,4,,CONV,12,14  ! TOP SURFACE LOAD OF CONCRETE
!
SFA,19,,CONV,4.3,14        ! Ambeient
SFA,23,,CONV,4.3,14        ! Ambeient
SFA,25,,CONV,4.3,14        ! Ambeient
!
ALLSEL
!
TIME,12
SFA,1,,CONV,12,11  ! SURFACE LOAD OF FORMWORK
SFA,5,,CONV,12,11  ! SURFACE LOAD OF FORMWORK
!
SFA,4,,CONV,12,11  ! TOP SURFACE LOAD OF CONCRETE
!
SFA,19,,CONV,4.3,11        ! Ambeient
SFA,23,,CONV,4.3,11        ! Ambeient
SFA,25,,CONV,4.3,11        ! Ambeient
BFV,1,HGEN,359
SOLVE
!
TIME,18
SFA,1,,CONV,12,11.6        ! SURFACE LOAD OF FORMWORK
SFA,5,,CONV,12,11.6        ! SURFACE LOAD OF FORMWORK
SFA,4,,CONV,12,11.6        ! TOP SURFACE LOAD OF CONCRETE
SFA,19,,CONV,4.3,11.6      ! Ambeient
SFA,23,,CONV,4.3,11.6      ! Ambeient
SFA,25,,CONV,4.3,11.6      ! Ambeient
BFV,1,HGEN,207
SOLVE
!
TIME,24
SFA,1,,CONV,12,17.2        ! SURFACE LOAD OF FORMWORK
SFA,5,,CONV,12,17.2        ! SURFACE LOAD OF FORMWORK
SFA,4,,CONV,12,17.2        ! TOP SURFACE LOAD OF CONCRETE
SFA,19,,CONV,4.3,17.2      ! Ambeient
SFA,23,,CONV,4.3,17.2      ! Ambeient
SFA,25,,CONV,4.3,17.2      ! Ambeient
BFV,1,HGEN,151
SOLVE
!
TIME,30
SFA,1,,CONV,12,10.9        ! SURFACE LOAD OF FORMWORK
SFA,5,,CONV,12,10.9        ! SURFACE LOAD OF FORMWORK
SFA,4,,CONV,12,10.9        ! TOP SURFACE LOAD OF CONCRETE
```

```
SFA,19,,CONV,4.3,10.9        ! Ambeient
SFA,23,,CONV,4.3,10.9        ! Ambeient
SFA,25,,CONV,4.3,10.9        ! Ambeient
BFV,1,HGEN,120
SOLVE
!
time,36
SFA,1,,CONV,12,7.7 ! SURFACE LOAD OF FORMWORK
SFA,5,,CONV,12,7.7 ! SURFACE LOAD OF FORMWORK
SFA,4,,CONV,12,7.7 ! TOP SURFACE LOAD OF CONCRETE
SFA,19,,CONV,4.3,7.7         ! Ambeient
SFA,23,,CONV,4.3,7.7         ! Ambeient
SFA,25,,CONV,4.3,7.7         ! Ambeient
BFV,1,hgen,100
SOLVE
!
time,42
SFA,1,,CONV,12,9.9 ! SURFACE LOAD OF FORMWORK
SFA,5,,CONV,12,9.9 ! SURFACE LOAD OF FORMWORK
SFA,4,,CONV,12,9.9 ! TOP SURFACE LOAD OF CONCRETE
SFA,19,,CONV,4.3,9.9         ! Ambeient
SFA,23,,CONV,4.3,9.9         ! Ambeient
SFA,25,,CONV,4.3,9.9         ! Ambeient
BFV,1,hgen,86
SOLVE
!
time,48
SFA,1,,CONV,12,22.1          ! SURFACE LOAD OF FORMWORK
SFA,5,,CONV,12,22.1          ! SURFACE LOAD OF FORMWORK
SFA,4,,CONV,12,22.1          ! TOP SURFACE LOAD OF CONCRETE
SFA,19,,CONV,4.3,22.1        ! Ambeient
SFA,23,,CONV,4.3,22.1        ! Ambeient
SFA,25,,CONV,4.3,22.1        ! Ambeient
BFV,1,hgen,75
SOLVE
!
time,54
SFA,1,,CONV,12,12.2          ! SURFACE LOAD OF FORMWORK
SFA,5,,CONV,12,12.2          ! SURFACE LOAD OF FORMWORK
SFA,4,,CONV,12,12.2          ! TOP SURFACE LOAD OF CONCRETE
SFA,19,,CONV,4.3,12.2        ! Ambeient
SFA,23,,CONV,4.3,12.2        ! Ambeient
SFA,25,,CONV,4.3,12.2        ! Ambeient
BFV,1,hgen,66
```

```
SOLVE
!
time,60
SFA,1,,CONV,12,5.7 ! SURFACE LOAD OF FORMWORK
SFA,5,,CONV,12,5.7 ! SURFACE LOAD OF FORMWORK
SFA,4,,CONV,12,5.7 ! TOP SURFACE LOAD OF CONCRETE
SFA,19,,CONV,4.3,5.7        ! Ambeient
SFA,23,,CONV,4.3,5.7        ! Ambeient
SFA,25,,CONV,4.3,5.7        ! Ambeient
BFV,1,hgen,60
SOLVE
!
time,66
SFA,1,,CONV,12,11.6         ! SURFACE LOAD OF FORMWORK
SFA,5,,CONV,12,11.6         ! SURFACE LOAD OF FORMWORK
SFA,4,,CONV,12,11.6         ! TOP SURFACE LOAD OF CONCRETE
SFA,19,,CONV,4.3,11.6       ! Ambeient
SFA,23,,CONV,4.3,11.6       ! Ambeient
SFA,25,,CONV,4.3,11.6       ! Ambeient
BFV,1,hgen,54
SOLVE
!
time,72
SFA,1,,CONV,12,19.1         ! SURFACE LOAD OF FORMWORK
SFA,5,,CONV,12,19.1         ! SURFACE LOAD OF FORMWORK
SFA,4,,CONV,12,19.1         ! TOP SURFACE LOAD OF CONCRETE
SFA,19,,CONV,4.3,19.1       ! Ambeient
SFA,23,,CONV,4.3,19.1       ! Ambeient
SFA,25,,CONV,4.3,19.1       ! Ambeient
BFV,1,hgen,49
SOLVE
!
time,78
SFA,1,,CONV,12,11.6         ! SURFACE LOAD OF FORMWORK
SFA,5,,CONV,12,11.6         ! SURFACE LOAD OF FORMWORK
SFA,4,,CONV,12,11.6         ! TOP SURFACE LOAD OF CONCRETE
SFA,19,,CONV,4.3,11.6       ! Ambeient
SFA,23,,CONV,4.3,11.6       ! Ambeient
SFA,25,,CONV,4.3,11.6       ! Ambeient
BFV,1,hgen,45
SOLVE
!
time,84
SFA,1,,CONV,12,11.5         ! SURFACE LOAD OF FORMWORK
```

```
SFA,5,,CONV,12,11.5          ! SURFACE LOAD OF FORMWORK
SFA,4,,CONV,12,11.5          ! TOP SURFACE LOAD OF CONCRETE
SFA,19,,CONV,4.3,11.5        ! Ambeient
SFA,23,,CONV,4.3,11.5        ! Ambeient
SFA,25,,CONV,4.3,11.5        ! Ambeient

BFV,1,HGEN,42
SOLVE
!
time,90
SFA,1,,CONV,12,10.8          ! SURFACE LOAD OF FORMWORK
SFA,5,,CONV,12,10.8          ! SURFACE LOAD OF FORMWORK
SFA,4,,CONV,12,10.8          ! TOP SURFACE LOAD OF CONCRETE
SFA,19,,CONV,4.3,10.8        ! Ambeient
SFA,23,,CONV,4.3,10.8        ! Ambeient
SFA,25,,CONV,4.3,10.8        ! Ambeient
BFV,1,hgen,39
SOLVE
!
time,96
SFA,1,,CONV,12,16.8          ! SURFACE LOAD OF FORMWORK
SFA,5,,CONV,12,16.8          ! SURFACE LOAD OF FORMWORK
SFA,4,,CONV,12,16.8          ! TOP SURFACE LOAD OF CONCRETE
SFA,19,,CONV,4.3,16.8        ! Ambeient
SFA,23,,CONV,4.3,16.8        ! Ambeient
SFA,25,,CONV,4.3,16.8        ! Ambeient
BFV,1,HGEN,36
SOLVE
!
time,102
SFA,1,,CONV,12,11.8          ! SURFACE LOAD OF FORMWORK
SFA,5,,CONV,12,11.8          ! SURFACE LOAD OF FORMWORK
SFA,4,,CONV,12,11.8          ! TOP SURFACE LOAD OF CONCRETE
SFA,19,,CONV,4.3,11.8        ! Ambeient
SFA,23,,CONV,4.3,11.8        ! Ambeient
SFA,25,,CONV,4.3,11.8        ! Ambeient
BFV,1,hgen,34
SOLVE
!
time,108
SFA,1,,CONV,12,10.9          ! SURFACE LOAD OF FORMWORK
SFA,5,,CONV,12,10.9          ! SURFACE LOAD OF FORMWORK
SFA,4,,CONV,12,10.9          ! TOP SURFACE LOAD OF CONCRETE
SFA,19,,CONV,4.3,10.9        ! Ambeient
```

```
SFA,23,,CONV,4.3,10.9        ! Ambeient
SFA,25,,CONV,4.3,10.9        ! Ambeient
BFV,1,hgen,31
SOLVE
!
time,114
SFA,1,,CONV,12,12.7          ! SURFACE LOAD OF FORMWORK
SFA,5,,CONV,12,12.7          ! SURFACE LOAD OF FORMWORK
SFA,4,,CONV,12,12.7          ! TOP SURFACE LOAD OF CONCRETE
SFA,19,,CONV,4.3,12.7        ! Ambeient
SFA,23,,CONV,4.3,12.7        ! Ambeient
SFA,25,,CONV,4.3,12.7        ! Ambeient
BFV,1,hgen,29
SOLVE
!
time,120
SFA,1,,CONV,12,22  ! SURFACE LOAD OF FORMWORK
SFA,5,,CONV,12,22  ! SURFACE LOAD OF FORMWORK
SFA,4,,CONV,12,22  ! TOP SURFACE LOAD OF CONCRETE
SFA,19,,CONV,4.3,22          ! Ambeient
SFA,23,,CONV,4.3,22          ! Ambeient
SFA,25,,CONV,4.3,22          ! Ambeient
BFV,1,hgen,28
SOLVE
```

APPENDIX D. THERMAL STRESS ANALYSIS MODEL

```
/filnam,Stress_1.5m
/title, DAM Thermal Stress Analysis : 1.5M(Size 4M*15M*1.5M) : Cement Type IV
/prep7
et,1,45
! Material properties
!
mp,alpx,1,10.3e-6      $mp,dens,1,2400     $mp,ex,1,1070      $MP,PRXY,1,0.18
mp,alpx,2,10.3e-6      $mp,dens,2,2400     $mp,ex,2,2060      $MP,PRXY,2,0.18
mp,alpx,3,10.3e-6      $mp,dens,3,2400     $mp,ex,3,2510      $MP,PRXY,3,0.18
mp,alpx,4,10.3e-6      $mp,dens,4,2400     $mp,ex,4,2880      $MP,PRXY,4,0.18
mp,alpx,5,10.3e-6      $mp,dens,5,2400     $mp,ex,5,3200      $MP,PRXY,5,0.18
mp,alpx,6,10.3e-6      $mp,dens,6,2400     $mp,ex,6,3490      $MP,PRXY,6,0.18
mp,alpx,7,10.3e-6      $mp,dens,7,2400     $mp,ex,7,3740      $MP,PRXY,7,0.18
mp,alpx,8,10.3e-6      $mp,dens,8,2400     $mp,ex,8,3980      $MP,PRXY,8,0.18
mp,alpx,9,10.3e-6      $mp,dens,9,2400     $mp,ex,9,4200      $MP,PRXY,9,0.18
mp,alpx,10,10.3e-6     $mp,dens,10,2400    $mp,ex,10,4400     $MP,PRXY,10,0.18
mp,alpx,11,10.3e-6     $mp,dens,11,2400    $mp,ex,11,4590     $MP,PRXY,11,0.18
mp,alpx,12,10.3e-6     $mp,dens,12,2400    $mp,ex,12,4770     $MP,PRXY,12,0.18
mp,alpx,13,10.3e-6     $mp,dens,13,2400    $mp,ex,13,5160     $MP,PRXY,13,0.18
mp,alpx,14,10.3e-6     $mp,dens,14,2400    $mp,ex,14,5560     $MP,PRXY,14,0.18
mp,alpx,15,10.3e-6     $mp,dens,15,2400    $mp,ex,15,5970     $MP,PRXY,15,0.18
mp,alpx,16,10.3e-6     $mp,dens,16,2400    $mp,ex,16,6380     $MP,PRXY,16,0.18
mp,alpx,17,10.3e-6     $mp,dens,17,2400    $mp,ex,17,6800     $MP,PRXY,17,0.18
mp,alpx,18,10.3e-6     $mp,dens,18,2400    $mp,ex,18,7220     $MP,PRXY,18,0.18
mp,alpx,19,10.3e-6     $mp,dens,19,2400    $mp,ex,19,7650     $MP,PRXY,19,0.18
mp,alpx,20,10.3e-6     $mp,dens,20,2400    $mp,ex,20,8080     MP,PRXY,20,0.18
!
BLOCK,0,-7.5,0,1.5,0,-2
BLOCK,0,-7.5,0,-4.5,0,-2
BLOCK,-7.5,-22.5,0,-4.5,0,-2
VGLU,ALL

LSEL,S,,,1
LSEL,A,,,3
LSEL,A,,,6
LSEL,A,,,8
LESIZE,ALL,,,10              ! X DIRECTION OF UPPER BLOCK
 !
LSEL,S,,,25
LSEL,A,,,39
LSEL,A,,,38
LSEL,A,,,40
```

```
LSEL,A,,,39
LSEL,A,,,32
LESIZE,ALL,,,10,10  ! X DIRECTION OF UNDER BLOCK
 !
LSEL,S,,,2
LSEL,A,,,16,17
LSEL,A,,,7
LESIZE,ALL,,,15            ! Y DIRECTION OF 7.5M BLOCK
 !
LSEL,S,,,41
LSEL,A,,,43,44
LSEL,A,,,42
LESIZE,ALL,,,15            ! Y DIRECTION OF 15M BLOCK
 !
LSEL,S,,,11
LSEL,A,,,12
LSEL,A,,,10
LSEL,A,,,36
LSEL,A,,,22
LSEL,A,,,33
LESIZE,ALL,,,8            ! X DIRECTION OF UNDER BLOCK
!
ALLSEL,ALL
VMESH,ALL

SAVE
FINISH

/SOLU
ANTYPE,STATIC
NROPT,2

NSEL,S,LOC,Z,-2
NSEL,U,LOC,Y,0,-4.5
D,ALL,UZ,0

NSEL,S,LOC,X,-7.5
NSEL,U,LOC,Y,0,-4.5
D,ALL,UX,0

NSEL,S,LOC,Y,-4.5
D,ALL,UY,0

NSEL,S,LOC,Y,0
```

```
NSEL,U,LOC,X,-7.5,-22.5
D,ALL,UY,0

NSEL,S,LOC,X,-22.5
D,ALL,UX,0

NSEL,S,LOC,X,0
CP,1,UX,ALL

NSEL,S,LOC,Z,0
CP,2,UZ,ALL

ALLSEL,ALL
!
time,0.1
solve
!
time,12
Ldread,temp,,,12,,THERM_1.5m.rth
MPDELE,EX,1
MPCHG,2,ALL
solve
!
time, 18
Ldread,temp,,,18,,THERM_1.5m.rth
MPDELE,EX,2
MPCHG,3,ALL
solve
!
time, 24
Ldread,temp,,,24,,THERM_1.5m.rth
MPDELE,EX,3
MPCHG,4,ALL
solve
!
time, 30
Ldread,temp,,,30,,THERM_1.5m.rth
MPDELE,EX,4
MPCHG,5,ALL
solve
!
time, 36
Ldread,temp,,,36,,THERM_1.5m.rth
MPDELE,EX,5
```

```
MPCHG,6,ALL
solve
!
time, 42
Ldread,temp,,,42,,THERM_1.5m.rth
MPDELE,EX,6
MPCHG,7,ALL
solve
!
time,48
Ldread,temp,,,48,,THERM_1.5m.rth
MPDELE,EX,7
MPCHG,8,ALL
solve
!
time,54
Ldread,temp,,,54,,THERM_1.5m.rth
MPDELE,EX,8
MPCHG,9,ALL
solve
!
time,60
Ldread,temp,,,60,,THERM_1.5m.rth
MPDELE,EX,9
MPCHG,10,ALL
solve
!
time,66
Ldread,temp,,,66,,THERM_1.5m.rth
MPDELE,EX,10
MPCHG,11,ALL
solve
!
time,72
Ldread,temp,,,72,,THERM_1.5m.rth
MPDELE,EX,11
MPCHG,12,ALL
solve
!
time,78
Ldread,temp,,,78,,THERM_1.5m.rth
MPDELE,EX,12
MPCHG,13,ALL
solve
```

```
!
time,84
Ldread,temp,,,84,,THERM_1.5m.rth
MPDELE,EX,13
MPCHG,14,ALL
solve
!
time,90
Ldread,temp,,,90,,THERM_1.5m.rth
MPDELE,EX,14
MPCHG,15,ALL
solve
!
time,96
Ldread,temp,,,96,,THERM_1.5m.rth
MPDELE,EX,15
MPCHG,16,ALL
solve
!
time, 102
Ldread,temp,,,102,,THERM_1.5m.rth
MPDELE,EX,16
MPCHG,17,ALL
solve
!
time,108
Ldread,temp,,,108,,THERM_1.5m.rth
MPDELE,EX,17
MPCHG,18,ALL
solve
!
time,114
Ldread,temp,,,114,,THERM_1.5m.rth
MPDELE,EX,18
MPCHG,19,ALL
solve
!
time,120
Ldread,temp,,,120,,THERM_1.5m.rth
MPDELE,EX,19
MPCHG,20,ALL
solve
```